ISSN: 0128-7680

Pertanika Journal of

SCIENCE & TECHNOLOGY

VOLUME 10 NO.2
JULY 2002

A scientific journal published by Universiti Putra Malaysia Press

Pertanika Journal of Science & Technology

About the Journal

Pertanika, the pioneer journal of UPM, began publication in 1978. Since then, it has established itself as one of the leading multidisciplinary journals in the tropics. In 1992, a decision was made to streamline Pertanika into three journals to meet the need for specialised journals in areas of study aligned with the strengths of the university. These are **(i) Pertanika Journal of Tropical Agricultural Science (ii) Pertanika Journal of Science & Technology (iii) Pertanika Journal of Social Science & Humanities.**

Aims and Scope

Pertanika Journal of Science & Technology welcomes full papers and short communications in English or Bahasa Melayu in the fields of chemistry, physics, mathematics, and statistics, engineering, environmental control and management, ecology and computer science. It is published twice a year in January and July.

Articles must be reports of research not previously or simultaneously published in other scientific or technical journals.

Communications are notes of a significant finding intended spaced typewritten pages and must be accompanied by a letter from the author justifiying its publication as a communication.

Reviews are critical appraisals of literature in areas that are of interest to a board specturm of scientist and researchers. Review papers will be published upon invitation.

Submission of Manuscript

Three complete clear copies of the manuscript are to be submitted to

The Chief Editor
Pertanika Journal of Science & Technology
Universiti Putra Malaysia
43400 UPM, Serdang, Selangor Darul Ehsan
MALAYSIA
Tel: 03-89468854; Fax: 03-89416172

Proofs and Offprints

Page proofs, illustration proofs and the copy-edited manuscript will be sent to the author. Proofs must be checked very carefully within the specified time as they will not be proofread by the Press editors.

Authors will receive 20 offprints of each article and a copy of the journal. Additional copies can be ordered from the Secretary of the Editorial Board.

Published by Universiti Putra Malaysia Press
ISSN No. 0128-7680

PERTANIKA EDITORIAL OFFICE
Research Management Centre (RMC)
1st Floor, IDEA Tower II
UPM-MTDC, Technology Centre
Universiti Putra Malaysia
43400 Serdang, Selangor, Malaysia
Tel: +603 8947 1622, 8947 1619, 8947 1616

Pertanika Journal of Science & Technology

Volume 10 No. 2, 2002

Contents

ISSN: 0128-7680
Pertanika J. Sci. & Technol. 10(2): 145 - 152 (2002)

Convergence of the Steepest Descent Method for Minimizing Convex Functions

Malik Hj. Abu Hassan, Mansor b. Monsi & Leong Wah June
Department of Mathematics
Universiti Putra Malaysia
43400, UPM Serdang,
Selangor

Received: 28 June 1999

ABSTRAK

Kiwiel dan Murty (1996) membincangkan sifat penumpuan bagi suatu kelas algoritma penurunan tercuram untuk meminimumkan fungsi kuasi cembung yang selanjar dan boleh beza f atas $\Re^n$. Di bawah syarat sederhana kita buktikan bahawa had infimum bagi $\|\nabla f(x_k)\|$ adalah sifar dan penumpuan palsu tidak berlaku walaupun bila cembung.

ABSTRACT

Kiwiel and Murty (1996) discuss the convergence properties of a class of steepest descent algorithm for minimizing a continuously differentiable quasiconvex function f on $\Re^n$. Under mild conditions, we prove that the limit infimum of $\|\nabla f(x_k)\|$ is zero and that false convergence does not occur even when f is convex.

Keywords: Convergence, steepest descent method, convex functions, minimization

INTRODUCTION

Consider the following unconstrained minimization problem:

$$\min \{ f(x): x \in \Re^n \}, \tag{1}$$

when f is assumed continuously differentiable on $\Re^n$.

Descent algorithms for solving (1) usually generate a sequence $\{x_k\}$ such that $f(x_{k+1}) < f(x_k)$ for all k. However, such a procedure does not always guarantee that $f(x_k)$ converges to the infimum of f on $\Re^n$, even if f is a convex function and $\lim_{k\to\infty} \nabla f(x_k) = 0$. In fact, Rockafellar (1970), Todd (1989), and Auslender and Crouzeix (1989) have given examples to confirm the above phenomenon, which has been called false convergence.

The Todd example has the following properties:

(i) f is convex and continuously differentiable;
(ii) the sequence $\{f(x_k)\}$ is monotonically decreasing and $\lim_{k\to\infty} \nabla f(x_k) = 0$;
(iii) $\lim_{k\to\infty} \nabla f(x_k) > \inf_{x\in\Re^n} f(x)$.

Steepest descent method with Armijo's stepsizes (1966) generates a sequence $\{x_k\}$ via

$$x_{k+1} = x_k + t_k d_k, \quad k = 0, 1, \ldots \tag{2}$$

where

$$d_k = -\nabla f(x_k) \tag{3}$$

and

$$t_k = \arg\max \{t: f(x^k + t_k d_k) \le f(x^k) + \alpha t \nabla f(x_k)^T d_k,\ t = 2^{-i},\ i = 0, 1, \ldots\}, \tag{4}$$

with $\alpha \in (0,1)$.

Under the following standing assumption that generalizes Armijo's condition (4),

Assumption 1.1. Let $\phi : \Re_+ \to \Re_+$ be a function such that:

(A1) $\exists \alpha \in (0,1), \tau_\alpha > 0, \forall t \in (0, \tau_\alpha] : \phi(t) \le \alpha t$,
(A2) $\exists \beta > 0, \tau_\beta \in (0, \infty), \forall t \in (0, \tau_\beta] \cap \Re : \phi(t) \ge \beta t^2$,
(A3) $\forall k, f(x_k + t_k d_k) \le f(x_k) + \phi(t) \nabla f(x_k)^T d_k$ and $0 < t_k < \tau_\beta$ in (1),
(A4) $\exists \gamma > 1, \tau_\gamma > 0, \forall k: t_k \ge \tau_\gamma$ or $[\exists t_k \in [t_k, \gamma t_k]: f(x_k + t_k d_k) \ge f(x_k) + \phi(t_k) \nabla f(x_k)^T d_k]$.

Kiwiel and Murty have proven that for the steepest descent method, the false convergence does not happen if f is quasiconvex. We present our global convergence results in the next section without the quasiconvexity restriction.

GLOBAL CONVERGENCE PROPERTIES

Theorem 2.1. Suppose that Assumption 1.1 holds, then:

(i) either $f(x_k) \to -\infty$ or $\liminf_{k \to \infty} \|\nabla f(x_k)\| = 0$;
(ii) either $f(x_k) \to -\infty$ or $\lim_{k \to \infty} \|\nabla f(x_k)\| = 0$,
if ∇f is Hölder continuous on $\Re^n$; i.e., there exist two positive scalar $l > 0$ and $M > 0$ such that, for all $x, y \in \Re^n$,

$$\|\nabla f(x) - \nabla f(y)\| \le M \|x - y\|^l. \tag{5}$$

Proof. Since for all k,

$$\nabla f(x_k)^T d_k = -\|\nabla f(x_k)\|^2 < 0,$$

we have

$$f(x_{k+1}) < f(x_k),$$

which implies that $\{f(x_k)\}$ is a monotonically decreasing sequence. If $f(x_k)$ tends to $-\infty$, then we complete the proof. Therefore, in the following discussion, we assume that $\{f(x_k)\}$ is a bounded set, i.e.,

$$f(x_0) \geq f(x_k) \geq f(\tilde{x}), \text{ for some fixed } \tilde{x} \text{ and all k.}$$

(I) Suppose that (i) is not true. Then, there exists $\varepsilon > 0$ such that, for all k,

$$\|\nabla f(x_k)\| \geq \varepsilon. \tag{6}$$

It follows from (3), (A2) and (A3) that

$$f(x_{k+1}) - f(x_k) \leq -\beta t_k^2 \|\nabla f(x_k)\|^2. \tag{7}$$

The above inequality, (6), and the boundedness of $\{f(x_k)\}$ yield

$$\sum_{k=0}^{\infty} t_k^2 \|\nabla f(x_k)\|^2 \leq (f(\tilde{x}) - f(x_0))/\beta,$$

and imply that

$$\sum_{k=0}^{\infty} t_k^2 \|\nabla f(x_k)\|^2 < +\infty. \tag{8}$$

By using (2) and (3), we obtain that, for any k,

$$\|x_{k+1} - x_k\|^2 = t_k^2 \|\nabla f(x_k)\|^2.$$

Then, (8) implies that

$$\sum_{k=0}^{\infty} \|x_{k+1} - x_k\|^2 \leq +\infty,$$

which yields that $\{x_k\}$ is convergent, say to a point x^*. From (6), (8), (A2) and (A3), we have

$$\lim_{k \to \infty} t_k = 0. \tag{9}$$

Without loss of generality, we may assume that there exists an index set **K** such that

$$\lim_{k \to \infty,\ k \in \mathbf{K}} d_k = d^*.$$

Then from (A1) and (A4), we deduce that, for $k \in \mathbf{K}$,

$$f(x_k + t_k d_k) - f(x_k) \geq \alpha t_k \nabla f(x_k)^T d_k.$$

Hence, for all k∈K, we have

$$[f(x_k + t_k d_k) - f(x_k)]/t_k \geq \alpha \nabla f(x_k)^T d_k.$$

Taking the limit for k∈K and by (9), we have

$$\nabla f(x^*)^T d^* \geq -\alpha \nabla f(x^*)^T d^* \tag{10}$$

which contradict (A1). (recall that $\nabla f(x_k)^T d_k < 0$.)
Therefore, Assumption 1.1, (10) and (3) imply that $\|\nabla f(x^*)\| = 0$. This completes the proof of (i).

(II) Suppose that there exists an infinite index set **K** and a positive scalar $\varepsilon > 0$ such that, for all k∈**K**,

$$\|\nabla f(x_k)\| \geq \varepsilon. \tag{11}$$

Analogous to the proof of (I), it is easy to prove that

$$\lim_{k\to\infty,\, k\in K} t_k = 0.$$

and

$$\lim_{k\to\infty,\, k\in K} t_k^2 \|d_k\|^2 = \lim_{k\to\infty,\, k\in K} t_k^2 \|\nabla f(x_k)\|^2 = 0. \tag{12}$$

Therefore, for all k∈K,

$$f(x_k + t_k d_k) - f(x_k) \geq \alpha t_k \nabla f(x_k)^T d_k.$$

Using (5) and the Taylor expansion formula, we have

$$\begin{aligned} &f(x_k + t_k d_k) - f(x_k) \\ &= t_k \nabla f(x_k)^T d_k + \int_0^1 [\nabla f(x_k + \theta t_k d_k) - \nabla f(x_k)]^T (t_k d_k)\, d\theta \\ &\leq t_k \nabla f(x_k)^T d_k + M\|t_k d_k\|^{1+l}. \end{aligned}$$

The above two inequalities and (2) yield

$$0 \geq (1 - \alpha) t_k \nabla f(x_k)^T d_k \geq -M\|t_k d_k\|^{1+l}.$$

Dividing the above inequality by $t_k\|d_k\|$, and taking the limit as $k \to \infty$, k∈**K**, we obtain by (12)

$$\lim_{k\to\infty,\, k\in K} (1 - \alpha) \nabla f(x_k)^T d_k / \|d_k\| = 0,$$

which contradicts (11), by (3) and Assumption 1.1.

Let

$$f^* = \inf \{f(x): x \in \Re^n\}, \ \tilde{f} = \lim_{k \to \infty} f(x_k).$$

The following results, given by Wei, Qi and Jiang (1997) show that our algorithm cannot exhibit the phenomenon of false convergence.

Theorem 2.2. If f is a convex function on $\Re^n$ and the algorithm of (2), (3) and Assumption 1.1 is used, then:

(i) $f(x_k) \to f^*$;
(ii) $\{x_k\}$ is an unbounded set if and only if f has an empty set of minima;
(iii) if f has a nonempty set of minima, then x_k converges to a minimal point of f.

Proof. Note that, for all x and all k,

$$\|x_{k+1} - x\|^2 = \|x_k - x\|^2 + \|x_{k+1} - x_k\|^2 + 2(x_{k+1} - x_k)^T(x - x_k), \quad (13)$$
$$f(x) - f(x_k) \geq \nabla f(x_k)^T(x - x_k),$$

by convexity of f. It follows from (2) and (3) that, for all $x \in \Re^n$ and all k,

$$\|x_{k+1} - x\|^2 \leq \|x_k - x\|^2 + \|x_{k+1} - x_k\|^2 + 2t_k(f(x) - f(x_k)). \quad (14)$$

(i) We prove this conclusion by the following three cases (ia), (ib), (ic).
(ia) $f^* = f$. This case is trivial, since $f^* = \tilde{f} = \lim_{k \to \infty} f(x_k)$.
(ib) $\{x_k\}$ is bounded. From the fact that $\{f(x_k)\}$ is a monotonically decreasing sequence, we have that

$$\lim_{k \to \infty} f(x_k) = \tilde{f} > -\infty,$$

which combined with (i) of Theorem 2.1 implies that there exists an index set **K** and a point $x^{**} \in \Re n$ such that

$$\lim_{k \to \infty, \, k \in K} x_k = x^{**},$$

$$\nabla f(x^{**}) = \lim_{k \to \infty, k \in K} \nabla f(x_k) = 0.$$

the convexity of f implies that x^{**} is a minimal point of f.
Therefore, $f^* = f(x^{**}) = \tilde{f}$.

(ic) We now assume that $\tilde{f} > -\infty$ and $\{x_k\}$ is unbounded. Suppose that there exists $\tilde{x} \in \Re^n$, $\varepsilon > 0$, and k_1 such that, for all $k \geq k_1$,

$$f(x_k) \geq f(\tilde{x}) + \varepsilon. \quad (15)$$

Setting $x = \tilde{x}$ in (14), we have

$$\|x_{k+1} - \tilde{x}\|^2 \leq \|x_k - \tilde{x}\|^2 + t_k[t_k\|\nabla f(x_k)\|^2 - 2\varepsilon]. \tag{16}$$

Therefore, the fact that $\{f(x_k)\}$ is bounded from below and the inequality

$$f(x_{k+1}) - f(x_k) \geq \alpha t_k\|\nabla f(x_k)\|^2$$

imply that

$$\sum_{k=0}^{\infty} t_k^2\|\nabla f(x_k)\|^2 < +\infty;$$

hence,

$$t_k^2\|\nabla f(x_k)\|^2 \to 0.$$

Then, (16) implies that $\{\|x_k - \tilde{x}\|^2\}$ is a descent sequence for sufficiently large k. It follows that $\{\|x_k\|\}$ is bounded, which contradicts our assumption.

(ii) [$\Rightarrow$]. Assume that f has an optimal solution point x^*. Setting $x = x^*$ in (14), and noting that $f(x^*) \leq f(x_k)$, we obtain

$$\|x_{k+1} - x^*\|^2 \leq \|x_k - x^*\|^2 + \|x_{k+1} - x_k\|^2. \tag{17}$$

By using Assumption 1.1, we have

$$\sum_{k=0}^{\infty} t_k^2\|\nabla f(x_k)\|^2 < +\infty.$$

Therefore, (2) and (3) yield

$$\sum_{k=0}^{\infty} \|x_{k+1} - x_k\|^2 \leq +\infty. \tag{18}$$

The inequality (17) implies that, for any k,

$$\sum_{i=0}^{k} (\|x_{i+1} - x^*\|^2 - \|x_i - x^*\|^2) \leq \sum_{i=0}^{k} \|x_{i+1} - x_i\|^2.$$

Hence, for any k,

$$0 \leq \|x_{k+1} - x^*\|^2 \leq \|x_0 - x^*\|^2 + \sum_{i=0}^{\infty} \|x_{i+1} - x_i\|^2,$$

which combined with (18) implies that $\{x_k\}$ is bounded. This is a contradiction.

(ii) [$\Leftarrow$]. Suppose that $\{x_k\}$ is bounded. By using the proof of (ib), we can deduce that there exists an accumulation point x^{**} of $\{x_k\}$ such that x^* is a minimal point of f. This contradicts the assumption.

(iii) Suppose that x^* is any fixed optimal solution of (1). Similar to the proof of (ii), (17)-(18) still hold. Then, we deduce that there exists a constant c such that

$$\lim_{k\to\infty} \|x_k - x^*\|^2 = c < +\infty \tag{19}$$

and that the sequence $\{x_k\}$ is bounded. Similar to the proof of (ii) [$\Leftarrow$], we see that $\{x_k\}$ has an accumulation point, which is an optimal solution of (1). By the monotonicity property of $\{f(x_k)\}$, any accumulation point of $\{x_k\}$ is an optimal solution of (1). Suppose that $\{x_k\}$ has two different accumulation points y_1 and y_2. It is clear that y_1 and y_2 are optimal solutions of (1) from the above argument. It follows from (19) that there exist constants c_1 and c_2 such that

$$\lim_{k\to\infty} \|x_k - y_i\|^2 = c_i < +\infty, \quad i = 1, 2. \tag{20}$$

It is easy to see by (2), (3) and (18) that $c_1 = c_2 = 0$ and $\|y_1 - y_2\| = 0$. This is a contradiction. Therefore, $\{x_k\}$ is convergent to an optimal solution point of (1).

DISCUSSION

First, the proof of Theorem 2.1 can be extended to more general search direction

$$d_k = -H_k \nabla f(x_k), \tag{21}$$

where H_k is an n×n symmetric positive-definite matrix, satisfied the following assumption:

(A5) There exist constants $\lambda_1, \lambda_2 > 0$ such that

$$\|H_k \nabla f(x_k)\| \le \lambda_1 \|\nabla f(x_k)\|$$

and

$$\nabla f(x_k)^T H_k \nabla f(x_k) \ge \lambda_2 \|\nabla f(x_k)\|^2,$$

for any integer k.

The conditions on $\{H_k\}$ are not very restrictive. In fact, the commonly used generating formulas of H_k, i.e., quasi-Newton updating methods in convex minimization, can guarantee Condition (A5). We refer the reader to the recent (Byrd and Nocedal 1989).

Second, by slightly modifying the proof of Theorem 3.1 in (Wu 1992), we can obtain the following results, which show that the algorithm with (21) and Assumption 1.1 cannot exhibit the phenomenon of false convergence.

Theorem 3.1. Suppose that (A5) holds. If f is convex function on $\Re^n$, then

$$f^* = \bar{f}. \tag{22}$$

Third, if f is quasiconvex, Theorem 9.2.4 in (Mangasarian 1969) ensures that case (ii) in Theorem 2.1 cannot happen. Furthermore, by the quasiconvexity of f (Theorem 9.1.4 in (Mangasarian 1969)),

$$\nabla f(x_k)^T(x - x_k) \leq 0.$$

Then, the inequality (13) is reduced to

$$\begin{aligned}\|x_{k+1} - x\|^2 &\leq \|x_k - x\|^2 + \|x_{k+1} - x_k\|^2 \\ &\leq \|x_k - x\|^2 + t_k^2\|\nabla f(x_k)\|^2,\end{aligned}$$

so that

$$\|x_l - x\|^2 \leq \|x_k - x\|^2 + \sum_{j=k} t_j^2\|\nabla f(x_j)\|^2 < +\infty,$$

if $l > k$. Hence, $\{\|x_k\|\}$ is bounded and therefore, the case where $\{x_k\}$ is an unbounded set is not considered in Theorem 2.2.

REFERENCES

Armijo, L. 1966. Minimization of functions having continuous partial derivatives. *Pacific Journal of Mathematics* **16**: 1-3.

Auslender, A. and J. P. Crouzeix. 1989. *Well-behaved Asymptotical Convex Functions*, p. 101-122. Analyse Non-Linéare, Gauthier-Villars, Paris.

Byrd, R. H. and J. Nocedal. 1989. A tool for the analysis of quasi-Newton methods with application to unconstrained minimization. *SIAM Journal on Numerical Analysis* **26:** 727-739.

Kiwiel, K. C. and K. Murty. 1996. Convergence of the steepest descent method for minimizing quasiconvex functions. *Journal of Optimization Theory and Applications* **89**: 221-226.

Mangasarian, O. L. 1969. *Nonlinear Programming.* New York: Mc-Graw-Hill.

Rockafellar, R. L. 1970. *Convex Analysis.* Princeton, New Jersey: Princeton University Press.

Todd, M. J. 1989. On convergence properties of algorithms for unconstrained minimization. *IMA Journal of Numerical Analysis* **9**: 435-441.

Wei, Z., L. Qi and H. Jiang. 1997. Some convergence properties of descent methods. *Journal of Optimization Theory and Applications* **95**: 177-188.

Wu, S. Q. 1992. Convergence properties of descent methods for unconstrained minimization. *Optimization* **26**: 229-237.

ISSN: 0128-7680
Pertanika J. Sci. & Technol. 10(2): 153 - 160 (2002)

Emulsion Properties of Mixed Tween20-Span20 in Non-Aqueous System

[1]W. M. Wan Rusmawati, *[2]K. Dzulkefly, [3]W.H. Lim & [4]S. Hamdan
[1]*Faculty of Science and Technology*
Universiti Pendidikan Sultan Idris (UPSI)
[2]*Department of Chemistry*
Universiti Putra Malaysia (UPM)
[3]*Advanced Oleochemical Technology Centre (AOTC)*
Malaysia Palm Oil Board (MPOB)
[4]*Faculty of Science and Technology*
University College Terengganu

Received: 27 June 2001

ABSTRAK

Emulsi minyak-dalam-gliserol (O/G) telah disediakan dari campuran surfaktan Tween20-Span20 dengan nisbah berat yang berbeza. Emulsi O/G didapati terbentuk bila kandungan minyak kurang dari 50 wt% dengan kepekatan campuran Tween20-Span20 3 wt%. Sifat-sifat fizikal emulsi ditentukan dengan mengguna mikroskop, penganalisis partikal dan pengukuran reologi. Kajian perkaitan antara nilai HLB campuran Tween20-Span20 dengan kestabilan emulsi juga dilakukan.

ABSTRACT

Oil-in-glycerol (O/G) emulsion was prepared in the presence of different weight ratios of mixed Tween20-Span20 surfactants. O/G emulsion was observed to form below 50 wt% of oil content at 3 wt% of mixed Tween20-Span20 surfactants. Physical properties of the emulsion were determined by using a microscope, particle counting and rheological measurement. An attempt to correlate HLB values of mixed Tween20-Span20 with emulsion stability was also carried out.

Keywords: Tween20, Span20, nonaqueous emulsion, droplets size, stability, rheology

INTRODUCTION

Emulsions have been defined as heterogeneous systems of one liquid dispersed in another in the form of droplets usually exceeding 0.1 μm in diameter. The two liquids are immiscible, chemically unreactive, and form systems characterized by a minimal thermodynamic stability. One of the important components for making an emulsion is the emulsifier, and a systematic selection of emulsifier type for a particular emulsion is frequently based on the hydrophilic-lipophilic balance (HLB) concept (1). It is known that mixtures of emulsifiers can have

*To whom correspondence should be addressed

synergistic effects in enhancing stability of emulsions. A suitable combination of emulsifiers leads to a greatly enhanced stability as compared to individual emulsifiers (2). Various reasons have been given for this, such as formation of intermolecular complexes at the oil/water (O/W) interface (3) and development of strong interfacial films that prevent coalescence by virtue of their high dilational elasticity (4).

Water-in-oil (O/W) and oil-in-water (O/W) emulsions have been widely studied since emulsion was recognized. In contrast, oil-in-glycerol (O/W) emulsion has not been fully explored and therefore remains rather limited. Thus, this paper presents some of the physical properties (emulsion stability, droplet size and flow behaviour) of a non-aqueous emulsion formed by mixing Tween20 and Span20.

MATERIALS AND METHODS

Materials

Polyoxyethylene (20) sorbitan monolaurate (Tween20) and sorbitan monolaurate (Span20) from Sigma were used as received. Glycerol (G) of 99.5% purity purchased from Sigma was also used throughout the experiment. Medium chain triglyceride (MCT) oil, obtained from a local manufacturer, was used as an oil phase.

Methods

Preparation of Emulsion

O/G emulsion was prepared by first dispersing a required amount of mixed emulsifier (Tween20-Span20) in glycerol (9.0 ml). The MCT oil (1.0 ml) was then added and the mixture was homogenised (using an IKA-T25 disperser) for 3 min at 8000 rpm to produce an emulsion. The emulsions were kept at 30.0±5°C for 24 hours to equilibrate before being analysed. The emulsifiers were blended together, to obtain HLB values within the range 8.7-16.7. HLB of mixed emulsifiers can be calculated as follows:

$$HLB_{mixture} = f\,HLB_A + (1\text{-}f)HLB_B \qquad (1)$$

Where f is weight fraction of emulsifier A and (1-f) is weight fraction of emulsifier B.

Particle Size

The O/G emulsions samples were viewed directly under a microscope (Olympus AX70) with a camera attached, and the stage of the microscope was thermostatically controlled. The undiluted samples were placed on a slide and were illuminated from below, i.e. transmitted light was used. The droplet sizes of emulsions were subjected to a laser light scattering instrument (Malvern Zetasizer 5000) for particle size determination.

Viscosity Measurement

The steady flow behaviour was studied using a Brookfield Rheometer (Model DV-III), which was attached to a cone and plate sensor system. The samples were allowed to reach the required test temperature in a suitable sensor system. Subsequently, the rheometer was operated at a steady rate and the shear rate was increased gradually from 1 and 250 s^{-1} and then decreased back to 1 s^{-1} over a period of scanning time. The flow behaviour of O/G emulsions systems containing different MCT:G ratio at 3% wt/wt of mixed emulsifiers was studied.

RESULTS AND DISCUSSION

The results of emulsion stability through visual observation in Table 1 showed that the emulsion was stable in the range of 10:90 to 30:70 of MCT:G ratios. The emulsions were unstable at higher content of MCT (i.e. 40:60 and 50:50 of MCT:G ratios). This might be due to the collapse of oil droplets in the emulsion system. Comparison among different weight ratios of mixed surfactants, 20:80 weight ratio of Tween20-Span20 system has the smallest stable emulsion region (between 10:90 and 20:80 of MCT:G ratios) as observed under a microscope. The decrease in emulsion region might be due to the strong repulsion between Tween20 and Span20 at the oil-glycerol interface, which was not able to retain the increase of oil droplets in the system.

Fig. 1 shows the variation of the emulsion droplets size of different HLB numbers for 10:90 of MCT:G weight ratio. On the first day, the droplet size increased with the increase of the HLB number. This means the increase of the HLB number - increase of Tween20 - played an important role in the increment of oil droplet in the continuous phase. On the seventh day, it was observed that the oil droplet at lower HLB numbers (8 to 13) increased to about the size of higher HLB numbers (13 to 16.7). This was due to the coalescence of the oil droplet cluster to form a more stable droplet. In contrast, there was no change in the droplet size of higher HLB number. The particle size was rather constant as compared to the first day. This suggests that the oil droplet in the emulsion

TABLE 1
Emulsion stability of mixed surfactants (3 wt%) in MCT/G emulsion systems

Tween20-Span20 (HLB)	MCT-in-G (%) 0:100	10:90	20:80	30:70	40:60	50:50
100:0 (16.70)	clr	S	S	S	B	B
80:20 (15.11)	clr	S	S	S	B	B
60:40 (13.82)	clr	S	S	S	B	B
40:60 (12.26)	clr	S	S	S	B	B
20:80 (10.41)	clr	S	S	B	B	B
0:100 (8.60)	clr	S	S	S	B	B

* clr -clear solution; S - stable emulsion; B - emulsion break

system was more stable even after seven days. This implied that the emulsion was more stable with the increase of Tween20 as it did not affect the oil droplet size.

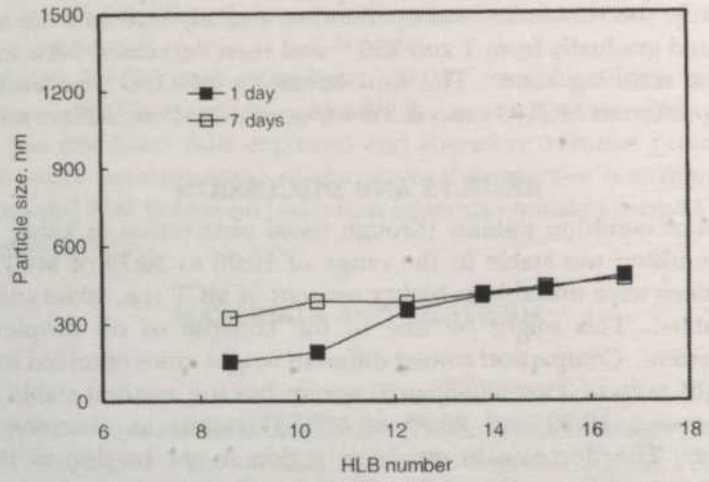

Fig. 1: O/G emulsion in mixed surfactants system of various HLB values (MCT:G, 10:90 weight ratio)

A similar phenomenon occurred in MCT:G of 20:80 weight ratio in mixed surfactants system as shown in *Fig. 2.* On the first day, the oil droplets increased steeply from 244 to 527 nm as the HLB number increased from 8 to 13. Further increase in HLB numbers from 13 to 16.7 did not show any significant increase in droplet size. After seven days, the oil droplet sizes of lower HLB (8 to 13) increased, whereas at higher HLB number, (13 to 16.7) the emulsion exhibited a rather constant droplet size. However, the droplet size of 20:80 weight ratio of MCT:G system was larger than the 10:90 system. The weak oil-glycerol interface of the 20:80 weight ratio contributed to the instability of the oil droplet as more oil droplet coalescence produced large oil droplets.

The oil droplet was further increased from 924 to 1061 nm (1st day) with the increase of oil (MCT) content as shown in *Fig. 3.* However, at lower HLB numbers, a rather consistent particle size was obtained after seven days. In contrast, at higher HLB numbers, the droplet size increased. This increase of size was due to the contribution of oil (MCT) content in the O/G emulsion system. The results showed that the increment of oil was still able to maintain the stability of emulsion except 20:80 weight ratio of Tween20-Span20 system.

Fig. 4 shows the plotted shear stress versus shear rate of O/G emulsion of different Tween20-Span20 weight ratios in MCT:G (10:90) in the mixed surfactants system. It was observed that the shear stress increased with the increase of shear rate. All mixed Tween20-Span20 studies showed a similar flow behaviour. The tangents of the curve indicate no changes in viscosity. The

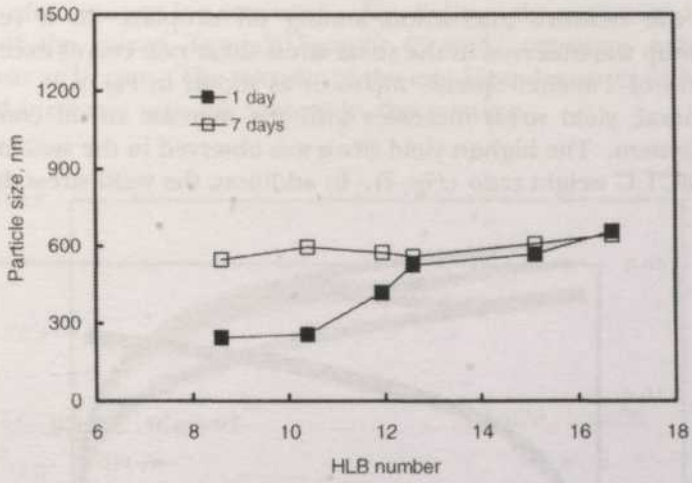

Fig. 2: O/G emulsion in mixed surfactants system of various HLB values (MCT:G, 20:80 weight ratio)

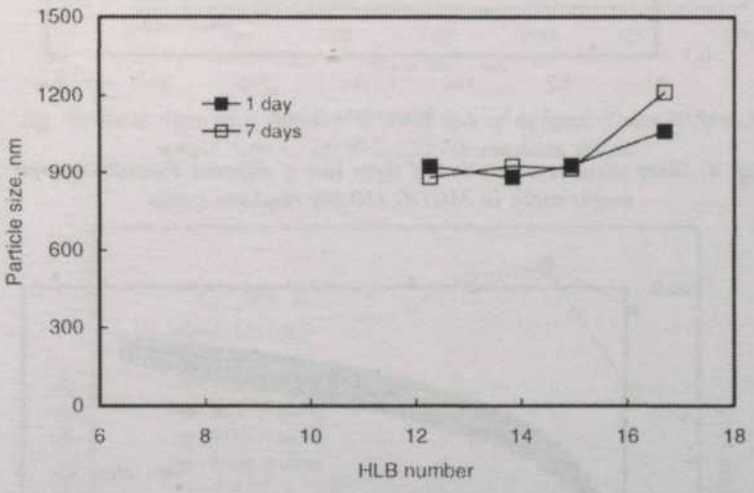

Fig. 3: O/G emulsion in mixed surfactants system of various HLB values (MCT:G, 30:70 weight ratio)

viscosity is constant regardless of the shear rate that shows Newtonian characteristics. As oil content increased to 20:80 of MCT:G in the mixed surfactant system, hysterisis loop was observed for all weight ratios of Tween20-Span20 mixtures except 0:100 and 20:80 of Tween20-Span20 (see *Fig. 5*). This indicates that the emulsion system was disturbed and unable to return to its original form. The network among oil droplets in the emulsion system was broken due to shear action. The increase of oil content in the emulsion system

increases the network interaction among oil droplets. As a result, larger hysterisis loop was observed in the shear stress-shear rate curves except for 0:100 weight ratio of Tween20-Span20 mixtures as shown in *Fig. 6.*

In general, yield stress increases with the increase of oil content in the emulsion system. The highest yield stress was observed in the system containing 30:70 of MCT:G weight ratio (*Fig. 7*). In addition, the yield stress does not vary

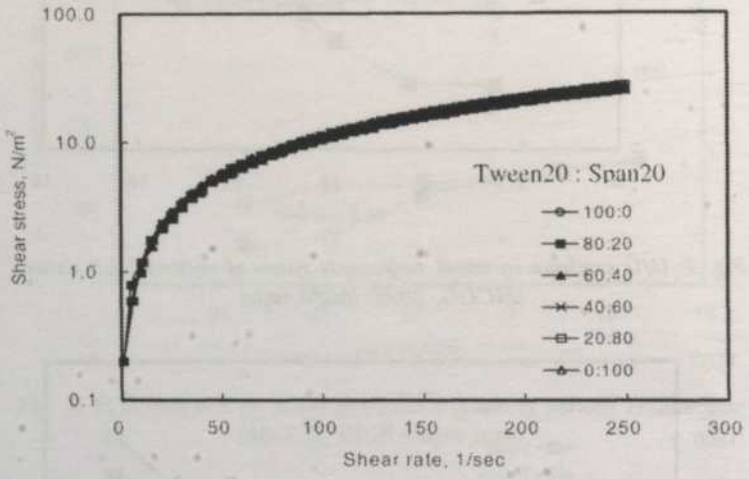

Fig. 4: Shear stress as a function of shear rate of different Tween20-Span20 weight ratios in MCT:G (10:90) emulsion system

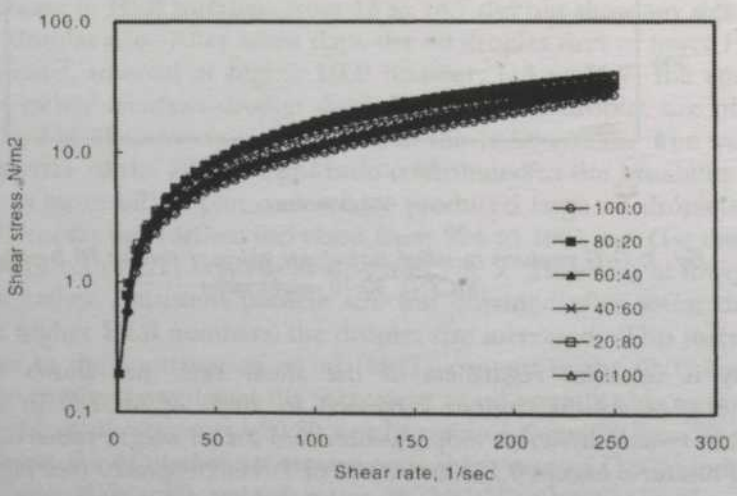

Fig. 5: Shear stress as a function of shear rate of different Tween20-Span20 weight ratio in MCT:G (20:80) emulsion system

significantly after storage for one week. *Fig. 8* shows the variation of viscosity with HLB of the mixed Tween20-Span20 (3 wt%) emulsion systems after applying shear at 10 rpm. The viscosity of the emulsion decreases with the HLB number and increases with oil content in the mixture.

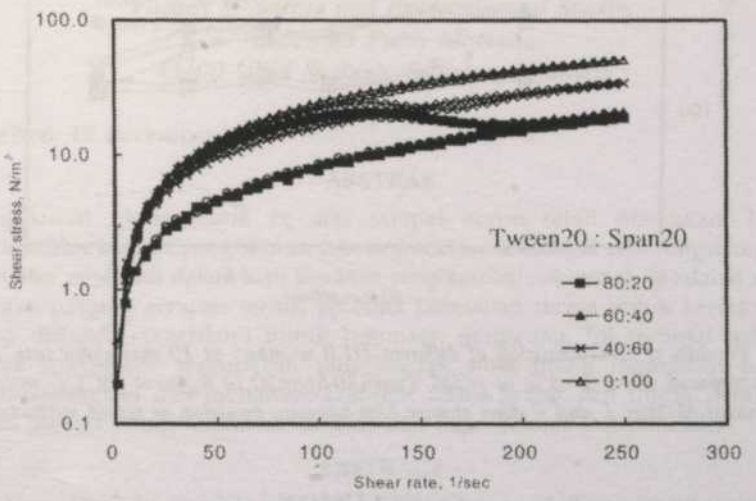

Fig. 6: Shear stress as a function of shear rate of different Tween20-Span20 weight ratio in MCT:G (30:70) emulsion system

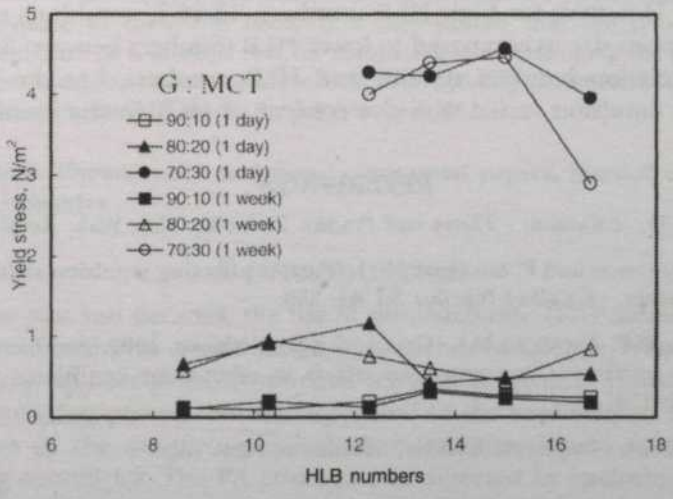

Fig. 7: Yield stress of O/G emulsions at different HLB numbers in 1 and 7 days. The emulsions were prepared using 3 wt% of mixed Tween20-Span20 in different MCT:G ratios

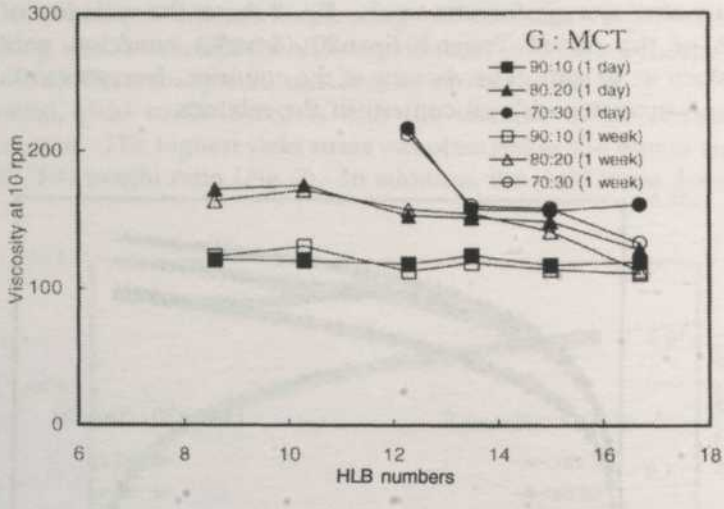

Fig. 8: Viscosity of O/G emulsion of different HLB numbers at 10 rpm shear rate. Emulsions were prepared using 3 wt% of mixed Tween20-Span20 in different MCT:G ratios and measured after 1 and 7 days storage.Non-aqueous emulsion of mixed surfactants

CONCLUSION

Stable O/G emulsion was obtained between 10:90 and 30:70 of MCT:G weight ratios. Further increase of oil content breaks the emulsion system. The increase of oil or MCT content also increases the droplet size and viscosity of the system. However, for high HLB numbers, 13-16.7, emulsions exhibited a stable oil droplet size as compared to lower HLB numbers between 8-13. There was no correlation between stability and HLB numbers, but the stability of nonaqueous emulsion varied with the content of MCT in the emulsion.

REFERENCES

BECHER, P. 1965. *Emulsions - Theory and Practice.* 2nd edn. New York: Reinhold.

BOYD, J., C. PARKINSON and P. SHERMAN. 1971. Factors affecting emulsion stability and the HLB concept. *J. Colloid Interface Sci.* **41**: 359.

FAIRHURST, D., M.P. ARONSON, M.L. GUM and E.D. GODDARD. 1983. Some comments on non-ionic surfactant concentration effects in oil-in-water emulsion. *Colloids and Surfaces* **7**: 153.

TADROS T.H. 1984. *Surfactant.* London: Academic Press Inc.

ISSN: 0128-7680
Pertanika J. Sci. & Technol. **10(2)**: 161 - 166 (2002)

Thermal Diffusivity Measurement of the Commercial Papers Using Photoacoustic Technique

Chan Kok Sheng & W. Mahmood bin Mat Yunus*

Department of Physics
Faculty of Science and Environmental Studies
Universiti Putra Malaysia
43400 UPM Serdang, Selangor, Malaysia

Received: 12 December 2001

ABSTRAK

Pengukuran photoakustik ke atas sampel kertas telah dilakukan. Ianya berdasarkan kepada pengukuran isyarat fotoakustik sebagai satu fungsi kepada frekuensi modulasi dalam satu kawasan yang ketebalan sampel, l_s, adalah sama dengan panjang serapan terma, μ_s. Nilai peresapan terma untuk kertas yang dikaji didapati mencukupi untuk kegunaan pengguna. Ini terbukti bahawa teknik fotoakustik merupakan satu kaedah yang boleh digunakan untuk membandingkan dan mengawal sifat-sifat terma kertas dan untuk penilaian kesan semasa pemprosesan di industri dan juga makmal penyelidikan.

ABSTRACT

We have carried out photoacoustic measurements of thermal diffusivity on samples of commercial papers. It is based upon the measurement of the photoacoustic signal as a function of the modulation frequency in the region where the sample thickness, l_s, was equal to the thermal diffusion length, μ_s. The value of the thermal diffusivities for the commercial papers was found to be adequate to their end users. It is also proven that the photoacoustic technique can be a valuable tool for comparing and controlling the properties of papers and for evaluating the effects of processing parameters upon these properties industrially or on the laboratory scale.

Keywords: Photoacoustic technique, commercial papers, thermal diffusivity, wood industries

INTRODUCTION

During the past two decades, the use of photoacoustic (PA) measurements has gradually diffused into a wide range of branches of science, from agricultural and medical sciences to environmental sciences in general (Lima *et al.* 2000). This encouraging process can be connected to the sensitivity of the PA signal to changes in the sample's physical characteristics due to modifications in processing conditions. The PA effect can be detected by enclosing a sample in an airtight cell and exposing it to a chopped light beam. As a result of the periodic heating of the sample, following the absorption of light, the pressure

*Corresponding Author

in the air chamber oscillates at the chopping frequency. A sensitive microphone coupled to the cell wall detects the resulting pressure fluctuation in the gas. The PA signal so produced depends not only on the amount of heat generated in the sample (i.e. on the optical absorption coefficient of the sample and its light-into-heat conversion efficiency), but also on how this heat diffuses through the sample and its exchange with the surrounding gas in the cell (Rosencwaig *et al.* 1976). The quantity that measures the rate of diffusion of heat in the sample is the thermal diffusivity α, given by:

$$\alpha = \frac{k}{\rho C_p} \tag{1}$$

where k is the thermal conductivity, ρ is the mass density and C_p is the specific heat at constant pressure of the sample.

The PA technique has proven to be a simple and reliable technique for measuring the thermal properties of almost any material. It has been used for measuring thermal diffusivity of materials as diverse as superconductor, semiconductors, glasses and polymers (Fanny *et al.* 1999; W. Mahmood Mat Yunus *et al.* 1999). The technique has also been used for direct assessment of change in material properties induced by processing, e.g. in composite preparation and food processing (Lima *et al.* 2000; Perondi *et al.* 1987). In this paper, we report on the photoacoustic measurement of the thermal diffusivity of several commercially available papers. These included white paper (for office printing), press paper (partially bleached), fax paper (for thermal printing), filtering paper, canson paper (for painting and drawing) and wrapping paper (tear resistant).

THEORY

The theory of the photoacoustic effect in solid sample was first described in 1976 (Rosencwaig and Gersho 1976). According to the proposed model, the heat generated in the sample will diffuse from the sample to the gas in immediate contact with the sample. An important parameter involved is the thermal diffusion length of the sample μ_s, which can be defined in terms of the thermal diffusivity by

$$\mu_s = \sqrt{\alpha / (\pi f)} \tag{2}$$

where f is the modulation frequency of the incident light. From Equation (2), it is obvious that μ_s decreases with the increasing modulation frequency. The chopping frequency is termed as characteristic frequency, f_c ($f = f_c$) when the thermal diffusion length, μs becomes equal to sample thickness, l_s (i.e. $\mu_s = l_s$). Thus, there are two possible regimes to be distinguished: first for $f > f_c$ which

$\mu_s < l_s$, in this case the sample is thermally thin. Then the amplitude of the photoacoustic (PA) signal decreases as f^{-1} one decreases the modulation frequency. At high modulation frequency, $f > f_c$ which $\mu_s < l_s$, the sample is thermally thick then the amplitude of PA signal varies as $f^{-1.5}$. Hence, by knowing f_c, l_s, and applying the Equation (2), which corresponds to the situation $l_s = \mu_s$, the thermal diffusivity can then be obtained as

$$\alpha_s = \pi f_c l_s^2 \qquad (3)$$

EXPERIMENTAL METHOD

The experimental set-up used for the present study is shown in *Fig. 1.* A 75 mW helium-neon laser, cw beam, is mechanically chopped by an optical chopper (SR540). The modulated beam then illuminated onto a sample kept inside a non-resonant PA cell. The cell was fitted with an electret microphone (Cirkit product, UK) and covered with a silica glass window. The absorption of the modulated beam on the sample produce in periodic heating. The generation of heat is transferred to the gas in contact. Consequently, the pressure in the air chamber oscillates at the chopping frequency. This phenomenon is known as a photoacoustic effect which can be detected by a sensitive microphone. The generated photoacoustic signal was then amplified by a preamplifier (SR 560) and further analyzed by using a lock-in amplifier (SR 530). The amplitude of photoacoustic signal is recorded as a function of the modulation frequency.

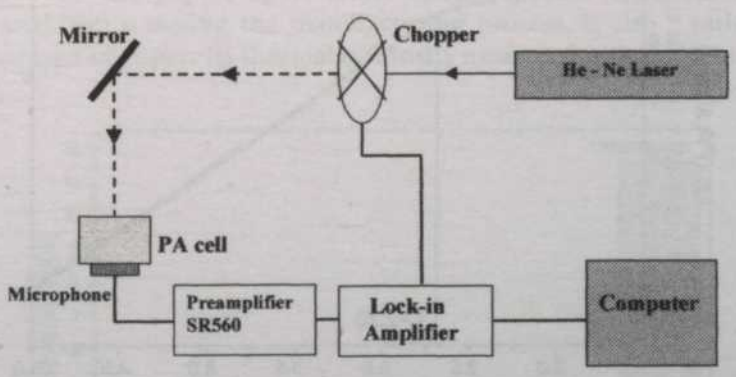

Fig. 1: Schematic diagram of the exprimental set-up

RESULTS AND DISCUSSION

The PA Signal of white paper (thickness 0.072 mm) varies exponentially with the frequency as shown in *Fig.2.* By using the analysis method proposed by Da Costa and Siqueira (1996), the ln (PA Signal) was plotted against ln (f) as shown in *Fig.3.* The characteristic frequency, f_c was obtained by measuring the frequency at which the sample changes its behavior from thermally thin to

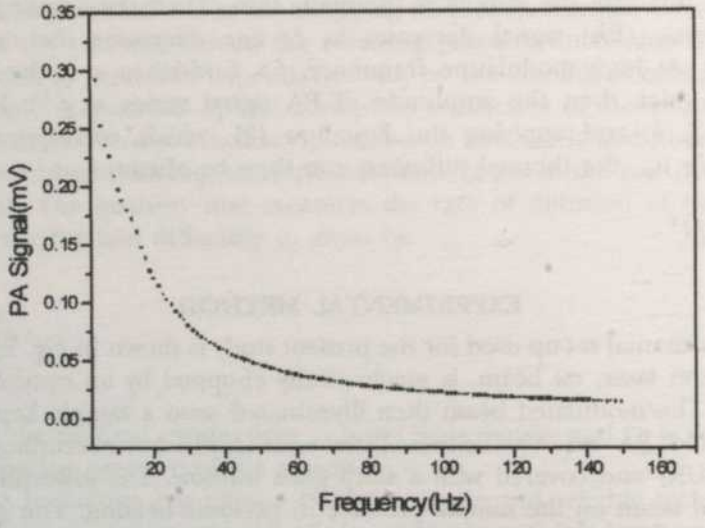

Fig. 2. Photocoustic signal amplitude as a function of the modulation frequency for white paper

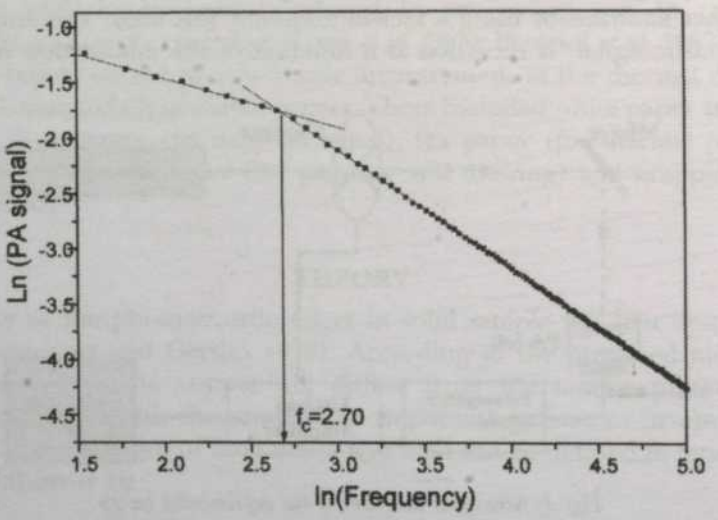

Fig. 3. ln (PA signal) versus ln (frequency) for white paper

thermally thick and it was found to be 14.89 Hz. By using the Equation (3), the thermal diffusivity of this sample was calculated as 2.42×10^{-3} cm^2s^{-1}. The same procedure was used for the other commercial paper samples and the measured thermal diffusivity values of all our samples are tabulated in Table 1.

TABLE 1
Thermal diffusivity of commercial paper samples obtained by a closed photoacoustic cell technique

Paper Samples	Thermal diffusivity (cm^2s^{-1})
Canson Paper	11.58×10^{-3}
Wrapping paper	2.85×10^{-3}
White Paper	2.42×10^{-3}
Filtering Paper	2.16×10^{-3}
Press Paper	1.22×10^{-3}
Fax Paper	0.53×10^{-3}

The measurements of thermal diffusivity for various commercial papers are summarized in the histogram of *Fig. 4*. The differences among the tested samples in this experiment indicate that different processing conditions were applied during manufacturing in order to satisfy the end user. These results are in agreement with those reported by Lima *et al.* (2000) using the open cell technique. It is known that canson paper has a considerably looser packing of the processed pulp, so that a large fraction of air filled space is present within the samples. Additionally, air has a rather high thermal diffusivity which is about 0.21 cm^2s^{-1}. These two factors are combined to explain why canson paper has a comparatively high thermal diffusivity.

In contrast, fax paper, apart from having specific chemical additives incorporated into it during the manufacturing process, is also a rather more compacted type of paper. Its thermal diffusivity measured with the printing side

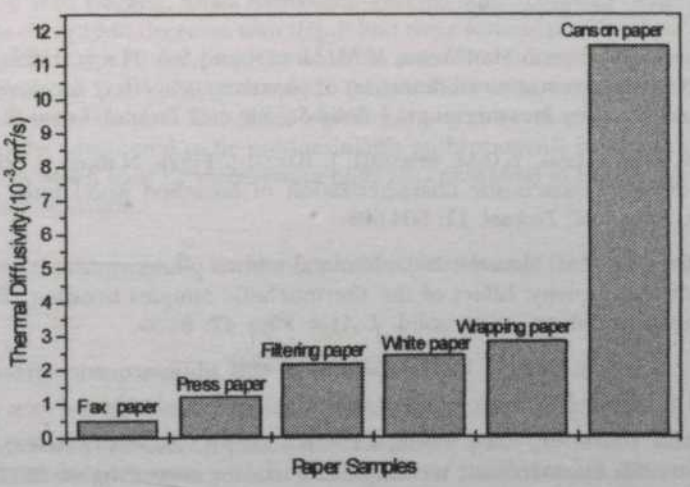

Fig.4. Thermal diffusivity of commercial papers measured by closed photoacoustic cell technique

facing the incoming light (α=0.53×10^{-3}cm^{2}s^{-1}) was the smallest among the tested papers. This finding is in due agreement with the expected end use of the material. Indeed, the formatted heat delivery to the printing surface is required to remain as localized as possible, both for good contrast and for high resolution in thermal printing. This requirement is satisfied better by a paper having a small thermal diffusivity, in agreement with our findings. In between these two extremes lie, in ascending order, the results for press paper and for wrapping paper (α=1.22×10^{-3}cm^{2}s^{-1} and 2.85×10^{-3}cm^{2}s^{-1}, respectively).

CONCLUSION

In this paper, the usefulness of the PA technique for measuring the thermal properties of several commercially available papers is demonstrated. The largest and the smallest thermal diffusivity of the tested papers are found to be canson paper and fax paper, respectively. Finally, PA measurements can be a valuable tool for researchers and in industrial plants for comparing, controlling and evaluating the effects of processing parameters particularly in wood-based industries.

ACKNOWLEDGEMENT

The authors wish to express their thanks to Universiti Putra Malaysia and the Malaysian Government for the financial support through IRPA and PASCA (CKS).

REFERENCES

Da Costa, A.C.R. and A.F. Siqueira. 1996. Thermal diffusivity of conducting polypyrrole. *J. Appl. Phys.* **80**: 5579-5582.

Fanny, C.Y.J., W. Mahmood Mat Yunus, M.M. Moksin and S.A. Halim. 1999. Piezoelectric and open photoacoustic cell detection of photoacoustic effect for power meter and thermal diffusivity measurement. *J. Solid St. Sci. and Technol. Letters* **6**: 15-22.

Lima, C.A.S., M.B.S. Lima, L.C.M. Miranda, J. Baeza, J. Freer, N.Reyes, J. Ruiz and M.D. Silva. 2000. Photoacoustic characterization of bleached wood pulp and finished papers. *Meas. Sci. Technol.* **11**: 504-508.

Perondi, L.F. and L.C.M. Miranda. 1987. Minimal-volume photoacoustic cell measurement of thermal diffusivity: Effect of the thermoelastic samples bending. Theory of the photoacoustic effect with solid. *J. Appl. Phys.* **47**: 64-69.

Rosencwaig, A. and A. Gersho. 1976 . Theory of the photoacoustic effect with solid. *J. Appl. Phys.* **47**: 64-69.

Mahmood Mat Yunus, W., C.Y.J. Fanny, I.V. Grozescu, A. Zakaria, Z.A. Talib, and M.M. Moksin. 1999. Photoacoustic technique as a tool for measuring thermal diffusivity of materials. *Acta Physica Sinica* **8**: S241-S245

Pertanika J. Sci. & Technol. **10(2)**: 167 - 177 (2002)
ISSN: 0128-7680

Accumulation of Barium, Uranium, Cadmium and Manganese in the Sediment Core from the Pulau Cik Wan Dagang Mangrove Forests, Terengganu, Malaysia

Kamaruzzaman, B. Y., Shazili, N. A. M., Mohd Lokman, H. & Sulong, I.
Mangrove Research Unit,
Institute of Oceanography,
Kolej Universiti Sains & Teknologi Malaysia,
21030 Kuala Terengganu,
Terengganu, Malaysia

Received: 9 May 2001

ABSTRAK

Akumulasi menegak unsur-unsur Ba, U, Cd dan Mn diukur pada teras sedimen sedalam 150 cm yang diperolehi di hutan paya bakau, Pulau Cik Wan Dagang, Kuala Kemaman, Terengganu, Malaysia. Secara keseluruhannya, kepekatan elemen kajian kecuali Mn menurun mengikut kedalaman dan menunjukkan satu sempadan yang jelas pada kedalaman 70 cm. Bagi menentukan pengaruh pencemaran logam berat, faktor pengkayaan (EF) bagi semua unsur dikira. Dalam kajian ini, nilai EF bagi U dan Cd secara signifikan adalah lebih besar daripada nilai piawai dan dianggap mempunyai sumber yang lebih dominan kepada antropogenik manakala sumber Ba dan Mn adalah dominan secara semula jadi kerana nilai EFnya didapati hampir sama dengan nilai piawai.

ABSTRACT

The accumulation of elements Ba, U, Cd and Mn with respect to depth was determined in a 150 cm sediment core obtained from the mangrove forests of Pulau Cik Wan Dagang, Kuala Kemaman, Terengganu, Malaysia. Generally, all elements except Mn decrease with depth and their vertical profiles show a clear boundary at about 70 cm deep. In order to assess the influence of heavy metal pollution more precisely, enrichment factors (EF) were calculated. In this study, U and Cd have EF values significantly greater than unity and may therefore be considered to be predominantly anthropogenic in origin whereas Ba and Mn which have EF values about unity are considered to be predominantly terigenous in origin.

Keywords: Anthropogenic, barium, cadmium, enrichment factors, manganese, uranium

INTRODUCTION

Mangroves are woody, seed-bearing, highly specialized plants and are found along sheltered intertidal coastlines of estuaries and lagoons. Their species possess unique adaptations which enable them to thrive in an environment where other plants cannot grow. Recently, reclamation of mangrove ecosystems for industrial, urban and other forms of development has been increasing and it causes irreversible damage in coastal regions throughout the tropics. Along

with the destruction of the mangroves comes the anthropogenic effects associated with the new developments. The sediments from mangrove areas contain a historical record of information on the temporal changes that have been brought about as a result of these actions. This record is altered or smeared by the effects of sediment mixing, which influences the preservation of the physical sedimentary structures (Nittrouer and Sternberg 1979). However, the alteration of the record depends on the intensity, depth and nature of the sediment mixing as well as the sediment accumulation rate. Sediment mixing also alters the biogenic components and pore water concentrations of dissolved chemical species within the sediment mixed layer (Berner 1980; Aller 1982). In addition, Yingst and Rhoads (1980) documented that microbial activities are influenced by sediment mixing rates.

Mangrove ecosystems are important sinks for particulate material supplied by rivers and the atmosphere to the oceans (Yeats and Bewers 1983). In urbanized regions, the sediment is very often influenced by domestic, industrial and mining activities leading to increased trace metal concentrations (Martin and Whitfield 1983; Martin *et al.* 1989). When these sediments are undisturbed, and sedimentation rates are known, they can provide us with a historical pollution record (Goldberg *et al.* 1977; Bertine 1980; Nolting and Helder 1991). Biological, physical, chemical and diagenetic processes can change the sediment properties and those processes can be applied to study the anthropogenic influences on the marine environment. In Malaysia, studies relating to mangroves are not well documented and only little information is available concerning the sedimentation of the mangrove forest (Mohd Lokman *et al.* 1994; Kamaruzzaman 1994). Furthermore, geochemical studies of sediments from the Malaysian mangrove forests have received little attention and only limited studies have been carried out regarding their role in the process of sedimentation (Kamaruzzaman *et al.* 2000). In view of the importance of the mangrove to various aspects of the environment, research on the concentration of heavy metals as well as their distribution pattern in sediment was carried out.

MATERIALS AND METHOD

Sampling Sites

Pulau Cik Wan Dagang is situated in the district of Kemaman, approximately 170 km south of Kuala Terengganu, Malaysia. The mangroves which are relatively undisturbed have been gazetted as a mangrove reserve forest by the Terengganu Forestry Department. The mangrove area lies on the southern bank of the Kemaman estuary, where both the Kemaman and Chukai rivers flow into. The tide floods the area twice daily as it is semi-diurnal with a mean range of 1.8 m. In this study, a 150 cm sediment core was collected with a D-section core sampler from this area (*Fig. 1*) and was cut into segments of approximately 5 cm intervals, labelled and stored in cleaned acid bottles for analysis. The sediment core was chosen for this study since the area is known to be highly productive (Kamaruzzaman 1994) and with a moderately high

sedimentation rate of 0.66 cm yr^{-1} (Kamaruzzaman *et al.* 2000), which is suitable for this kind of study.

Analytical Methods

The sediment samples were digested according to the published methods (Noriki *et al.* 1980; Sen Gupta and Bertrand 1995; Kamaruzzaman 1999) with some modifications. An inductively-coupled plasma mass spectrometer (ICP-MS) was used for the quick and precise determinations of Al, Ba, U, Cd and Mn

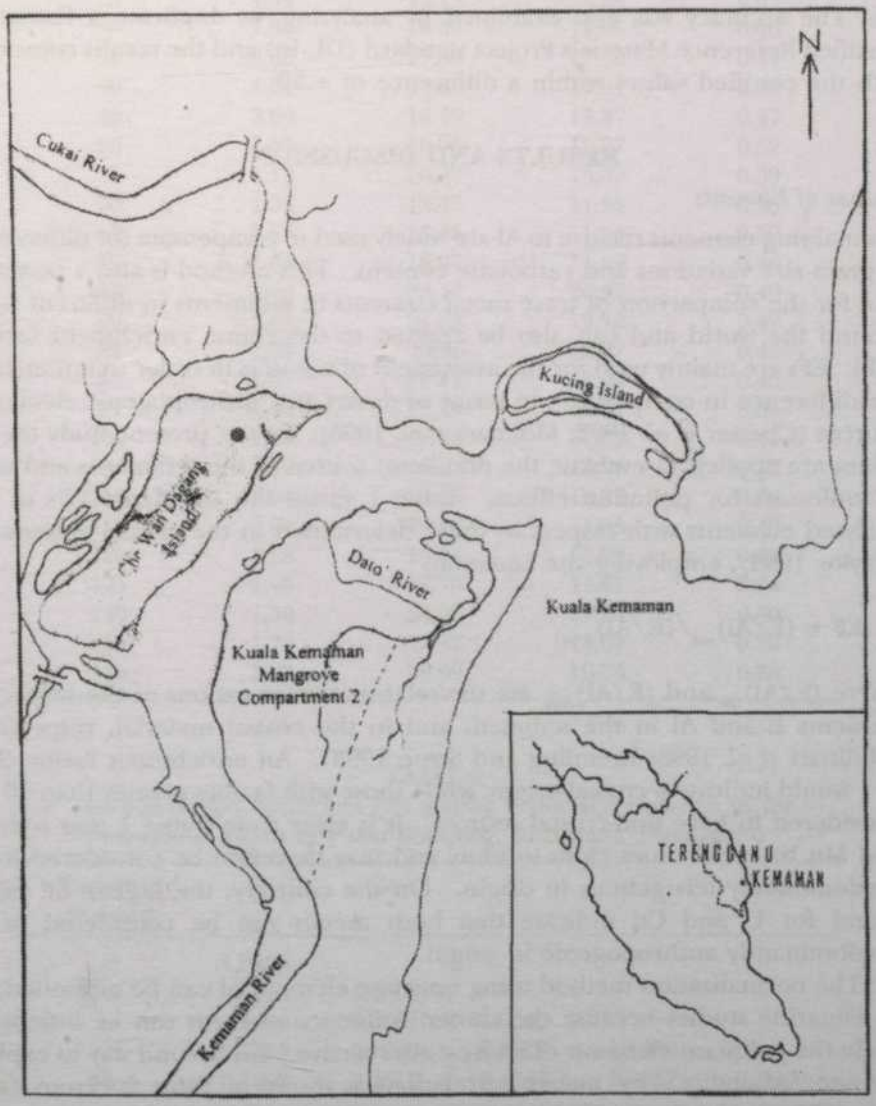

Fig. 1: Location of the core (-) study area in the Pulau Che Wan Dagang, Mangrove Forests, Kemaman, Terengganu, Malaysia

in the digested marine sediment. Briefly, the digestion method involved the heating of 50 mg of a < 63 μm size sample in a sealed teflon vessel with a concentrated acid mixture of HF, HNO_3 and HCl in the ratio of 2.5 : 3.5 : 3.5. The teflon vessels were kept at 150 °C for 3 – 5 hours. After cooling, a mixed solution of boric acid and EDTA was added, and the vessel was again heated at 150 °C for at least 5 hours. After cooling to room temperature, the content of the vessel was transferred into a 10 ml polypropylene test tube and was diluted to 10 ml with deionized water. A clear solution with no residue had to be obtained at this stage. The precision assessed by replicate analyses was within 3%. The accuracy was also examined by analyzing, in duplicate a Canadian Certified Reference Materials Project standard (DL-1a) and the results coincided with the certified values within a difference of ± 3%.

RESULTS AND DISCUSSION

Sources of Elements

Normalising elements relative to Al are widely used to compensate for differences in grain size variations and carbonate content. This method is also a powerful tool for the comparison of trace metal contents in sediments in different areas around the world and can also be applied to determine enrichment factors (EF). EFs are mainly used for the assessment of aerosols in order to understand the difference in composition in terms of desert and anthropogenic elemental sources (Chester *et al.* 1992; Molinari *et al.* 1993). In the present study the EF values are applied to evaluate the dominant source of the sediments and used as indicators for pollution effects. Table 1 shows the calculated EFs of the analysed elements with respect to those determined in the crustal abundance (Taylor 1964), employing the equation:

$$EF = (E/Al)_{sed} / (E/Al)_{crust},$$

where $(E/Al)_{sed}$ and $(E/Al)_{crust}$ are the relative concentrations of the respective elements E and Al in the sediment and in the crustal material, respectively (Molinari *et al.* 1993; Kremling and Strue 1993). An enrichment factor close to 1 would indicate a crustal origin, while those with factors greater than 10 are considered to have non-crustal sources. It is clear from Table 1 that only Ba and Mn have EF values close to unity and may therefore be considered to be predominantly terrigenous in origin. On the contrary, the higher EF values found for U and Cd indicate that both metals can be considered to be predominantly anthropogenic in origin.

The normalization method using only one element Al can be of limited use in estuarine studies because the chosen reference element can be unreactive while the pollutant elements of interest are reactive. The second way to explore element variability is by matrix correlations as shown in Table 2. From Table 2, only Ba, U and Mn showed a fairly moderate correlations coefficient ($r > 0.5$) with Al, indicating the co-occurrence with the lithigenous fraction of the

TABLE 1
Calculated enrichment factors (EF) of Ba, U, Cd and Mn based on the mean concentrations determined in the whole sub-cores

Depth (cm)	Ba	U	Cd	Mn
5	3.63	24.17	13.14	0.66
10	2.88	14.37	6.09	0.38
15	3.55	18.44	7.67	0.46
20	1.67	20.09	10.28	0.49
25	4.54	25.13	21.48	0.67
30	1.56	18.59	14.06	0.46
35	3.63	17.89	12.49	0.47
40	1.74	24.87	17.21	0.48
45	3.64	18.49	13.37	0.47
50	1.80	19.95	15.27	0.57
55	1.12	20.97	15.49	0.59
60	1.34	18.45	11.35	0.58
65	1.53	15.68	11.24	0.50
70	1.64	18.97	11.37	0.46
75	1.86	23.12	20.27	0.49
80	2.81	21.88	12.78	0.47
85	1.55	20.50	12.87	0.42
90	1.67	19.11	12.00	0.40
95	1.46	17.44	10.97	0.39
100	1.66	18.52	11.82	0.41
105	1.49	18.24	10.98	0.42
110	1.53	18.75	12.32	0.39
115	1.62	19.32	11.96	0.40
120	1.58	19.01	12.98	0.43
125	1.40	17.70	11.41	0.34
130	1.90	24.92	12.97	0.40
135	1.72	19.49	11.07	0.38
140	1.69	15.69	10.74	0.38

TABLE 2
The correlation coefficient (r^2) among 5 analysed elements in the mangrove forests of Pulau Sekeping, Kemaman, Terengganu

Elements analysed	Al	Ba	U	Cd	Mn
Al	1.0000				
Ba	0.5974	1.0000			
U	0.4992	0.0081	1.0000		
Cd	0.0633	0.1920	0.3018	1.0000	
Mn	0.5792	0.2612	0.4756	0.5037	1.0000

sediment. A fairly moderate correlations, ($r > 0.5$) with Mn is showed by U and Cd which indicates their occurrence in fine minerals that make up the bulk of the heavy mineral fraction of the sediment.

Depth Distribution

Depth profiles of Ba, U, Cd and Mn are shown in *Fig. 2*. Based on the previous studies (Mohd Lokman *et al.* 1994; Kamaruzzaman *et al.* 2000), sediments from the mangrove forests of Kemaman seem to be well mixed, and the sediment supply homogeneous. Although some of these profiles show an increase in concentration toward the surface layer, this is not necessarily an indication for anthropogenic input. It is more likely that early diagenetic processes are responsible for this phenomenon (Ridgway and Price 1987; Macdonald *et al.* 1991). It was noted that the vertical profiles of Ba, U, Cd and Mn show a distint contrast in the upper and lower parts of the sediments as shown in *Fig. 2*. The concentrations of all elements except for Mn were comparably high and varied widely whereas at greater depth, their vertical profiles showed only slight variation. The mean concentration and relative standard deviations of all four elements for each 5 cm subcore were calculated (Table 3). From the table, we can easily see the existence of a boundary at about 70 cm depth. For the first layer above 70 cm, the average percentage of relative standard deviations for all elements are higher (0.22%) and for greater depths they are relatively smaller (0.05%). Assuming the sedimentation rate obtained from a previous study (Kamaruzzaman *et al.* 2000) can be applied to the boundary, its age turned out to be 91 years old. The average of percentage relative standard deviations of Ba, U, Cd and Mn in the upper layer are 10% or more higher than those in the deeper layer, with Ba showing the greatest contrast of about 25%.

The concentration of Ba ranged from 231 ppm to 760 ppm with an average of 413 ppm. The vertical profile initially decreased steeply with depth (*Fig. 2*). The sharp decrease of Ba in the surface layer may be due to the early diagenetic loss of Ba, being a common phenomenon in the sediments. In other studies at a Pulau Cik Wan Dagang mangrove forest (Leong 2001), Ba has a fairly good correlation with organic matter, suggesting that the sedimentation of Ba is controlled largely by the biogenic matter, although the detrital fraction was dominant in the sediments. Therefore, the low Ba present in the sediments might be due to the low productivity during that period and/or probably due to the dilution of the biogenic matter with very high amounts of terrigenous material transported to the sea.

Uranium was generally constant ranging from 11.5 ppm to 20.1 ppm and averaged at 15.7 ppm (*Fig. 2*). Its mean value was 5 times higher than its average U shale value and calculated EF values suggesting that most of the U might have come from the anthropogenic sources. The slight decrease of U in the surface layer may be due to the early diagenetic loss of U in oxic sediment (Thomson *et al.* 1990), where the bottom water U has diffused downwards into the sediment a few cm deep. The vertical variations in the depth profile might be due probably to temporal changes in biological productivity. However,

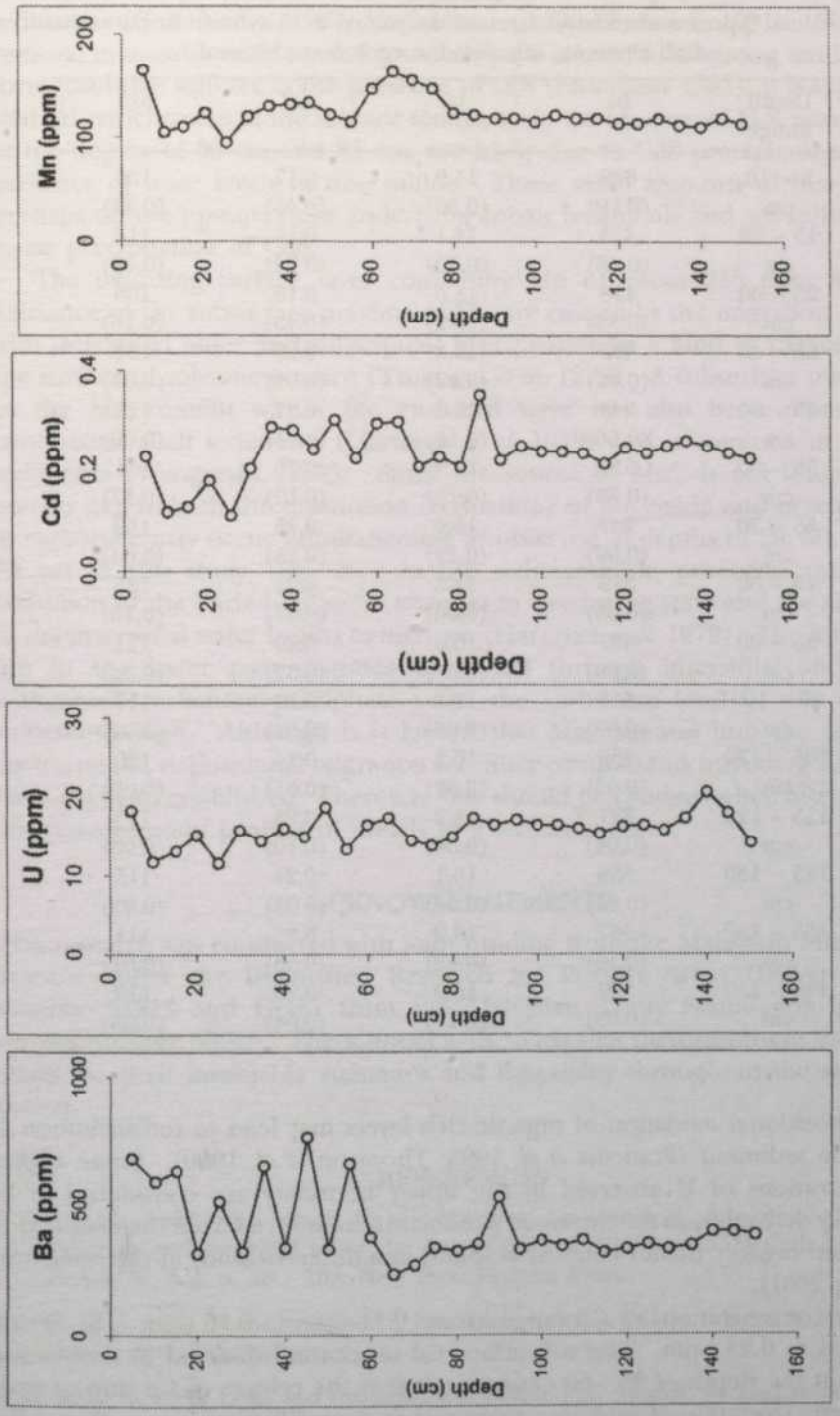

Fig. 2: Vertical profiles of Ba, U, Cd and Mn plotted against depth. The division in the graph is described in the text.

TABLE 3
Mean values (ppm) and relative standard deviations in % (shown in parentheses) of all elements calculated at each 5 cm interval

Depth Range	Ba	U	Cd	Mn
5 – 10 cm	638 (0.10)	14.9 (0.30)	0.17 (0.46)	135 (0.31)
15 – 20 cm	473 (0.48)	14.1 (0.10)	0.15 (0.24)	116 (0.08)
25 – 30 cm	418 (0.33)	13.6 (0.22)	0.16 (0.43)	108 (0.16)
35 – 40 cm	495 (0.46)	15.3 (0.07)	0.29 (0.01)	131 (0.01)
45 – 50 cm	543 (0.56)	16.8 (0.16)	0.27 (0.15)	128 (0.06)
55 – 60 cm	516 (0.39)	14.9 (0.15)	0.26 (0.19)	131 (0.17)
65 – 70 cm	247 (0.09)	15.9 (0.12)	0.25 (0.25)	159 (0.04)
75 – 80 cm	329 (0.03)	14.3 (0.06)	0.22 (0.07)	135 (0.13)
85 – 90 cm	437 (0.29)	16.8 (0.03)	0.29 (0.32)	121 (0.02)
95 – 100 cm	342 (0.08)	16.8 (0.03)	0.25 (0.03)	117 (0.02)
105 – 110 cm	350 (0.03)	16.2 (0.02)	0.24 (0.01)	120 (0.02)
115 – 120 cm	321 (0.04)	15.8 (0.04)	0.23 (0.10)	117 (0.03)
125 – 130 cm	336 (0.04)	16.1 (0.04)	0.24 (0.03)	116 (0.03)
135 – 140 cm	367 (0.10)	18.9 (0.12)	0.25 (0.03)	111 (0.01)
145 – 150 cm	389 (0.03)	16.0 (0.17)	0.23 (0.04)	117 (0.03)

postdepositional oxidation of organic rich layers may lead to redistribution of U in the sediment (Francois *et al.* 1993; Thomson *et al.* 1990). Some higher concentrations of U observed in the upper boundary are considered to be primarily derived from the increased productivity as inferred from the distribution of Ba and organic matter content as found in a different study at the same area (Leong 2001).

The concentrations of Cd ranged from 0.11 ppm to 0.35 ppm (*Fig. 2*) and averaged to 0.23 ppm. The subsurface Cd maximum observed in the vertical profile at the depth of 35 - 65 cm suggests that the release of Cd during early diagenetic oxidation of organic matter rather than diffusion from water at the

bottom is the primary source of dissolved Cd into pore water of suboxic sediments (Gobeil *et al.* 1987; McCorkle and Klinkhammer 1991). Since Cd removal in anoxic, sulfide bearing sediments is related to its strong tendency to form insoluble sulfides in the presence of H_2S (Elderfield 1981), it is suggested that Cd enrichments in the suboxic sediments in the absence of H_2S, particularly at the depths of 65 cm and 85 cm, are likely due to CdS precipitation in the presence of trace levels of free sulfide. These small amounts of free sulfide perhaps diffuse upward from underlying anoxic sediments and are sufficient to cause precipitation of CdS.

The oxidizing surface layer containing Mn of about 250 ppm and the existence of the subsurface maxima of Mn are caused by the migration of Mn^{2+} with interstitial water and subsequent precipitation as a kind of carbonate on the surface of volcanic pumice (Tsunogai *et al.* 1979). A subsurface maximum in the Mn content within the enriched layer has also been observed in continental shelf sediments (Hartman *et al.* 1979) and is common in pelagic sediments (Wangersky 1962). Since the source of Mn^{2+} is not limited at a certain depth, both the dissolution (reduction) of Mn oxide and precipitation as carbonate may occur simultaneously as observed at depths of 20, 50, 60 and 70 cm in this study (*Fig. 2*). As the sedimentation proceeds, the redox condition of the buried sediment changes to a reducing state and the alkalinity in the interstitial water begins to increase (Hartman *et al.* 1979). The interstitial Mn in the lower part migrates downward through interstitial and forms manganese carbonate precipitate when the carbonate level in the water is sufficiently high. Although it is known that Mn migrates into the reducing environment, depositional migration for other components including Ba and U have not been established. Therefore one should be cautious when interpreting the concentration profiles of metals in a sediment core.

ACKNOWLEDGEMENTS

This research was conducted with joint funding from the Malaysian Ministry of Science under the Intensified Research for Priority Areas (IRPA) project number 51513 and Grant from the Malaysian Toray Foundation (MTSF) project number 63905. The authors wish to express their gratitude to MARU teams for their invaluable assistance and hospitality throughout the sampling period.

REFERENCES

ALLER, R. C. 1982. The effects of microbenthos on chemical properties of marine sediment and overlying water. In *Animal-Sediment Relations* ed. McCall, P. L. and Tevesz, M. S. J. p. 53 – 102. New York: Plenum Press.

BERNER, R. A. 1980. *Early Diagenesis: A Theoretical Approach.* 241 p. Princeton, New York: Princeton University Press.

BERTINE, K. K. 1980. Lead and the historical sedimentary record. In *Lead in the Marine Environment* ed. Branica, M. and Konrad, Z. p 319 – 324. Oxford: Pergamon Press.

CHESTER, R., M. NIMMO, M. ALARCON and P. CORCORAN. 1992. The chemical character of the North Western Mediterranean aerosols. In *Water Pollution Research Report* ed. Martin, J. M. and Barth, H. **28**: 495 – 504. Commission of the European Communities, Brussels.

ELDERFIELD, H. 1981. Metal-organic associations in interstitial waters of Narragansett Bay sediments. *Am. J. Sci.* **281**: 1021 - 1055.

FRANCOIS, R., S. EMERSON and S. S. HUESTED. 1993. Glacial/interglacial changes in sediment rain rate in the SW Indian sector of sunAntartic waters as recorded by ^{231}Th, ^{231}Pa, U and δ^{15} N. *Paleocanography* **8**: 611 – 629.

GOBEIL, C., S. EMERSON and S. S. HUESTED. 1987. Cadmium diagenesis in Laurentian Trough sediments. *Geochim. Cosmochim. Acta* **51**: 589 - 596.

GOLDBERG, E. D., E. GAMBLE, J. J. GRIFFIN and M. KOIDE. 1977. Pollution history of Narragansett Bay as recorded in the sediments. *Estuarine and Coastal Marine Science* **5**: 37 – 47.

HARTMAN, M., P. J. MULLER, E. SUESS and C. H. VAN DER WEIJDEN. 1979. Chemistry of late quarternary sediments and their interstial waters from the NW African continental margin. *Meteor* **24**: 1 – 67.

KAMARUZZAMAN, K. Y. 1999. Geochemistry of the marine sediments: Its paleoceanographic significance. D.Sc Theses. Hokkaido University. 143 p.

KAMARUZZAMAN, K. Y, H. SUHAIMI, E. K. TEH, H. F. LEONG, K. H. SOON and K.Y. CHONG. 2000. The determination of ^{230}Th in the sediments: Sedimentation in the mangrove forests of Pulau Sekeping, Kemaman, Terengganu. *Journal of Ultra Scientist of Physical Sciences* **13(2)**: 239 – 245.

KAMARUZZAMAN, K. Y. 1994. A study of some physico-chemical parameters in the estuarine system of Chukai-Kemaman rivers, Terengganu. M. Sc. Theses. Universiti Putra Malaysia. 222 p.

KREMLING, K. and P. STREU. 1993. Saharan dust influence trace element fluxes in deep North Atlantic subtropical waters. *Deep Sea Research* **40**: 1155 – 1168.

LEONG, H. F. 2001. Geochemical proxy for mangrove forest of Pulau Sekeping, Kemaman. Final year report, Bachelor Science (Marine Science), Faculty of Applied Science and Technology, Universiti Putra Malaysia Terengganu. 71p.

MACDONALD, R. W., D. M. MACDONALD, M. C. O'BRIEN and C. GOBEIL. 1991. Accumulation of heavy metals (pb, Zn, Cu Cd), carbon and nitrogen in sediments from strait of Georgia, B. C., Canada. *Marine Chemistry* **34**: 109 – 135.

MARTIN, J. M. and M. WHITFIELD. 1983. The significance of the river input of chemical elements to the ocean. In *Trace Metals in Sea Water* ed. Wong, C. C., Boyle, E. A., Bruland, K. W., Burton, J. D. and Goldberg, E. D. p. 265 – 296. New York: Plenum.

MARTIN, J. M., F. ELBAZ-POULICHET, C. GUIEU, M. D. LOYE-PILOT and G. HAN. 1989. River versus atmospheric input to the Western Meditereanean. In *Water Pollution Research Reports. A Summary.* ed. Martin, J. M. and Barth, H. p. 423 – 434. **13**. EROS 2000. CEC Brussels.

McCorkle, D. C. and G. P. Klinkhammer. 1991. Porewater cadmium geochemistry and the porewater cadmium: (13 C relationship *Geochim. Cosmochim. Acta* **55**: 161 - 168.

Mohd Lokman, H., S. Merehojono, N. A. M. Shazili, Y. Rosnan and A. R. M. Kamil. 1994. Neap tidal transport of particulate organic matter (POM) in a mangrove creek at Pulau Sekeping, Kemaman, Terengganu. In *Proc. of 3rd. Symposium of Applied Biology*, p. 106 – 109. 28- 29 May.

Molinari, E., S. Guerzoni and G. Rampazzo. 1993. Contribution of Saharan dust to the central Mediterranean Basin. *Geological Society of America, special paper* **284**: 303 – 312.

Nittrouer, C. A., R. W. Sternberg, R. Carpenter and J. T. Bennett. 1979. The use of ^{210}Pb geochronology as a sedimentological tool: Application to the Washington continental shelf. *Marine Geology* **31**: 297 – 316.

Nolting, R. F. and W. Helder. 1991. Lead and zinc as indicators for atmospheric and riverine particle transport to sediments in the Gulf of Lions. *Oceanologica Acta* **14(4)**: 357 – 367.

Noriki, S., K. Nakanishi, T. Fukawa, M. Uematsu, T. Uchida and S. Tsunogai. 1980. Use of a teflon vessel for the decomposition followed by the determination of chemical contituents of various marine samples. *Bull. Fac. Fish, Hokkaido Univ.* **31**: 354 - 465.

Ridway, I. M. and N. B. Price. 1987. Geochemical associations and post depositional mobility of heavy metals in coastal sediments: Loch Etive, Scotland. *Marine Chemistry* **21**: 229 – 248.

Sen Gupta, J. G. and N. B. Bertrand. 1995. Direct ICP-MS determination of trace and ultratrace elements in geological materials after decomposition in a microwave oven, Quantitation of Y, Th, U and the lanthanides. *Talanta* **42**: 1595 - 1607.

Taylor, S. R. 1964. Abundance of chemical elements in the continental crust: A new table. *Geochimica et Cosmochimica Acta* **28**: 1273 – 1285.

Thomson, J., H. E. Wallace, S. Colley and J. Toole. 1990. Authigenic uranium in Atlantic sediments of last glacial stage – a diagenetic phenomenon. *Earth Planet. Sci. Lett.* **98**: 222 – 229.

Tsunogai, S., I. Yonemaru and M. Kusakabe. 1979. Post depositional migration of Cu, Zn, Ni, Co, Pb and Ba in deep sea sediments. *Geochem. J.* **13**: 239 - 252.

Wangersky, P. J. 1962. Sedimentation in three carbonate cores. *J. Geol.* **70**: 364 – 375.

Yeats, P. A. and J. M. Bewers. 1983. Potential anthropogenic influences on trace metals distribution in the North Atlantic. *Canadian Journal of Fisheries and Aquatic Sciences* **40**: 124 – 131.

Yingst, J. Y. and D. C. Rhoads. 1980. The role of bioturbation in the enhancement of microbial turnover rates in marine sediments. In *Marine Benthic Dynamics* ed. Tenore, K. R. and Coull, B. C. p. 407 – 422. Columbia: University of South Carolina Press.

Pertanika J. Sci. & Technol. **10(2)**: 179 - 186 (2002)
ISSN: 0128-7680

Strength Estimation of Concrete in Different Environments Using UPV

Mohd Saleh Jaafar, Waleed A Thanoon, Shibli R.M Khan & DN Trikha
Faculty of Engineering, Universiti Putra Malaysia
43400 UPM Serdang, Selangor

Received: 15 November 2001

ABSTRAK

Kelusuhan konkrit dalam satu struktur disebabkan oleh beberapa mekanisme dalaman dan luaran mengurangkan kekuatan atau keutuhan struktur. Kertas ini mengemukakan keputusan ujian-ujian tanpa musnah halaju denyut ultrasonik (UPV) unutk menentukan kekuatan konkrit dalam tiga keadaan yang berbeza iaitu keadaan kering ketuhar, kering udara dan tepu kerana potensi sebenar penggunaan UPV dalam berbagai-bagai keadaan masih belum dipelopori. Kandungan lembapan keberkesanan UPV bagi meramal kekuatan konkrit, darjah kandungan lembapan dalam konkrit perlu dipertimbangkan. Laluan halaju dalam beberapa keadaan juga perlu dikaji. Dalam kajian ini terdapat empat gred konkrit yang didedahkan kepada tiga keadaan yang berbeza. Banyak siri ujian makmal yang telah dilakukan untuk mendapatkan hubung kait antara keputusan ujian UPV dan kekuatan sebenar konkrit. Sebanyak 108 kiub telah disediakan. Simen yang digunakan adalah simen Portland biasa dan agregat kasar adalah batu granit dengan saiz maksimum 19mm seperti mana yang digunakan dalam kebanyakan binaan struktur konkrit. Kaedah reka bentuk campuran DOE telah digunakan untuk menghasilkan empat gred konkrit yang biasa digunakan dalam amalan binaan konkrit. Keputusan uji kaji menunjukkan kehadiran lembapan dalam konkrit mengubah nilai-nilai UPV dengan ketara. Ujian-ujian UPV melalui ukuran secara langsung menunjukkan ramalan yang lebih baik berbanding ukuran secara tidak langsung. Beberapa persamaan telah dicadangkan untuk meramal kekuatan konkrit dalam keadaan kering ketuhar dan kering udara.

ABSTRACT

Deterioration of concrete in a structure is a result of several internal and external degradation mechanisms which decrease the strength or the integrity of the structure. This paper presents results of use of non-destructive ultrasonic pulse velocity tests (UPV) to determine the strength of concrete in three different environments, namely oven-dry, air-dry and saturated conditions, as the full potential of UPV in different environments is still not fully explored. Moisture is known to have a significant effect on ultrasonic pulse velocity. In order to improve the efficiency of UPV in estimating the concrete strength, the degree of moisture present in the concrete i.e. the physical condition of the concrete is to be considered. Pulse velocity path in the different physical conditions of concrete also has to be examined. In the present investigations, four different grades of concrete in three different environments were considered. Extensive series of tests were carried out in the laboratory to obtain a correlation of the UPV test results with the actual compressive strength of concrete. A total of 108 cubes were cast. The cement used was the ordinary

Portland cement and the coarse aggregate consisted of granite with the maximum aggregate size of 19mm as is generally used in conventional R.C structures. The DOE-method of mix-design was used to design four different grades of concrete in order to simulate concrete strengths found in practice. Test results indicated that the presence of moisture in concrete changes the UPV values significantly. The UPV tests through the direct transmission measurements display better estimates compared to the indirect measurements. Exponential expressions have been proposed for the strength estimation of concrete under oven dry and air dry conditions.

Keywords: Concrete, compressive strength, ultrasonic pulse velocity (UPV)

INTRODUCTION

The strength of in-situ concrete may be measured using semi-destructive and non-destructive test techniques. Ultrasonic Pulse Velocity (UPV) is one of the most frequently used NDT techniques to measure the physical properties of concrete. The reliability of UPV technique to estimate the compressive strength of concrete has come about as a result of enormous data gained through extensive testing. UPV test technique has been used for more than two decades for concrete quality evaluation and concrete compressive strength (f_{cu}) determination. UPV test provides indirect data that can be empirically related to standard cube compressive strength. Factors influencing the test results and their interpretation have been widely reported.

According to Castro (1985) age, mix proportions, water/cement ratio, cement type and aggregate type have an influence on the pulse velocity test results and their relationship to f_{cu}. Using different concrete mixes, but with the same ingredients Castro (1987) showed similar relationship for the cylindrical specimens. In their research, the effect of UPV on the concrete constituent material was established. But the concrete physical condition was ignored and the mode of test was not investigated. Ferreira *et al.* (1999) established the UPV and other NDT correlations with compressive strength of concrete. They considered different mix proportions of concrete with different compressive strength of coarse aggregate in their investigations. The concrete physical conditions were, however, not reported.

This paper describes the results of an experimental program on the use of UPV for assessing concrete strength. The concrete specimens have varying strengths of 10 to 40MPa and have been subjected to oven dry, air dry and saturated conditions. Direct and indirect modes of measurements have been used on all the cubes as shown in *Fig. 1.* Table 1 gives the number of the cube samples of size 150×150×150mm used in the investigations. A total of 108 cubes have been cast for testing. The cement used in this experiment was ordinary Portland cement, which is mostly used in the R.C structure. The aggregate used in this experiment was broken granite stone with compressive strength of 95 to 120MPa.

TABLE 1
Schedule of test specimen 150×150×150 mm test cubes

Concrete Grade	Physical Condition	Number of Cubes at the Age of Testing			Sub-total
		7 days	14 days	28 days	
	Oven dry	3	3	3	9
Grade 10	Air dry	3	3	3	9
	Saturated	3	3	3	9
	Oven dry	3	3	3	9
Grade 20	Air dry	3	3	3	9
	Saturated	3	3	3	9
	Oven dry	3	3	3	9
Grade 30	Air dry	3	3	3	9
	Saturated	3	3	3	9
	Oven dry	3	3	3	9
Grade 40	Air dry	3	3	3	9
	Saturated	3	3	3	9

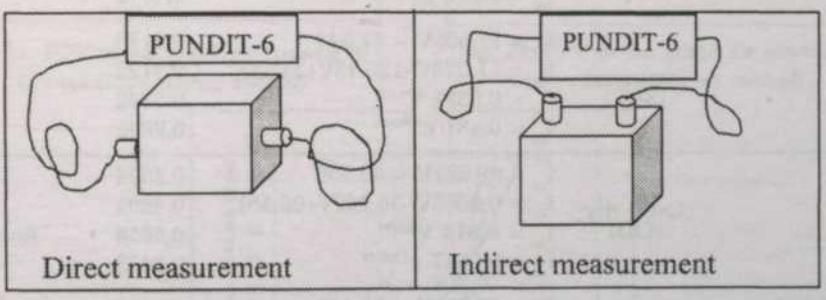

Fig. 1: UPV mode of tests on specimen

TEST RESULTS AND DISCUSSION

The UPV measurements as obtained during the investigations for different concrete grades and different physical conditions using direct and indirect methods of measurements are not reported but available Shibli (2001). Similarly, the corresponding actual cube strengths are also not reported. Both exponential and polynomial expressions have been tried to co-relate the UPV values and the cube strength to best fit through regression analysis. The best-fit expression is obviously the one which has correlation coefficient value nearly equal to 1.0. It was found that the correlation between[1] UPV values and the[2] concrete strength for any measurement made and[3] the physical conditions did not improve when such correlations were developed separately for different grades of concrete. It was then thought advisable to determine expressions, which would be identical for all grades of concrete as considered in the present investigation. Separate

expressions were, however, determined for different measurement modes and physical conditions.

Table 2 gives the polynomial/exponential expressions for each measurement mode and physical condition valid for concrete strengths ranging from 10MPa to 40MPa. The correlation coefficient values are also given in each case to select the best-fit expression, which is highlighted in bold.

TABLE 2
Co-relation expressions for direct and indirect transmission measurement

Mode of Test	Physical conditions	Regression Equations	Correlation coefficient	Remarks
Direct Transmission	Oven dry (OD)	$f_{cu} = 21.04V - 90.63$	0.8403	
		$f_{cu} = 3.441V^2-16.073V+8.874$	**0.8451**	Best-fit
		$f_{cu} = 0.0019\ V^{5.5257}$	0.8125	
		$f_{cu} = 0.0831\ e^{1.0230V}$	0.8035	
	Air dry (AD)	$f_{cu} = 14.378V - 61.594$	0.5238	
		$f_{cu} = 12.124V^2-126.18V+342.79$	**0.5901**	Best-fit
		$f_{cu} = 0.0135\ V^{4.1414}$	0.4617	
		$f_{cu} = 0.292\ e^{0.7222V}$	0.4672	
	Saturated (SAT)	$f_{cu} = 11.395V - 47.844$	0.3176	
		$f_{cu} = 11.023V^2-120.13V+341.38$	0.3722	
		$f_{cu} = 0.0321\ V^{3.526}$	0.2842	
		$f_{cu} = 0.481\ e^{0.5995V}$	0.2895	
Indirect Transmission	Oven dry (OD)	$f_{cu} = 29.781V - 86.705$	0.4894	
		$f_{cu} = 0.8983V^2-36.262V+98.351$	0.4895	
		$f_{cu} = 0.013\ V^{5.6747}$	**0.5558**	Best-fit
		$f_{cu} = 0.0647\ e^{1.5702V}$	0.5493	
	Air dry (AD)	$f_{cu} = 26.758V - 79.409$	0.4516	
		$f_{cu} = 0.5359V^2-22.694V-71.74$	**0.4516**	Best-fit
		$f_{cu} = 0.0187\ V^{5.2218}$	0.4267	
		$f_{cu} = 0.1069\ e^{1.3731V}$	0.4205	
	Saturated (SAT)	$f_{cu} = 32.582V - 106.6$	0.603	
		$f_{cu} = 21.447V^2-134.78V+218.51$	**0.6275**	Best-fit
		$f_{cu} = 0.0019\ V^{6.7338}$	0.5619	
		$f_{cu} = 0.020\ e^{1.7365V}$	0.5641	

Figs. 2a, 2b and *2c* show the best-fit curve on the test values for the direct mode of transmission with regard to three physical conditions. From the figures and the respective regression equations, it is observed that the UPV test techniques using direct measurement cannot estimate the concrete strength to any acceptable level of accuracy in a saturated environment. The method, however, does estimate the concrete strength sufficiently accurately when concrete is subjected to the oven dry or air-dry environment. It is also observed

that the UPV values are affected by the presence of moisture in the structure and this must be considered in estimating the compressive strength of concrete from the UPV values.

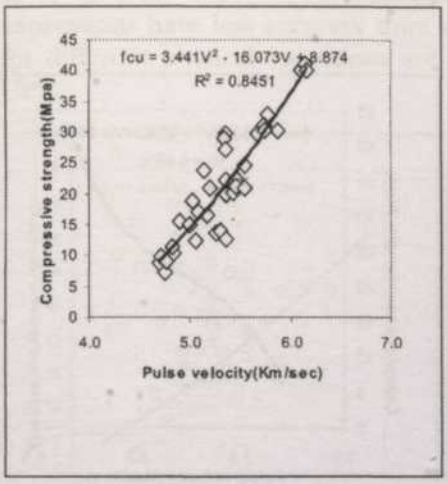

Fig. 2a: UPV vs fcu graph for concrete at OD condition (Direct method)

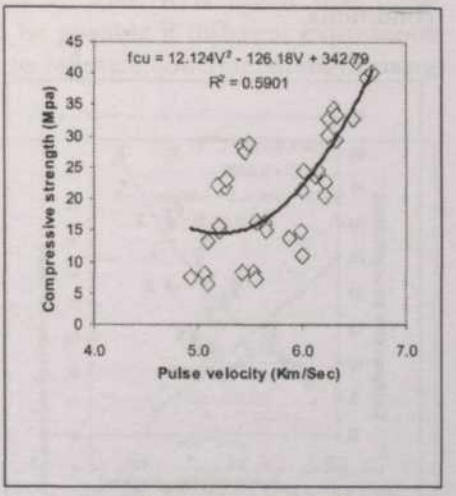

Fig. 2b: UPV vs fcu graph for concrete at AD condition (Direct method)

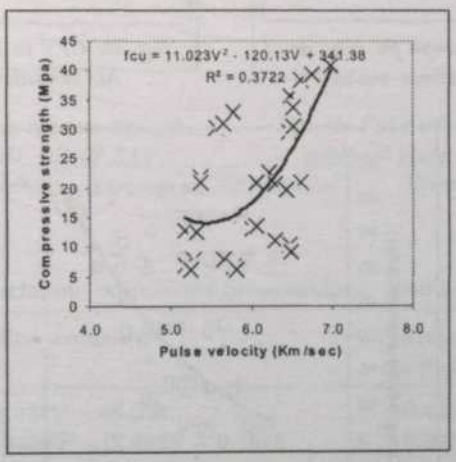

Fig. 2c: UPV vs fcu graph for concrete at SAT condition (Direct method)

Figs. 3a, 3b and *3c* similarly show graphically the best-fit curves for indirect mode of transmission with regard to three physical conditions with the UPV test values. From the figures and respective regression equations, it is observed that the co-relation is not very satisfactory between the best-fit values and the test values, as indicated by correlation coefficient values for concrete in dry conditions.

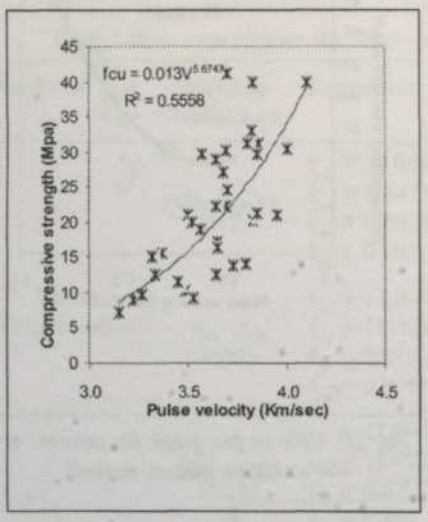

Fig. 3a: UPV vs fcu graph for concrete at OD condition (Indirect method)

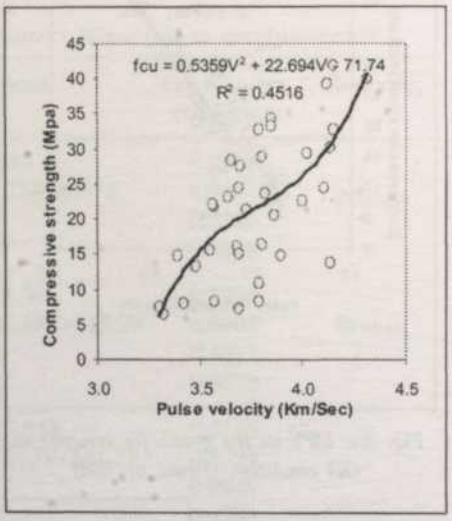

Fig. 3b: UPV vs fcu graph for concrete at AD condition (Indirect method)

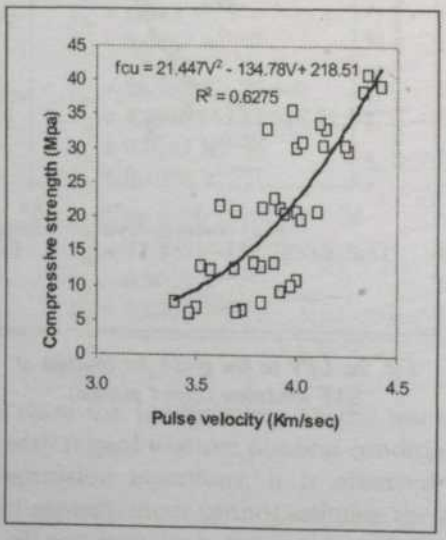

Fig. 3c: UPV vs fcu graph for concrete at SAT condition (Indirect method)

As indicated earlier, attempts were made to recommend as few expressions as possible that are valid in different conditions. One such attempt is shown in *Figs. 4a* and *4b*, which display the best-fit curves to the UPV values obtained for all three different physical conditions and concrete grades. Various regression analysis equations to fit the aggregate data are tabulated in Table 3, where the most accurate expressions are highlighted in bold. It is noted that these expressions have less accuracy than would be possible if different expressions for different physical conditions are used to estimate concrete strength using UPV.

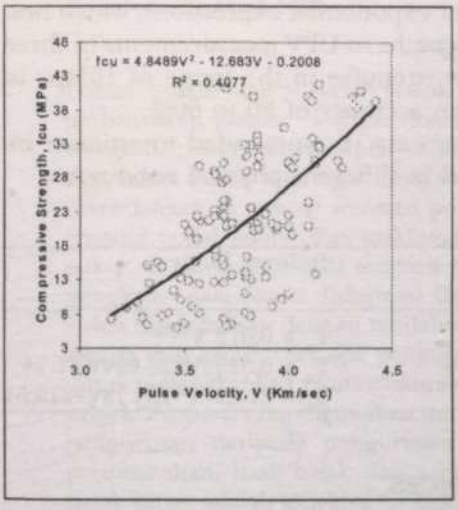

Fig. 4a: Pulse velocity vs concrete strength combined graph of OD, AD & SAT (Indirect method)

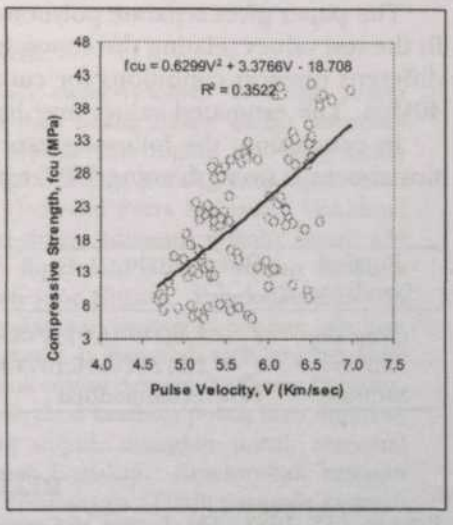

Fig. 4b: Pulse velocity vs concrete strength combined graph of OD, AD & SAT (Direct method)

TABLE 3
Co-relation expressions for combined conditions

Mode of Tests	Regression equation	Correlation coefficient	Remarks
Indirect transmission	$f_{cu} = 24.034V - 69.37$	0.4058	
	$f_{cu} = 4.8489V^2 - 12.683V - 0.2008$	**0.4077**	Better
	$f_{cu} = 0.0398\ V^{4.6448}$	0.3790	
	$f_{cu} = 0.1817e^{1.2293V}$	0.3764	
Direct transmission	$f_{cu} = 10.638V - 39.44$	0.3518	
	$f_{cu} = 0.6299V^2 + 3.3766V - 18.708$	**0.3522**	Better
	$f_{cu} = 0.107\ V^{2.9737}$	0.2977	
	$f_{cu} = 0.9787\ e^{0.5173V}$	0.2950	

CONCLUSIONS

It may be concluded that it is necessary to use different expressions for predicting concrete strength using UPV method for different physical conditions. It is also concluded that presence of moisture in concrete may change the UPV values significantly and as such expressions developed from co-relation tests on saturated concrete may not be suitable. Similarly, the UPV values obtained through direct transmission tests are usually 1.50 times higher than those through indirect transmission test values. Separated expressions are needed for the two modes of measurements.

The paper gives separate polynomial or exponential expressions, which best fit the test values relating the concrete strengths to UPV measurements in three different physical conditions for concrete strengths in the range of 10Mpa to 40Mpa. The estimated values may have an accuracy of 50 to 60%.

In conclusion, the following expressions are recommended to estimate in-situ concrete strength using UPV method in different physical conditions:

Physical Condition	Direct Mode	Indirect Mode
Oven dry	$f_{cu} = 3.441V^2-16.073V+8.874$	$f_{cu} = 0.013\ V^{5.6747}$
Air dry	$f_{cu} = 12.124V^2-126.18V+342.79$	$f_{cu} = 0.5359V^2-22.694V-71.74$
Saturated	Not recommended	$f_{cu} = 21.447V^2-134.78V+218.51$

REFERENCES

BUNGEY, J.H. 1982. *The Testing of Concrete in Structure.* p.35. New York, USA: Surrey University Press.

CASTRO, P.F. 1985. An expandable sleeve test for assessing concrete strength. PhD thesis. University College London, England.

CASTRO, P.F. 1987. Concrete Strength – Comparison Between Non-destructive Tests. In *Proc. of Fourth International Conference on Durability of Building Materials & Components,* p. 885-890. Singapore.

FERREIRA, ALMIR P. 1999. Application of NDT to Concrete Strength Estimation. In *Proc. of International Symposium on NDT Contribution to the Infrastructure Safety Systems.* Vol.5. RS, Brazil.

KONSTANTIN KOVLER and ISAAK SCHAMBAN. 1999. Building Research Institute. Faculty of Engineering, Technion – Israel Institute of Technology, Haifa, Israel.

SHIBLI R.M KHAN. 2001. Effectiveness of nondestructive test technique to assess the quality of concrete. M.S Thesis to be submitted. Universiti Putra Malaysia, Serdang, Selangor.

THOMSETT, H.N. 1980. Ultrasonic pulse velocity measurement in assessment of concrete quality. *Magazine of Concrete Research* **32 (110)** March: 7-16.

Pertanika J. Sci. & Technol. 10(2): 187 - 199 (2002)
ISSN: 0128-7680

A Simple GIS Data for Tree Management in Universiti Putra Malaysia's Arboretum

Kamaruzaman Jusoff & Iwan Setiawan
Forest Production Department
Faculty of Forestry
Universiti Putra Malaysia, 43400 UPM Serdang
Email: kamaruz@forr.upm.edu.my

Received: 20 April 1999

ABSTRAK

Lokasi pokok dan ciri-ciri pokok adalah elemen-elemen berharga sistem perbandaran pokok. Dengan mencipta data pokok dalam sistem informasi Geografi, pengguna mempunyai akses kepada data digital lain yang boleh digunakan dalam hubungan dengan pengkalan data pokok. Satu kajian telah dikendalikan di tempat semaian pokok Universiti Putra Malaysia. Maklumat tentang posisi pokok dan maklumat ciri-cirinya (dimensi pokok) untuk 434 pokok di kawasan tempat semaian boleh diperolehi dengan mudah daripada pengkalan data Sistem Informasi Geografi yang ringkas. Pangkalan data GIS boleh dikendalikan dengan mudahnya bersama parameter-parameter lain juga spesies dan lokasi. Sebagai pengurusan rutin, ia hanyalah satu langkah kecil untuk melengkapkan ukuran-ukuran pokok piawai dengan data yang berguna, subjektif seperti yang digunakan untuk merekod keadaan pokok atau tindakan pengurusan daripada pengurusan yang wujud, mungkin untuk meramal pertumbuhan, hasil balak dan juga impak landskap. Keseluruhan kawasan tapak kajian adalah kira-kira 5.7 hektar. Pembahagian famili daripada kawasan mengandungi 12 famili, 19 genus dan 15 spesies. *Hopea odorata* adalah jumlah spesies pokok yang paling tinggi dengan pembahagian diameter daripada 4.2cm hingga 65.7 cm. Kira-kira 75 pokok di dalam kawasan tersebut didapati mati disebabkan oleh sistem pengairan yang tidak sempurna. Kerja melabel dan mengecat pokok mesti dilakukan untuk mengawasi pertumbuhannya, mortaliti dan pengukuran kedudukan pokok masa hadapan.

ABSTRACT

Tree location and tree attributes are valuable elements of municipal tree management systems. By creating the tree data in Geographic Information System, users have access to other digital data that can be used in conjunction with tree database. A study was conducted at the Universiti Putra Malaysia's arboretum with an objective to establish a computerized information system for Universiti Putra Malaysia's arboretum. Information about tree position and their attributes information (tree dimension) for 434 trees in arboretum area can be easily retrieved from a simple Geographic Information System database. The GIS database can cope just as easily with other parameters besides species and location. As for routine management, it is only a small step to complement standard tree measurements, with data of a useful, subjective kind, such as that used to record tree condition or management action from existing measurement, perhaps to predict growth, timber yields and even landscape impact. The total area of study site is about 5.7 ha. Family distribution from the area consisted of 12 families, 19 genus and 15 species. *Hopea odorata* was the highest number

of the tree species present with diameter distribution ranging from 4.2 cm to 65.7 cm. About 75 trees inside the area were found dead due to water logging and improper drainage. Labeling or painting of trees should be done in order to monitor their growth, mortality and future tree stand measurement.

Keywords: Geographic Information System, database, tree management, arboretum

INTRODUCTION

Trees have served as sources of untold wealth from primitive times to today. They contribute to worldwide comfort and convenience by providing many usable materials for construction and industrial purposes, attractive woods for furniture, potent medicines for healing, fuels for heating and valuable sustenance for all types of wildlife.

Trees provide shade from intense sun, shelter from the wind, act as a barrier against sound, contribute importantly to erosion control and to dust removal from the air. Trees, when they are properly selected, placed and maintained, can greatly improve the microclimate of urban areas. Therefore, trees are an important part of human lives-around homes, schools, shopping centers, places of work, along streets and highways, in the city centres, parks and other landscaped areas such as arboretum (Minkler 1980; Harris 1983; James 1990 and Boyce 1995).

Tree location and tree attributes are valuable elements of arboretum tree management system. By creating the tree data in GIS, users have access to other digital data that can be used in conjunction with tree database. These elements, if used together, will help in the cost effectiveness of tree management (Goodwin 1996). With a GIS database, recording for each tree dimension in the collection will be maintained in an electronic database, and detailed planting locations will be plotted on a digital map. Therefore, the establishment of a simple geographic information system database that have the capability to expand, rapidly update and retrieve information (both graphic and non graphic information) will be a useful tool for the proper planning and management of the arboretum.

The general objective of this study is therefore, to establish a computerized information system for UPM's arboretum. The specific objectives of this study are two-fold, namely: (i) To establish an initial GIS database and to produce digital map for the arboretum in UPM and (ii) To develop an inventory of tree species and their growth, in term of diameter and height.

MATERIALS AND METHODS

Site Description

The study was conducted at the Universiti Putra Malaysia's arboretum. The total area of study site is about 5.7 ha (*Fig. 1*). Based on a tree inventory

prepared in December 1996, the number of trees inside the area is about 1107 trees, 15 families, and 28 species with Acacia mangium constituting the highest number. There are two types of tree spacing available in this study i.e. 6 x 12 m and 3 x 2 m. Due to the time constraint in this study, only a total of 434 trees (12 families, 19 genus and 15 species) were enumerated and mapped in the area excluding Acacia mangium planted with a spacing of 3 m x 2 m. The geographical position of the UPM arboretum is located at latitudes 3° 00' 11.28" N - 3° 00' 27.43" N and longitude :101° 43' 22.11" E - 101° 43' 30.73" E.

METHOD

Hardware and Software

The hardware used for this study is a microcomputer and its accessories such as digitizer, printer and plotter. To determine the position of the area studied, a Global Position System (GPS) Geo explorer II was used with 30 m accuracy. The GIS software selected for use in this study was ARC/INFO version 3.4.2 and ARCVIEW version 3.1, produced by Environmental System Research Institute (ESRI), Redlands, California. ARC/INFO and Arc View were used to translate both the location and properties of spatial features into digital form. Data conversion is the process of creating digital map files from other sources.

Data Collection and Mapping

Primary data that were collected from the field included measurement of diameter at breast height and tree position and spacing. Secondary data comprised UPM land-use map which was obtained from UPM Development Unit and the inventory data from the Faculty of Forestry UPM collected in December 1996.

A map of UPM's arboretum at a scale of 1:1000 was developed using compass and meter tape.

Procedure

Database Structure and Design

Database structure has been performed in such a way that information can only be derived as required. The database structure consists of digital graphic (arboretum digitized map) and non graphic data that describe map features, tree attributes such as diameter, height and species. Graphic data use four types of graphic elements to depict map features and annotation (i.e. points, lines, area, and symbols). They include digital descriptions of map features, logical geographic relationships among features. Non graphic data are representations of the characteristics, qualities or relationships of map features and geographic locations. They are stored in conventional alphanumeric formats. In this study non graphic data was stored in Excel format. The graphic and non graphic data formats are linked with GIS technology.

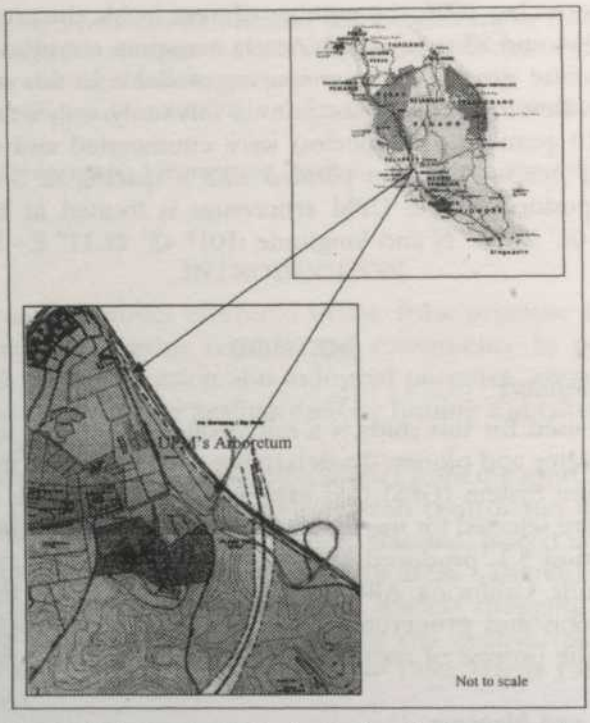

Fig. 1: A map of Peninsular Malaysia showing the location of the study site

The data was designed by separating tree family, genus and species in separate columns in Excel format. To ease data retrieval, the genus and species names are put in different columns to enable choosing genus name only or species name of the required trees. The digitized map (graphic data) which describes tree location was linked with the attribute data by transferring all the attribute data from Excel format to dbase format in Arc View software.

Digitizing

The position of trees and the boundary of the arboretum area were digitized manually using four tics. The position of the trees was plotted in points and stored in a separate file to make further editing easier. The boundary of the study was delineated using a polygon and stored in different layers. To display the information about each family, every family has its own layer. The segment and point as a result of digitizing were then overlaid to create a digital map with the complete information about a particular tree. Editing the polygon and build topology were conducted in ARC/INFO. ARCVIEW was used for overlaying and processing the tabular data and for map display.

Attribute data

In the beginning, tree data were inputted in ARC/INFO but for data processing like querying and sorting data ARCVIEW was used. The tabular data consists

of the number of trees, diameter of trees (Years of measurement 1996 and 1999), height (measured in 1996), family, genus and species. The tabular data were incorporated with the spatial data resulting from digitizing in ARCVIEW.

RESULTS AND DISCUSSION

Pattern of Tree Distribution (Family, Genus and Species)

Family distribution from the area consists of 12 families (*Fig. 2* and Table 1), 19 genus and 15 species. To retrieve the information about the distribution of the family of Dipterocarpaceae by using the query that was already facilitated in ARCVIEW, the computer selected the tree distribution of this family (*Fig. 2*) and by clicking on the information on the tree position, the information and description about that tree such as family name, genus, species and local name appear in the tabular format (Table 2) as well as the coordinate of trees inside the plot, diameter and height.

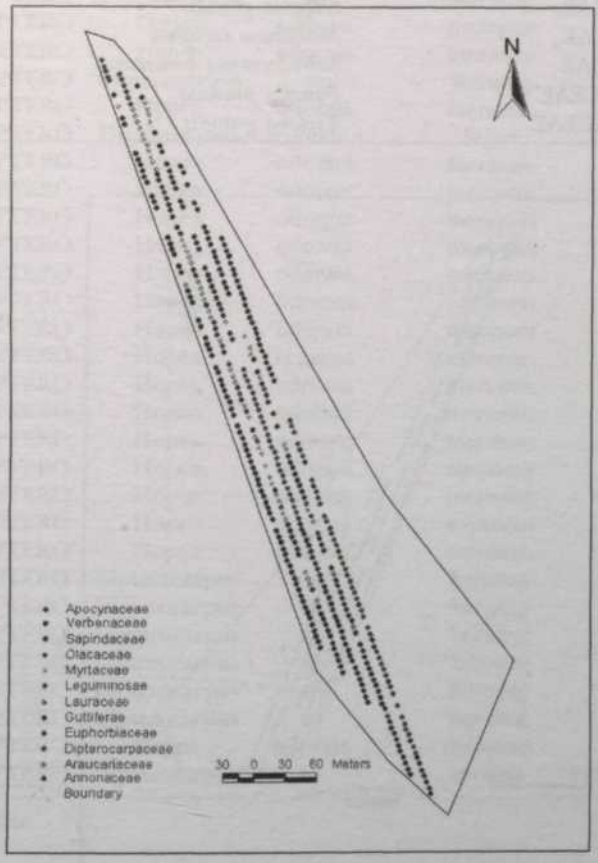

Fig. 2: Family distribution inside the arboretum area

TABLE 1
List of family distribution in the arboretum area

No	Family	Species
1	ANNONACEAE	*Polyathia longifolia*
2	APOCYNACEA	*Dyera costulata*
3	AURACARIACEA	*Agathis borneensis*
4	DIPTEROCARPACEAE	*Dipterocarpus sp*
5	DIPTEROCARPACEAE	*Dryobalanops aromatica*
6	DIPTEROCARPACEAE	*Hopea odorata*
7	DIPTEROCARPACEAE	*Shorea acuminata*
8	EUPHORBIACEAE	*Pimelodendron griffithianum*
9	GUTTIFERAE	*Mesua ferrea*
10	LAURACEAE	*Cinnamomum iners*
11	LEGUMINOSAE	*Acacia mangium*
12	LEGUMINOSAE	*Adenanthera pavonina*
13	LEGUMINOSAE	*Delonix regia*
14	LEGUMINOSAE	*Pongamia pinnata*
15	MYRTACEAE	*Eugenia grandis*
16	MYRTACEAE	*Malaleuca cajuputi*
17	OLACACEAE	*Scorodocarpus borneensis*
18	SAPINDACEAE	*Pometia pinnata*
19	VERBENACEAE	*Tectona grandis*

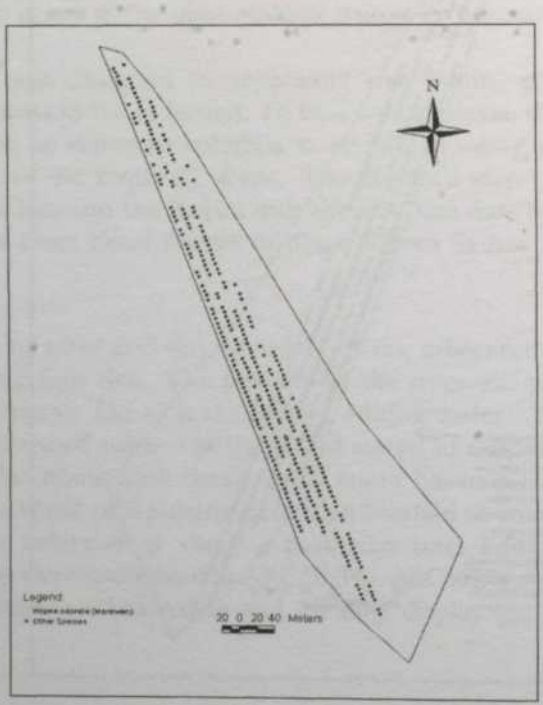

Fig. 3: Distribution of Hopea odorata (Merawan) inside the arboretum area

TABLE 2
Attribute information about Dipterocarpaceae family

Tree no.	Family	Genus	Species	Local Name	D99 (cm)	D96 (cm)
68	DIPTERO	Hopea	odorata	merawan	23.9	21.5
69	DIPTERO	Hopea	odorata	merawan	23	22
71	DIPTERO	Hopea	odorata	merawan	24.4	21.6
77	DIPTERO	Hopea	odorata	merawan	10.9	9.2
83	DIPTERO	Shorea	acuminata	meranti tembaga	18	15.2
101	DIPTERO	Hopea	odorata	merawan	31.6	30
102	DIPTERO	Hopea	odorata	merawan	32	31.1
105	DIPTERO	Hopea	odorata	merawan	25.9	24.5
106	DIPTERO	Dipterocarpus	sp	Keruing	13.4	12.7
107	DIPTERO	Dipterocarpus	sp	Keruing	26.9	26.2
108	DIPTERO	Hopea	odorata	merawan	22.3	20.3
109	DIPTERO	Hopea	odorata	merawan	25.3	23.2
110	DIPTERO	Hopea	odorata	merawan	25.7	24.8
116	DIPTERO	Hopea	odorata	merawan	27.5	25.3
117	DIPTERO	Hopea	odorata	merawan	25.5	24.8
122	DIPTERO	Dipterocarpus	sp	Keruing	12.3	NA
126	DIPTERO	Hopea	odorata	merawan	14.3	NA
127	DIPTERO	Hopea	odorata	merawan	26.5	NA
130	DIPTERO	Dipterocarpus	sp	Keruing	16.7	NA
137	DIPTERO	Hopea	odorata	merawan	32.1	NA
149	DIPTERO	Dryobalanops	aromatica	kapur	15.4	NA
155	DIPTERO	Hopea	odorata	merawan	18.6	NA
164	DIPTERO	Hopea	odorata	merawan	29.4	NA
173	DIPTERO	Hopea	odorata	merawan	37.8	NA
174	DIPTERO	Hopea	odorata	merawan	27	NA
175	DIPTERO	Hopea	odorata	merawan	30.5	NA
176	DIPTERO	Hopea	odorata	merawan	29.9	NA
177	DIPTERO	Hopea	odorata	merawan	21.5	NA
178	DIPTERO	Hopea	odorata	merawan	24.2	NA
179	DIPTERO	Hopea	odorata	merawan	33.2	NA
180	DIPTERO	Hopea	odorata	merawan	40.8	NA
181	DIPTERO	Hopea	odorata	merawan	33.1	NA
182	DIPTERO	Hopea	odorata	merawan	28.7	NA
183	DIPTERO	Hopea	odorata	merawan	28.7	NA
184	DIPTERO	Hopea	odorata	merawan	34.1	NA
185	DIPTERO	Hopea	odarata	merawan	37.2	NA
186	DIPTERO	Dipterocarpus	sp	keruing	21.4	NA
187	DIPTERO	Dipterocarpus	sp	keruing	21	NA
189	DIPTERO	Dipterocarpus	sp	keruing	19.9	NA
190	DIPTERO	Dipterocarpus	sp	keruing	19.6	NA
191	DIPTERO	Dipterocarpus	sp	keruing	20.9	NA
192	DIPTERO	Dipterocarpus	sp	keruing	25.1	NA
193	DIPTERO	Hopea	odorata	merawan	30.7	NA
194	DIPTERO	Dipterocarpus	sp	keruing	17.6	NA

NA = not available

TABLE 3
Attribute information about Hopea odorata (Merawan)

Tree No.	Family	Genus	Species	Local Name	D99 (cm)	D96 (cm)	Ht96 (m)
68	DIPTEROCARPACEAE	Hopea	odorata	merawan	23.9	21.5	7
69	DIPTEROCARPACEAE	Hopea	odorata	merawan	23	22	7
71	DIPTEROCARPACEAE	Hopea	odorata	merawan	24.4	21.6	7
77	DIPTEROCARPACEAE	Hopea	odorata	merawan	10.9	9.2	4
101	DIPTEROCARPACEAE	Hopea	odorata	merawan	31.6	30	18
102	DIPTEROCARPACEAE	Hopea	odorata	merawan	32	31.1	18
105	DIPTEROCARPACEAE	Hopea	odorata	merawan	25.9	24.5	19
108	DIPTEROCARPACEAE	Hopea	odorata	merawan	22.3	20.3	6
109	DIPTEROCARPACEAE	Hopea	odorata	merawan	25.3	23.2	8
110	DIPTEROCARPACEAE	Hopea	odorata	merawan	25.7	24.8	10
116	DIPTEROCARPACEAE	Hopea	odorata	merawan	27.5	25.3	11
117	DIPTEROCARPACEAE	Hopea	odorata	merawan	25.5	24.8	10
126	DIPTEROCARPACEAE	Hopea	odorata	merawan	14.3	NA	NA
127	DIPTEROCARPACEAE	Hopea	odorata	merawan	26.5	NA	NA
137	DIPTEROCARPACEAE	Hopea	odorata	merawan	32.1	NA	NA
155	DIPTEROCARPACEAE	Hopea	odorata	merawan	18.6	NA	NA
164	DIPTEROCARPACEAE	Hopea	odorata	merawan	29.4	NA	NA
173	DIPTEROCARPACEAE	Hopea	odorata	merawan	37.8	NA	NA
174	DIPTEROCARPACEAE	Hopea	odorata	merawan	27	NA	NA
175	DIPTEROCARPACEAE	Hopea	odorata	merawan	30.5	NA	NA
176	DIPTEROCARPACEAE	Hopea	odorata	merawan	29.9	NA	NA
177	DIPTEROCARPACEAE	Hopea	odorata	merawan	21.5	NA	NA
178	DIPTEROCARPACEAE	Hopea	odorata	merawan	24.2	NA	NA
179	DIPTEROCARPACEAE	Hopea	odorata	merawan	33.2	NA	NA
180	DIPTEROCARPACEAE	Hopea	odorata	merawan	40.8	NA	NA
181	DIPTEROCARPACEAE	Hopea	odorata	merawan	33.1	NA	NA
182	DIPTEROCARPACEAE	Hopea	odorata	merawan	28.7	NA	NA
183	DIPTEROCARPACEAE	Hopea	odorata	merawan	28.7	NA	NA
184	DIPTEROCARPACEAE	Hopea	odorata	merawan	34.1	NA	NA
185	DIPTEROCARPACEAE	Hopea	odorata	merawan	37.2	NA	NA
193	DIPTEROCARPACEAE	Hopea	odorata	merawan	30.7	NA	NA
200	DIPTEROCARPACEAE	Hopea	odorata	merawan	31.9	NA	NA
210	DIPTEROCARPACEAE	Hopea	odorata	merawan	22.5	NA	NA
211	DIPTEROCARPACEAE	Hopea	odorata	merawan	24	NA	NA
255	DIPTEROCARPACEAE	Hopea	odorata	merawan	34.8	NA	NA
256	DIPTEROCARPACEAE	Hopea	odorata	merawan	22	NA	NA
267	DIPTEROCARPACEAE	Hopea	odorata	merawan	16.1	NA	NA
268	DIPTEROCARPACEAE	Hopea	odorata	merawan	13	NA	NA
269	DIPTEROCARPACEAE	Hopea	odorata	merawan	40.6	NA	NA
270	DIPTEROCARPACEAE	Hopea	odorata	merawan	42.3	NA	NA
271	DIPTEROCARPACEAE	Hopea	odorata	merawan	42.1	NA	NA
272	DIPTEROCARPACEAE	Hopea	odorata	merawan	49.9	NA	NA

NA = not available

By using the same procedure, the selected genus, species or local name of the tree that we require can easily be retrieved and displayed on the screen (Table 2). To ease data retrieval, the genus and species names are put in different columns to enable the users to choose genus names only or the species names of the required trees.

In this study, *Hopea odorata* constitutes the highest number (109 trees) of available species followed by Dyera costulata (69 trees) and Dipterocarpus sp (68 trees) as shown in Table 4.

The graphic data which represent map images in this study was performed in point elements i.e. the position of the tree. A point is a zero-dimensional object that specifies a geometric location through a set of coordinates (The American Cartographer, Jan 1988 cited by Antenucci *et al.* 1994). Graphic images can be stored as vectors or raster of uniform grid cells or pixels. Vector data are represented by horizontal (i.e., x and y) coordinates of point and line locations or as rules for computing the coordinates and connecting the points as lines or areas.

The attribute information which contains the information about the tree is called textual data. This data relates to geographic locations or graphic elements in this case related to position of the trees. The attribute data was managed separately from the graphic data because of their different characteristics or their maintenance and use in other systems. Although this attribute data was stored in the table, it was integrated or related to graphic data through common identifiers or other mechanisms, which can still be opened to be expanded with additional information, if required.

TABLE 4
Distribution of tree number in each species in arboretum area

No	Species	Local name	Number of Trees
1	Agathis borneensis	Damar	1
2	Delonix regia	Semarak Api	1
3	Pimelodendron griffithianum	Perah ikan	1
4	Shorea acuminata	Meranti tembaga	1
5	Scorodocarpus borneensis	Kulim	1
6	Polyathia longifolia	Mempisang	1
7	Cinnamomum iners	Kayu manis	2
8	Dryobalanops aromatica	Kapur	2
9	Mesua ferrea	Panaga Lilin	7
10	Pometia pinnata	Kasai	10
11	Tectona grandis	Jati	11
12	Eugenia grandis	Kelat	15
13	Pongamia pinnata	Mempari	16
14	Adenanthera pavonina	Saga	31
15	Malaleuca cajuputi	Gelam	41
16	Acacia mangium	Mangium	45
17	Dipterocarpus sp	Keruing	68
18	Dyera costulata	Jelutong	69
19	Hopea odorata	Merawan	109

Distribution of Tree Diameter and Tree Height

The same procedure was used to obtain information on the distribution of tree diameter and tree height. Using the query icon, tree growth information was easily retrieved from database. Inventory data obtained in December 1996 showed that the minimum and maximum diameters were 3 cm and 52.7 cm, respectively. In this study, the diameter ranged from 4.2 cm (minimum) to 65.7 cm (maximum). The selected diameters (*Figs. 4, 5* and Table 5) were chosen to describe how GIS database provides an easy way to retrieve huge data including geographic data (in this case the tree position).

Based on previous inventory data completed in December 1996, the distribution of tree height ranges from 2 m to 20 m can be easily retrieved using the query icon that was developed in the ARCVIEW.

GIS database can also provide a combined information on species; diameter and height distribution in one occasion. For example, if the user needs information on *Hopea odorata* distribution with diameter > 40.8 cm, the computer displays that information (*Fig. 6*) and at the same time provides attribute data from each tree (Table 6) using the combination command (logical command).

Fig. 6 shows empty spaces among the tree spacing (6x 12 m) due to dead trees which still exist in the previous inventory. About 75 dead trees in the northern part of the arboretum were caused by water logging. It is necessary to have a proper drainage system in this area or to rehabilitate the affected area with suitable tree species that can adapt in this "wetland" space.

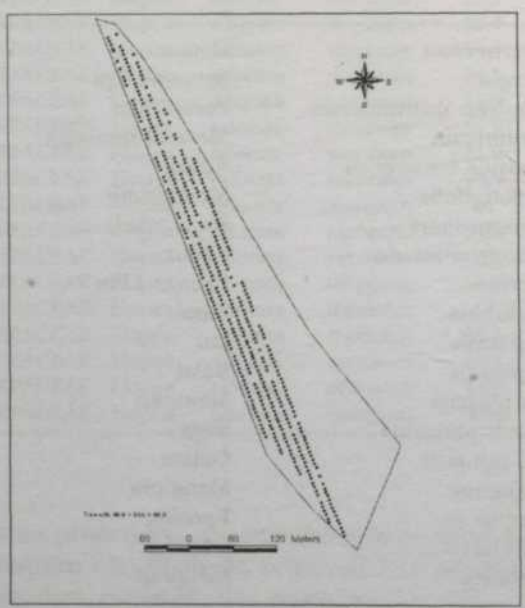

Fig. 4: Distribution of trees with Dbh > 45.5 cm and Dbh < 49.9 cm

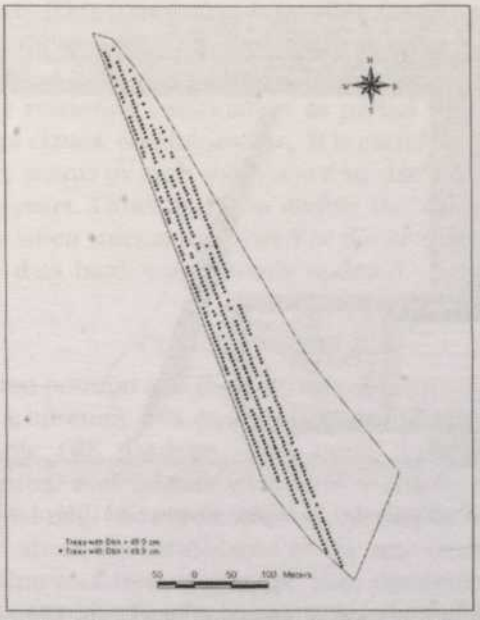

Fig. 5: Distribution of trees with Dbh > 49.9 cm

TABLE 5
Attribute information about distribution of trees with Dbh > 49.9 cm

Tree No.	Family	Genus	Species	Local Name	D99 (cm)	D96 (cm)	Ht96 (m)
103	LEGUMINOSAE	Acacia	mangium	Mangium	53.1	52.7	20
139	LEGUMINOSAE	Acacia	mangium	Mangium	57.2	NA	NA
143	LEGUMINOSAE	Acacia	mangium	Mangium	65.7	NA	NA

NA = Not Available

In order to know tree growth or tree increments, tree deaths or losses, it is essential to know the individual identity of each tree, so that each measurement can be allocated for the appropriate tree record. Labeling or painting the enumerated trees will avoid confusion between trees of similar sizes or species or when the relative size or status changes between measurements. It is recommended that the labeling or numbering should not be omitted even if plot maps of tree position and number are drawn and regularly revised. Numbered labels are best nailed to the tree at a standard height above the point of diameter measurement, where they are clearly visible and help to define the point of measurement. However, they may be exposed to theft and lost if the tree is harvested or dead. It is sometimes an advantage to fix the nail just above the buttress.

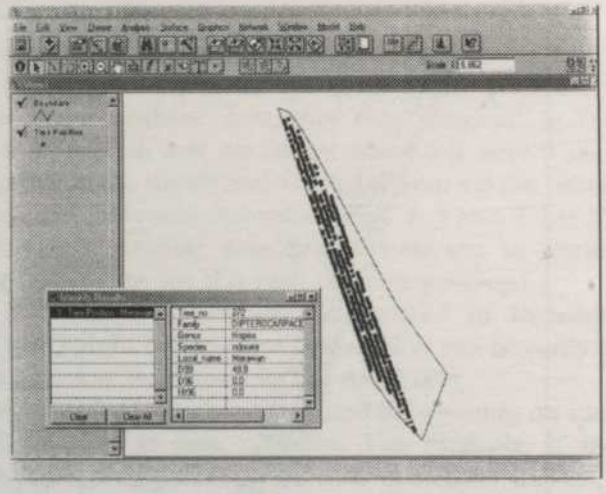

Fig. 6: Distribution of Hopea odorata with Dbh > 40.8 cm

TABLE 6
Attribute information of Hopea odorata with Dbh > 40.8 cm

Tree No.	Family	Genus	Species	Local Name	D99 (cm)	D96 (cm)	Ht96 (m)
270	DIPTERO	Hopea	odorata	merawan	42.3	NA	NA
271	DIPTERO	Hopea	odorata	merawan	42.1	NA	NA
272	DIPTERO	Hopea	odorata	merawan	49.9	NA	NA
273	DIPTERO	Hopea	odorata	merawan	41.8	NA	NA
275	DIPTERO	Hopea	odorata	merawan	48.6	NA	NA
355	DIPTERO	Hopea	odorata	merawan	41.2	NA	NA
357	DIPTERO	Hopea	odorata	merawan	45.3	NA	NA

NA = Not Available

The GIS database can cope just as easily with other parameters besides species and location. As for a routine management, it is only a small step to complement standard tree measurements, with data of a useful, subjective kind, such as that used to record tree condition or management action from existing measurement, perhaps to predict growth, timber yields and even landscape impact.

The resource planner's problem is how to compare and combine selected information from these two kinds of databases. In order to relate a given geographic location to its specific attributes (such as tree dimension), computer technology especially GIS has long since made it possible to manipulate and analyze statistical information. However, only recently has the technology been developed which can convert maps into a computer-usable digital format and allow the simultaneous manipulation of both geographical spatial data and

related attribute data. This now makes it possible for the resource planner to rapidly produce a combination of maps and tables that show where and what.

The users concerned with tree surveys will be satisfied to use the system as a library file, simply retrieving information as partial lists under headings of species, locations, age classes, conditions, etc. It is useful, in these circumstances, to retain blank entry points in each tree record so that further parameters can be added in future years. Other facilities enable the users to delete obsolete information, such as when trees are removed or die or to extend the file to new entries keeping the data bank continuously updated.

CONCLUSIONS

Information about tree position and their attribute information (tree dimension) for 434 trees in the arboretum area can be easily stored, retrieved, analyzed and displayed in a simple GIS database. Tree stand management can also be depicted both in spatial and tabular criteria in a simple and comprehensive manner using a digital map of tree location which can be stored in ARCVIEW.

The information about the distribution of the tree family, genus or species as well as the coordinate of trees inside the plot, diameter, and height of the required tree, can be retrieved easily by using the query that was developed in ARCVIEW. Family distribution in the area consists of 12 families, 19 genus and 15 species with *Hopea odorata* constituting the largest number inside the area. Tree diameter distribution ranges from 4.2 cm to 65.7 cm with lots of dead trees (75 trees) inside the area due to problem of waterlogging.

REFERENCES

ANON. 1999. The Morton Arboretum. http://www.mortonarb.org. 6p.

ANTENUCCI, J.C., B. KEY, L. C. PETER, J.K. MICHAEL and A. HUGH. 1991. *Geographic Information System: A Guide to the Technology.* New York: Van Nostrand Reinhold.

BOYCE, S.G. 1995. *Landscape Forestry.* New York: John Wiley & Sons, Inc.

GOODWIN, D.W. 1996. A street tree inventory for Massachusetts using GIS. *Journal of Arboriculture* **22 (1)**: 19-28.

HARRIS, R.W. 1983. *Arboriculture. Care of Trees, Shrubs and Vines in the Landscape.* New Jersey: Practice-Hall Inc.

JAMES, N.D.G. 1990. *The Arboriculturalist's Companion. A Guide to the Care of Trees.* United Kingdom: Basil Blackwell Ltd.

MINKLER, L.S. 1980. *Woodland Ecology. Environmental Forestry for the Small Owner.* New York: Syracuse University Press.

Pertanika J. Sci. & Technol. 10(2): 201 - 208 (2002)
ISSN: 0128-7680

Study on CCB (Chromated Copper Boric Acid) Dip Preservation of Golpata *(Nypa fruticans)*

G. N. M. Ilias[1], M. A. Rahman[2], M. O. Hannan[2], S. M. Feroz[2] & Faridah Abdullah[3]

[1]Rural Electrical Board, Joarsahara, Khilkhet, Dhaka - 1227, Bangladesh

[2]Forestry and Wood Technology Discipline, University of Khulna, Khulna, Bangladesh

[3]Department of Biology, Faculty of Science and Environmental Studies, Universiti Putra Malaysia, 43400 UPM Serdang, Selangor, Malaysia

Received: 2 August 1999

ABSTRAK

Golpata (*Nypa fruticans*) ialah satu sumber atap yang murah di Bangladesh. Bagaimanapun, jangka hayat semula jadi selama 2-3 tahun membuatkannya tidak sesuai untuk penggunaan jangka panjang. Kajian ini dilakukan untuk menyiasat kemungkinan jangka hayat Golpata dipanjangkan melalui rawatan secara celupan ke dalam larutan pengawet kimia CCB (Kuprum berkromat dan Asid Borik). Sampel ujian terdiri daripada daun dan urat-tengah Golpata dengan julat kandungan kelembapan di antara 16.63% hingga 70.67% pada permulaan uji kaji. Sampel-sampel dicelup ke dalam larutan CCB pada 4 kepekatan berbeza selama 2, 4, 6 dan 8 jam setiap satu dan seterusnya diperiksa kemasukan dan kesimpanan CCB di dalam sampel. Kemasukan ditentukan dengan mengguna penunjuk kuprum dan boron sementara kesimpanan dihitung melalui spektroskopi sinar-X. Keputusan menunjukkan yang dua faktor, iaitu kepekatan CCB dan jangka masa celupan, mempengaruhi keberkesanan rawatan Golpata. Kemasukan CCB yang paling baik ialah untuk rawatan celupan 6 jam untuk kedua-dua sampel. Kesimpanan CCB pula adalah paling baik pada rawatan celupan 6 jam untuk daun dan 8 jam untuk urat tengah daun. Masa rawatan menunjukkan keberkesanan bererti pada 5% paras keyakinan. Kajian ini mendapati jangka hayat Golpata boleh dipanjangkan dengan cara celupan dalam pengawet CCB.

ABSTRACT

Golpata *(Nypa fruticans)* is a cheap source of roof thatches in Bangladesh. However, its short life span of 2-3 years makes it unsuitable for long-term use. This study was carried out to investigate the treatability of Golpata by dipping in CCB (Chromated Copper Boric acid) mixture. Samples of leaves and midribs of Golpata with moisture contents ranging from 16.63% to 70.67% at the start of the experiment, were dipped into CCB solution of four different concentrations for 2, 4, 6 and 8 hours and examined for CCB penetration and retention. Penetration was determined by using a copper and boron indicator whereas retention was calculated by X-ray spectroscopy. Results revealed that two factor chemical (CCB) concentrations and duration of dipping period have considerable effect on the preservation of Golpata but not the moisture content. Better CCB penetration was observed after 6 hours of dipping time in

both leaves and midribs but better CCB retention was found for both 6 and 8 hours dipping time for both specimen types respectively. Treatment time showed a significant effect at 5% level of confidence. Chemical (CCB) concentration had a significant effect on penetration of Golpata leaves but had no effect on the retention.

Keywords : *Nypa fruticans*, CCB dip treatment, penetration, retention

INTRODUCTION

Nypa fruticans locally called Golpata is a mangrove palm with a wide variety of uses. It is one of the valuable non-wood forest plant species of mangroves of Asia and the Pacific. Its leaves are made into roof thatches in Bangladesh, India, Burma, Vietnam, Malaysia and the Philippines (FAO 1994). The leaves are also used in the manufacturing of bags, baskets, hats, mats, raincoats, wrappers and such like. Sun-dried Golpata petioles are a source of firewood, whilst the skin of fresh petioles can be turned into ropes for tying purposes. Sap can be extracted from its inflorescence and made into sugar, alcohol or vinegar. The fruits are edible and can be consumed fresh or preserved (FAO 1994). Besides the economic significance, Golpata is also of ecological importance as it protects soil erosion. However, the use of Golpata as thatching material in Bangladesh is mainly confined to people of low income category, particularly those living in the sundarban (mangrove forests) areas (Source : ADB 1992). Golpata is the third most important commercial product from the sundarban forests of Bangladesh. The country has a yearly estimated production of one fortieth million of US dollars. The revenues collected from Golpata showed an increase from 2 to 5.8 million taka between 1980 - 1991, which is an increase of about 200% over a ten-year period (Source : ADB 1992).

The demand for Golpata is expected to rise to commensurate with an increasing population growth; and in due time, it is anticipated that demand will exceed the supply. Besides high demand, a decrease in supply may also be attributed to gradual ecological changes, unplanned harvesting as well as the fast turnover of the product due to its limited life-span. To sustain the supply, planned cultivation and harvesting of Golpata should be implemented. An immediate and short-term approach to overcome this problem would be to prolong the durability period of the thatching material, which is normally between 2 to 3 years, to several times more (Hunt and Garratt 1953). Preservative treatment previously done on thatching materials of sungrass, rice stalk and bamboos showed that the service life could be prolonged 10 to 15 times more than when they were not treated (Anon 1984).

The objective of this study was to investigate the treatability of Golpata leaves by using a mixture of chromated-copper-boric acid (CCB, with modification from FRI 1970) in the ratio of 2:2:1 as a chemical preservative. This study undertakes to determine the optimum preservative concentration and the optimum dipping period of Golpata leaves and midribs.

MATERIALS AND METHODS

Golpata Sample Collection and Preparation

In practice air-dried, wet and fresh or green Golpata leaves and midribs are used and hence these forms were used to investigate the treatability using CCB dip treatment. Air-dried and wet Golpata were collected from the local market, whilst fresh or green Golpata were harvested from the field. Fronds selected for dip treatment were cut into approximately six-inch length pieces. The leaves were separated from the midribs and they were all marked with non-leachable ink for reference. The density and moisture content of leaf and midribs before treatment were determined by oven drying them at 60° C (AWPA 1986). The leaf length, breadth and lamina thickness of Golpata leaves were also recorded.

CCB Preparation and Treatment

The main components of 'CCB' were Sodium Dichromate, Copper Sulphate and Boric Acid. These were purchased from the local market. The compound 'CCB' was prepared by mixing the three chemicals in the ratio of 2 : 2 : 1 respectively (FRI 1970). The basic mixture consisted of 260g Sodium dichromate, 260g Copper sulphate and 130g Boric acid.

The mixture was added to 2.24 kgs (5 pounds) of water to make up a homogenous stock solution from which dilutions of 10%, 8%, 6% and 4% were made. Each concentration was then placed in four separate plastic containers. Samples from each homogenous dilution were taken and each concentration was verified by X-ray Spectroscopy. After verification the solutions were found to be 2.24%, 3.16%, 4.20% and 5.00% instead of 4, 6, 8 and 10% respectively. This happened due to the presence of large amounts of impurities in the chemicals especially in copper sulphate which were unavoidable.

Assay of CCB Penetration and Retention

The dry weights of each of the samples were recorded before they were dipped into the various preservative concentrations. The samples were each submerged for durations of 2, 4, 6 and 8 hours in each of the 4 concentrations. At each time interval, the samples were taken out, dried with tissue papers and weight readings recorded. Penetration of CCB preservatives into the leaves and midribs were checked by using Copper indicator (Chrome-azurol solution) and Boron indicator (solution 1 & 2, as per AWPA, A3-84, 1986). The samples were checked and categorized as "all-through deep" (ATD) penetration or "all-through light" (ATL) penetration. If the penetration was not all-through, they were recorded as "side and end" (SE), "cuticle deep and inner-side light" (CL), "cuticle deep and inner-side no" (CN), or "cuticle deep and inner-side deep" (LD) penetrations. If the penetration is ambiguous, it is categorized as not clear (NC), and "end and middle" (EM) penetration.

Retention of CCB preservatives into the leaves and midribs were determined by using X-Ray Spectroscopy (AWPA 1986) and the reading was expressed in pound per cubic feet (pcf).

RESULTS AND DISCUSSION

The production of Golpata increased approximately 6% but its revenue (price) collection increased to about 200% over a ten - year period between 1980 - 1991. This may be due to the higher demand of Golpata than the production and supply. As an increase in Golpata production is neither easy nor practical at this moment, the use of CCB preservative treatment may increase the life-span (durability) of Golpata to 5 - 10 times more than the normal life-span. This may indirectly help to satiate the demand quickly. The average density of leaves was found to be 0.57 g/cc or 36.197 lb/cft (pcf) and that of midribs was 0.43 g/cc or 26.75 lb/cft (pcf).

CCB Penetration in Leaves

For dry leaves of 16.63% moisture content, ATD penetration of Cu was observed at concentrations 2.24 to 4.2 % of CCB during the first 2 hours (Table 1). However, the penetration became ATL when the duration was more than 2 hours (with one exception of at 8 hours). This indicated that Cu penetration was limited by two factors. Firstly, at concentrations of higher than 4.2 % and secondly, for dipping durations of more than 2 hours where beyond these points, performance decreases. The reason for the good penetration during 2 hours dipping rather than 4, 6 and 8 hours is still unknown from this study.

For wet leaves of 70.67% moisture content, the best penetration results were found in the 2 hours' dipping duration. Here, 75% of samples exhibited ATD penetration for both the Copper and Boron tests and the remainder 25% ATL for 2 hours' dipping period.

For fresh or green leaves of 59.23% moisture, content, ATL and ATD penetration occurred haphazardly for 2 and 4 hours dipping period. For fresh or green leaves, the best preservative penetration was for 6 and 8 hours' dipping duration for all concentrations.

Hence, it is recommended that Golpata treatment of dry and wet leaves be of 2 hours' dipping duration with 3.00% - 4.00% of CCB concentration, and 6 or 8 hours' dipping duration for fresh green leaves with the same chemical concentration.

CCB Penetration in Midribs

For dry midribs which contained 30.03% moisture content, 25% of samples showed only side and end penetration (SE) at 2.24% of CCB concentration for 2 hours in the Copper test (Table 2). However, for cuticle deep and inner-side, no penetrations (CN) were observed in 100% samples at 5% of CCB concentration for all soaking durations in the Copper test. For the Copper test alone, 75% of samples gave an ATL penetration in 4 hours' soaking time, but this was 25% ATD and 25% ATL for other time periods. On the other hand, Boron test exhibited better penetration results than Copper. In all concentrations and time periods it was either ATD or ATL.

For wet midribs having 116.91% MC, ATL penetration was observed in all concentrations for 2, 4 and 6 hours in the Copper test except for one case at

TABLE 1
Penetration of CCB in Golpata leaves at two hourly intervals

Concentration %	Penetration							
	Duration (hours)							
	2 hours		4 hours		6 hours		8 hours	
	Cu	Br	Cu	Br	Cu	Br	Cu	Br
	Dry leaf =16.63% MC							
2.24	ATD	ATL	ATL	ATD	ATL	ATD	ATD	ATL
3.16	ATD	ATD	ATL	ATL	ATL	ATD	ATL	ATD
4.20	ATD	ATD	ATL	ATD	ATL	ATD	ATL	ATL
5.00	ATL	ATD	ATL	ATD	ATL	ATD	ATL	ATD
	Wet leaf = 70.67% MC							
2.24	ATD	ATL	ATL	ATD	ATL	ATD	ATL	ATL
3.16	ATD	ATD	ATL	ATL	ATL	ATD	ATL	ATL
4.20	ATD	ATD	ATL	ATD	ATL	ATD	ATL	ATD
5.00	ATL	ATD	ATL	ATD	ATL	ATD	LD	ATD
	Fresh or Green = 59.23% MC							
2.24	ATL	ATD	LD	ATL	ATL	ATD	ATL	ATD
3.16	CN	ATD	ATL	ATD	ATL	ATD	ATL	ATD
4.20	ATL	ATL	LD	ATL	ATL	ATL	ATL	ATD
5.00	CN	ATL	ATL	ATL	ATD	ATD	CL	ATD

4 and 6 hours in 5.0% and 3.16% of CCB concentration, which gave SE and LD penetration respectively. In the case of 8 hours' soaking time, copper penetration was 75% LD and 25% ATL. No ATD was found for any concentration at any time for the Copper test. Results of Boron penetration were better than Copper in all cases where it was either ATD or ATL. For wet midribs, 2 hours' soaking time in 2.25 to 5.0% concentration is recommended.

For fresh or green midribs containing 66.40% moisture content, 100% samples showed end and middle section (EM) penetration at 2.24% of CCB concentration for all soaking times and at all concentrations for 4 hours in Copper test. Boron penetration was better than Copper. It was found to be either ATD or ATL penetration at all CCB concentrations for all time periods. This study found that for fresh midribs, 4 hours' soaking time with 3.16% to 5.0% chemical concentration may be recommended.

CCB Retention in Leaves

For dry leaves, the best retention at 0.273 pound per cubic feet (pcf) was found in 4.20% of CCB solution for 6 hours and 0.262 pcf retention was found at 5.00% of CCB solution for 8 hours (Table 3). An overall good retention was found for 6 hours of soaking with CCB at all concentrations. So, for dry leaves,

TABLE 2
Penetration of CCB in Golpata midribs at two hourly intervals

Concentration %	Penetration							
	Duration (hours)							
	2 hours		4 hours		6 hours		8 hours	
	Cu	Br	Cu	Br	Cu	Br	Cu	Br
	Dry midribs =30.03% MC							
2.24	SE	ATL	ATL	ATL	ATD	ATD	ATD	ATD
3.16	ATL	ATD	ATL	ATL	ATL	ATD	ATL	ATL
4.20	ATD	ATL	ATL	ATL	LD	ATL	CD	ATL
5.00	CN	ATL	CN	ATL	CN	ATL	CN	ATL
	Wet midribs = 116.91% MC							
2.24	ATL	ATD	ATL	ATD	ATL	ATD	LD	ATL
3.16	ATL	ATD	ATL	ATD	LD	ATL	LD	ATD
4.20	ATL	ATL	ATL	ATD	ATL	ATL	ATL	ATL
5.00	ATL	ATD	SE	ATL	ATL	ATD	LD	ATD
	Fresh or Green midribs =66.40% MC							
2.24	EM	ATL	EM	ATL	EM	ATD	EM	ATL
3.16	EM	ATL	EM	ATD	ATL	ATL	EM	ATD
4.20	NC	ATD	EM	ATD	EM	ATL	NC	ATL
5.00	EM	ATD	EM	ATD	EM	ATD	EM	ATD

6 hours' soaking time with 4.20 - 5.0% chemical concentration may be recommended.

For wet leaves, the best retention of 0.263 pcf and 0.264 pcf were found in 5% solution for 6 hours and 4.20% solution for 8 hours respectively. But the good retention was found as a whole at 2.24%, 3.16% and 4.20% CCB for 8 hours. So, for wet leaves, 8 hours' soaking time with 2.24 - 4.20% chemical concentration or 6 hours with 5.0% chemical concentration might be recommended.

In fresh leaves, the best retention of 0.252 pcf and 0.272 pcf were found at 4.20% and 5.00% of CCB concentrations respectively, for 6 hours' dipping. But the overall good retention was found for all solutions for 4 hours. So, for fresh leaves, 4 hours' soaking time with 4-5% of CCB concentrations may be recommended.

CCB Retention in Midribs

For dry midribs, the best retention of 0.267 pcf and 0.366 pcf were found at 4.20% and 5.00% of CCB solution respectively for 8 hours (Table 4), with an overall good retention found for all solutions during 8 hours of soaking. So, for dry midribs, 8 hours' soaking time with any of the four chemical concentrations, especially 4.20 - 5.0% concentrations, may be recommended.

For wet midribs, the best retention at 0.795 pcf was found at 5.00% concentration for 8 hours. The overall good retention was found for all solutions during 6 hours of soaking. So, for wet midribs, 6 hours' soaking time with any of the four solutions at 4-5% or 8 hours' soaking time with 5.0% solution may be recommended.

TABLE 3
Retention of CCB in the Golpata leaves at two hourly intervals

Retention (pcf)

Concentration %	Duration (pcf)			
	2 hrs	4 hrs	6 hrs	8 hrs
		Dry leaf= 16.63 % MC		
2.24	0.034	0.026	0.198	0.120
3.16	0.027	0.032	0.182	0.092
4.20	0.048	0.092	0.273	0.099
5.00	0.085	0.068	0.241	0.262
		Wet leaf= 70.67 % MC		
2.24	0.081	0.058	0.111	0.228
3.16	0.178	0.087	0.095	0.257
4.20	0.031	0.058	0.163	0.264
5.00	0.033	0.103	0.263	0.012
		Fresh or Green leaf = 59.23 % MC		
2.24	0.021	0.159	0.071	0.238
3.16	0.073	0.120	0.048	0.034
4.20	0.129	0.215	0.252	0.231
5.00	0.025	0.281	0.272	0.000

For fresh or green midribs, the best retention at 0.194 pcf, was found at 5.00% concentration for 8 hours. So, for fresh midribs, 8 hours' soaking time with 3.16 - 5.0% chemical concentration may be recommended.

CONCLUSION

It is obvious from this study that Golpata can be treated with the preservative CCB (Chromated Cupper Boric Acid) mixture. This study recommends that Golpata should be dipped for 6 - 8 hours, in 4 - 5% CCB for optimum preservation. To minimize costs, treatment should be carried out commercially to fulfill the nation's demand for Golpata. As the chemicals are easily available locally at minimum cost, Golpata should be chemically treated so as to increase their durability and hence minimize thatching cost.

TABLE 4
Retention of CCB in the Golpata midribs in two hourly intervals

Concentration %	Retention (pcf) Duration (pcf)			
	2 hrs	4 hrs	6 hrs	8 hrs
		Dry leaf= 30.03 % MC		
2.24	0.046	0.061	0.083	0.161
3.16	0.083	0.095	0.118	0.165
4.20	0.063	0.122	0.230	0.267
5.00	0.079	0.114	0.236	0.366
		Wet leaf= 116.91 % MC)		
2.24	0.088	0.057	0.179	0.093
3.16	0.017	0.027	0.149	0.184
4.20	0.027	0.149	0.203	0.032
5.00	0.048	0.029	0.178	0.795
		Fresh or Green leaf = 66.40 % MC		
2.24	0.054	0.065	0.075	0.096
3.16	0.079	0.079	0.085	0.147
4.20	0.093	0.101	0.116	0.162
5.00	0.077	0.101	0.100	0.194

REFERENCES

ADB. 1992. Non-wood Forest Products. Project 372001/9; Forestry Master Plan, Bangladesh TA 1355-BAN Asian Development Bank, Manila, Philippines. p. 46 - 50.

AWPA. 1986. American Wood Preservers Association Standard. Maryland, U.S.A. p. M5-6, A9-1 to 2, A3-1 to 2.

ANON. 1984. Wood preservation and wood products treatment. Bulletin 823, cooperative extension service/ The University of Georgia College of Agriculture/Athens, Greece, p. 29.

FRI. 1970. India Forest Utilization Vol-1, Forest Research Institute and Colleges, Dehra Dun. Publications, FRI and Colleges Dehra Dun Delhi, India.

FAO. 1994. Environmental Aspects of Industrial Wood Preservation : A technical guide, UNEP IE/PAC technical reports series, **20**:20-21.

HUNT, G.M. and G.A. GARRATT. 1953. *Wood Preservation.* p. 417. U.S.A: New York.

Pertanika J. Sci. & Technol. 10(2): 209 - 227 (2002)
ISSN: 0128-7680

Development of a GIS Based Water Management Tool for a Large Scale Rice Irrigation Scheme

Rowshon M. K., Kwok C. Y. & Lee T. S.
Department of Biological and Agricultural Engineering
Faculty of Engineering, Universiti Putra Malaysia
43400 UPM Serdang, Selangor, Malaysia
Email: kwokcy@eng.upm.edu.my

Received: 23 November 2000

ABSTRAK

Satu model berasaskan GIS telah direka untuk menggabungkan pelbagai maklumat spatial dari kawasan pengairan Kerian. Kawasan pengairan ini dibahagi kepada lapan kompatmen yang terdiri daripada 28 blok. Model ini mengandungi tiga modul, iaitu Penjadualan (Scheduling) yang mengira pembekalan air berasaskan maklum balas spatial dan temporal daripada sawah, sementara modul Pemantauan (Monitoring) menunjukkan maklumat tentang keseragaman bekalan air antara semua blok dan kompatmen. Petunjuk-petunjuk seperti Relative Water Supply (RWS), Water Use Efficiency (WUE), Cumulative Relative Water Supply (CRWS), dan Water Productivity Index (WPI) ditentukan dengan modul Penilaian (Evaluation). Analisis lepas musim menggunakan maklumat hidro-klimatik mingguan, bekalan air dan indeks pengairan mingguan bagi setiap blok. Berdasarkan tempoh seminggu, didapati bahawa julat RWS ialah antara 1.01 hingga 2.24 dan WUE ialah antara 45% hingga 99% bagi musim utama, sementara pada luar musim nilai RWS ialah antara 1.04 hingga 1.87 dan WUE ialah antara 53.57% hingga 96.15%. Nilai purata WPI ialah 0.13kg/m^3 pada musim utama dan 0.22kg/m^3 di luar musim. Peta tematik berkod warna telah disediakan untuk mengesan Hasil Musim, dan Keamatan Penanaman Musim (Cropping Intensity), mengikut blok dan kompatmen. Maklumat dipamerkan dalam bentuk jadual dan graf akan memudahkan proses membuat keputusan sepanjang musim oleh pihak pengurusan. Model yang berasaskan maklum balas daripada sawah ini dapat mempertingkatkan lagi sistem pengurusan pengairan di jelapang padi.

ABSTRACT

A GIS based model was developed to integrate the vast amounts of spatially distributed information from the Kerian Irrigation Scheme comprising eight compartments which are further subdivided into 28 blocks. The model consists of three modules. The "Scheduling" program computes irrigation deliveries based on spatial and temporal demand of the paddy field by each compartment, block or secondary canal. The "Monitoring" program gives information by compartment and by block on the uniformity of water distribution and the shortfall or excess. Relative Water Supply (RWS), Water Use Efficiency (WUE), Cumulative Relative Water Supply (CRWS), and Water Productivity Index (WPI) were computed by the "Evaluation" module. The post-season analysis uses weekly information on hydro-climatic parameters, irrigation delivery and irrigation indices by block within each compartment. On a weekly basis, RWS and WUE were found to range from 1.01 to 2.24 and 45% to 99% respectively

in the main season and 1.01 to 1.87 and 53.57% to 96.15% respectively in the off season. The average values of RWS and WUE were found to be 1.53 and 68.15% in the main season and 1.33 and 78.47% in the off season respectively. The average values of WPI were also found to be 0.13 and 0.22 kg/m^3 in the main season and off seasons respectively. Color-coded thematic maps were produced for the monitoring of Seasonal Yields and Cropping Intensity (CI) by block and compartment of the scheme. The results are displayed allowing the manager to view maps, tables and graphs in a comprehensible form to ease decision making as the season progresses. This study would be useful to improve the irrigation system management based on feedback of field information.

Keywords: Water management, rice irrigation, user-interface and GIS

INTRODUCTION

Rice is the staple food in Malaysia. The Government has targeted rice production of 1.20 million tons by 2010 at a self-sufficiency level of 65 percent in National Agricultural Policy, NAP 1992-2010. According to a JICA and DID report (Anon 1998), effective use of water resources by rationalizing irrigation systems and impartial water allocation with a suitable water management practice are key factors for increasing rice production. Irrigation performance has received growing attention during the last decades. Vast amounts of data are distributed spatially at district levels. These could be integrated to help improve water management. Geographical Information Systems (GIS) is a tool with great potential for structuring information to improve monitoring and evaluation of irrigation and drainage projects and assist in related policy decisions. Salman *et. al.* (1997) used Remote Sensing (RS) and GIS to monitor and evaluate irrigation and drainage projects in Pakistan. This study concentrated on the estimation of crop related indicators such as area under different crops and cropping intensity. Assessing performance requires a clear identification of the performance indicators, the scale at which performance is to be assessed, and the level of accuracy required by the potential users of this information. A GIS based software (NAGA Version 1) is being tested for monitoring and diagnosis of irrigation projects in Thailand. It expects improved stability of delivery at the secondary level by "real time" monitoring; monitoring of the global indices of efficiency and identification of mismanagement, easy weekly assessment of performance.

In irrigation projects there is significant variation in the spatial and temporal data. GIS capabilities to integrate spatial data from different sources, with diverse formats, structures, projections or resolution levels, constitute the main characteristic of these systems, thus providing needed aid for those models that incorporate information in which spatial data has a relevant role (Goodchild 1993). Bradly (1993) stated that the capability of GIS makes it appropriate for decision-making. GIS provides a platform for retrieval and structuring of that information to improve irrigation deliveries, monitoring and evaluation of irrigation and drainage projects and related policy decisions. The objective of

this study is to develop a GIS interface program for Water Management of rice irrigation to improve regular or periodic irrigation delivery and monitoring, and post-season analysis to evaluate the irrigation performance.

Study Area

The Kerian Irrigation Scheme is one of the oldest Schemes in Malaysia. It is situated at the northwest corner of the State of Perak in Peninsular Malaysia. *Fig. 1* shows the layout of the 28 blocks which make up a total irrigated area of 23,800 ha. The catchment area of the reservoir is 489 km^2 and active storage of the reservoir is 56 MCM with a dead storage of 19 MCM. It serves as the source of irrigation water for compartments (E to H), while a pumping station supplements four compartments (A to D) at the tail end of the scheme.

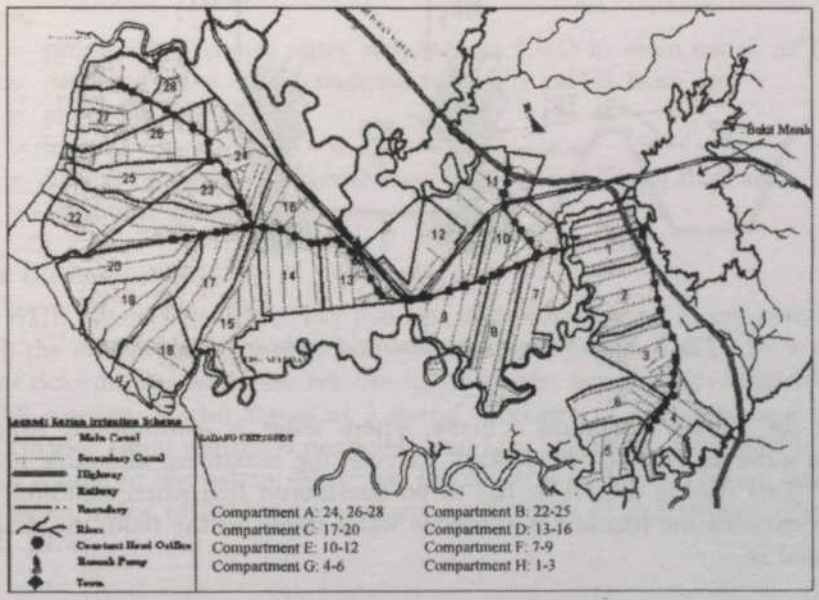

Fig. 1. Digitized layout of Kerian Irrigation

METHODOLOGY

Water Balance in a Rice Field

The field water balance is used to characterise scheduling, monitoring and evaluation of the rice irrigation system. For a continuous irrigation system, how well water is distributed among plots within a block for a particular irrigation period needs to be answered. Adequate monitoring and evaluation of performance is needed to improve water management practices to achieve a satisfactory level of efficiency. The schematic diagram of water balance components in a paddy field is shown in *Fig. 2*, while the balance equation is expressed as follows:

$$WD_j = WD_{j-1} + IR_j + RF_j - ET_j - SP_j - DR_j \quad (1)$$

Where,

WD_j = depth of water in the paddy field at the end of period, cm.
WD_{j-1} = depth of water in the paddy field at the beginning of a period, cm.
IR_j = depth of diversion of irrigation water supply during the period, cm
RF_j = rainfall during the irrigation period, cm.
ET_j = evapotranspiration from the paddy field during the period, cm.
SP_j = average seepage and percolation loss from the paddy field, cm.
DR_j = drainage requirement during the period, cm.
j = period of water management for irrigation scheme, days.

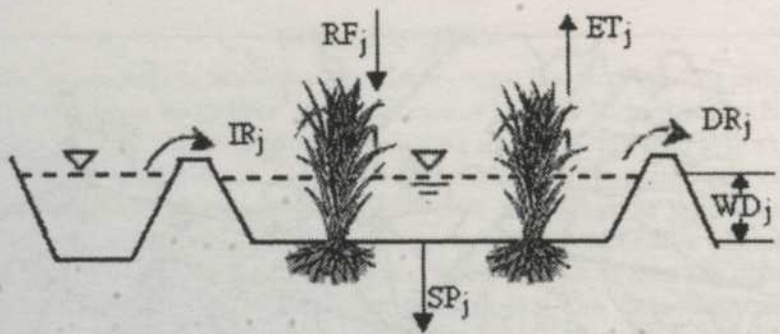

Fig. 2. Water balance components of a model in a paddy field

In the Kerian Irrigation Scheme, where water is continuously supplied, excess water is drained whenever it exceeds the maximum allowable level of water (Dd) during season. It has to be considered that when standing water depth exceeds the maximum allowable water depth in the field, the drainage required is:

$$DR_j = WD_j - Dd \text{ if } WD_j > Dd \quad (2)$$

Targeted Diversion Irrigation Supply

Precise estimation of irrigation delivery is a key element in any irrigation system. Accurate estimation of the expected rainfall and evaporation is difficult. Taking into account expected rainfall before performing the scheduling processes can save significant amounts of irrigation water. Spatial and temporal irrigation supply for a single CHO can be estimated according to paddy field requirements. If WD_j is less than the targeted depth, Dd (ie., $WD_j < Dd$) then the sum of depleted standing water depth (WD_j - Dd) cm, and losses from the paddy field and expected rainfall ($ET_j + SP_j - ER_j$) are considered in the scheduling process, using the following equation:

$$Q_p = \frac{\left[(Dd - WD_j) + (ET_j + SP_j - ER_j) * t\right] A}{244.66\ t * Es} \quad (3)$$

When only the amount of losses from the paddy field and expected rainfall ($ET_j + SP_j - ER_j$) are considered during the scheduling processes when water depth remains the same as the maximum allowable water depth, then the diversion supply will be

$$Q_p = \frac{\left[(ET_j + SP_j - ER_j) * j\right] A}{244.66\ j * Es} \quad (4)$$

Where,

Q_p = predicted diversion water supply from CHO in main canal, m^3/sec
Dd = designed water depth maintained in the paddy field, cm
ER_j = expected rainfall, cm
A = irrigation area, ha
j = period of water management for irrigation scheme, days and
Es = irrigation system efficiency.

Water Use Efficiency, WUE

The WUE involves the efficiency concept traditionally used in engineering in which the efficiency is a comparison of output with input. It provides a simple way of determining water use relative to total water supply from irrigation and rainfall sources. It also serves as a useful indicator of the irrigation system performance when rainfall is negligible and how efficiently the available water supply is used in the system. Water use efficiency as defined as below, has been used as an index of field water utilization efficiency in rice irrigation systems (IRRI 1974).

$$WUE = \left(\frac{ET_j + SP_j}{IR_j + ER_j}\right) * 100 \quad (5)$$

Where,

IR_j = depth of diversion water supply during the period in cm.
ER_j = effective rainfall during the irrigation period in cm.
ET_j = evapotranspiration from the paddy field during the period in cm.
SP_j = average seepage and percolation loss during the period, cm.

Relative Water Supply, RWS

Relative water supply proposed by Levin (1982) is the ratio of total water supply from rainfall and irrigation sources to total evapotranspiration need and seepage and percolation losses.

$$RWS = \left(\frac{IR_j + ER_j}{ET_j + SP_j} \right) \tag{6}$$

It is a simple ratio of supply to demand. It is useful for analysis and interpretation of irrigation system performance for different time intervals, monthly, annual, seasonal or special periods such as land preparation and for the different locations at system and subsystem levels. RWS is a more practical indicator than the irrigation system efficiency for rice irrigation practices. It represents the amount utilized for crop production and the amount of water delivered to meet crop water demand. Due to this, it gives a clear understanding and planning for the behavior of the major parameters in the irrigation management process to the irrigation managers and farmers.

Cumulative Relative Water Supply, CRWS

It is defined as the accumulated value of the ratio of supply to the demand computed over short intervals of time (i.e. daily, weekly or any period) starting from a particular time of the season. The RWS helps to identify acute access or shortage while the CRWS gives the integrated value. It is also useful at the end of every season as part of the evaluation of the irrigation process. It is expressed mathematically as follows:

$$CRWS = \sum RWS_j \tag{7}$$

Where, $\sum RWS_j$ is the cumulative value of all the RWS values over short time duration up to that time.

Water Productivity Index, WPI

The water productivity index measures effectiveness of the irrigation in terms of gross rice yield per volume of water applied. The realistic range of the water productivity index should be from 0.30 to 0.60 kg/m^3. Both the increases of rice yield per hectare and water use efficiency are essential to improve Water Productivity Index. However, yields are not a function of water alone, it also depends on soil fertility, climate, pests, diseases and agricultural practices. It is expressed as:

$$WPI = \frac{\text{Specific Yield in kg / ha}}{\text{Specific Supply in ha / m}^3} = \frac{Y}{q_s * 1000} \text{kg / m}^3 \tag{8}$$

where, Y the specific yield is the yield per ha (kg/ha) for the season in the area concerned, and q_s the specific supply is the total supply including rainfall per ha for the season in the area concerned, m^3/ha.

GIS User-interface

The design of the GIS user-interface and its application in the Kerian Irrigation Scheme are presented below. The desktop mapping software package MapInfo for Windows and MapBasic Programming Language were used for developing the user-interface tools. The schematic in *Fig. 3* illustrates the components and operation strategies.

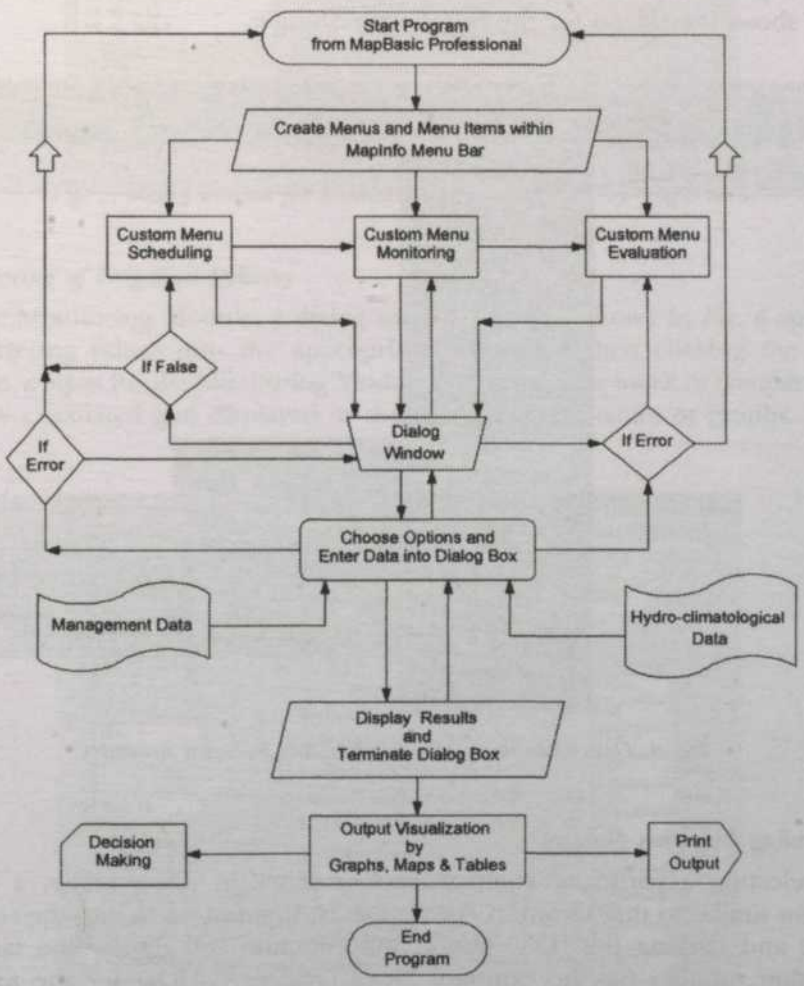

Fig. 3. Schematic diagram illustrates the operation procedure of the user-interface technique

Three modules were developed, namely Scheduling, Monitoring and Post Season Analysis (Evaluation). Scheduling was used to determine the Target Irrigation Delivery, while the second was used to monitor Irrigation Deliveries such as Relative Water Supply and Water Use Efficiency. The last, as its name implies, is carried out at the end of the season to consider yields, Water Productivity Index and Cumulative Relative Water Supply. An identical user interface was implemented at the beginning of the model. The selected module's name appears in the MapInfo menu bar. Clicking on this menu item activates a drop-down menu which allows the user to select any one of the eight compartments. Within each compartment, further selection of an individual block is possible. After this point, menus specific to the module will be used. *Fig. 4* shows the screen for the Scheduling Module.

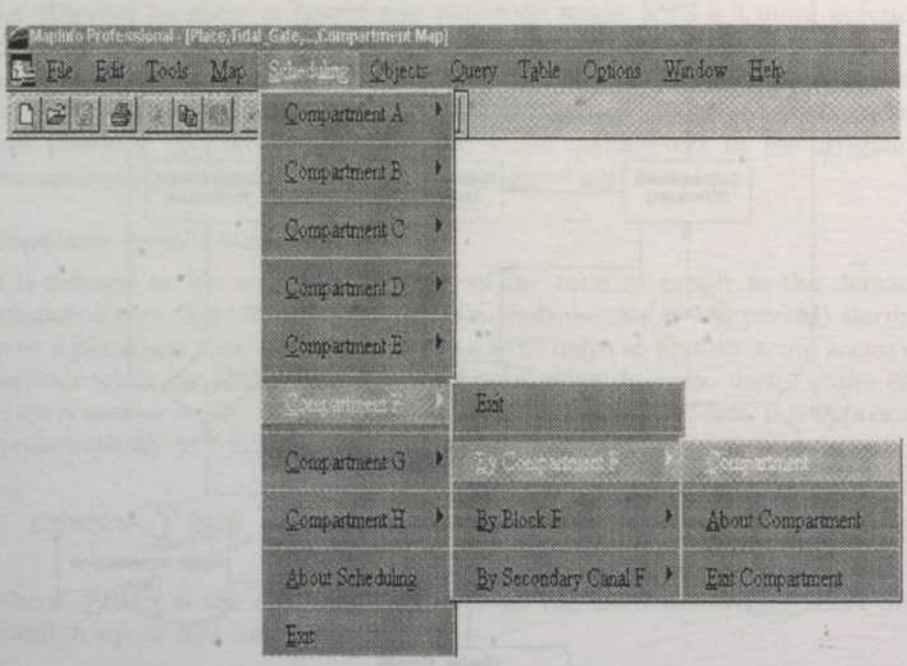

Fig. 4. Customized menu of scheduling and its menu structures

Scheduling Irrigation Delivery

On selecting a particular compartment or block in this module, a dialog window similar to that shown in *Fig. 5* appears. Inputting data into the relevant boxes and clicking the "OK" button will compute and display the targeted diversion supplies for the Constant Head Orifices (CHOs) for the selected blocks/compartments.

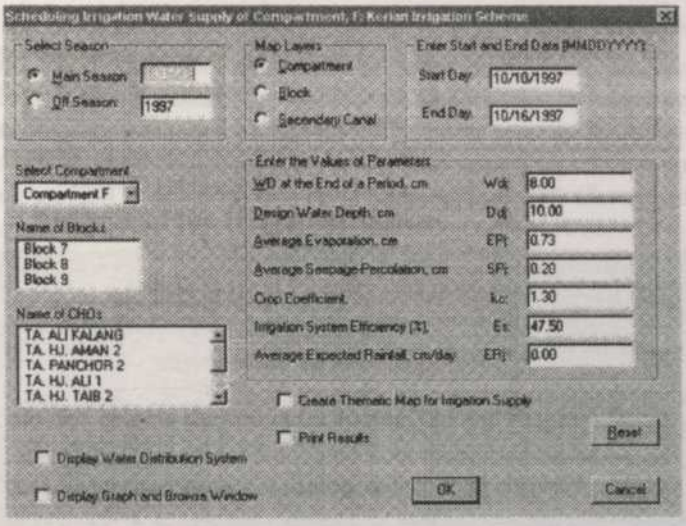

Fig. 5. Dialog window for scheduling of compartment F by compartment

Monitoring of Irrigation Delivery

In the Monitoring Module, a dialog window like that shown in *Fig. 6* appears. By entering values into the appropriate boxes and then clicking the "OK" button, output for the Monitoring Module for a particular block or compartment will be calculated and displayed in the form of maps, tables or graphs.

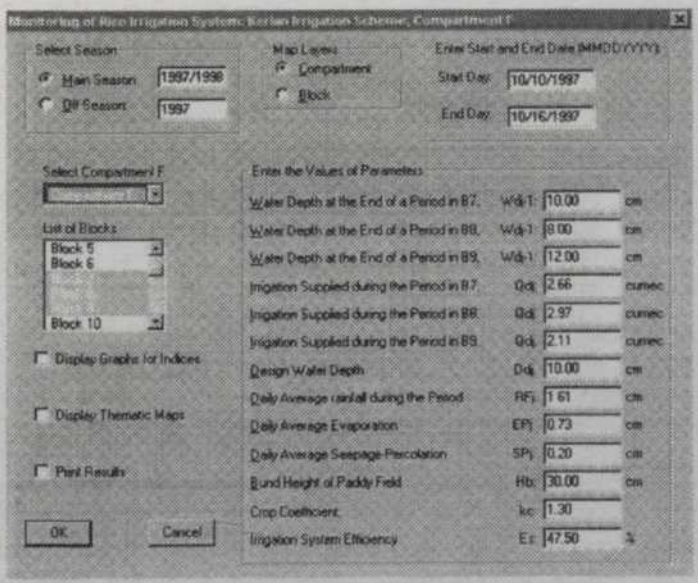

Fig. 6. Dialog window for Monitoring Module by compartment

Post-season Analysis of the Irrigation System

The "Evaluation" module is used to carry out post-season analysis for the irrigation system. On selection of this module a dialog window similar to that in *Fig. 7* appears. The user enters data and selects the indicator to analyse and display. When yield and Water Productivity Index are to be determined a dialog window as shown in *Fig. 8* appears.

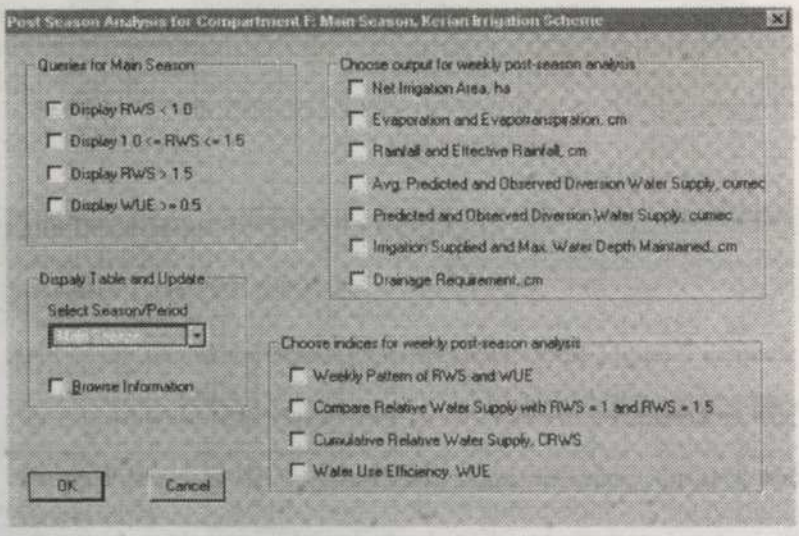

Fig. 7. Dialog window for post-season analysis for the main season, 1997/98

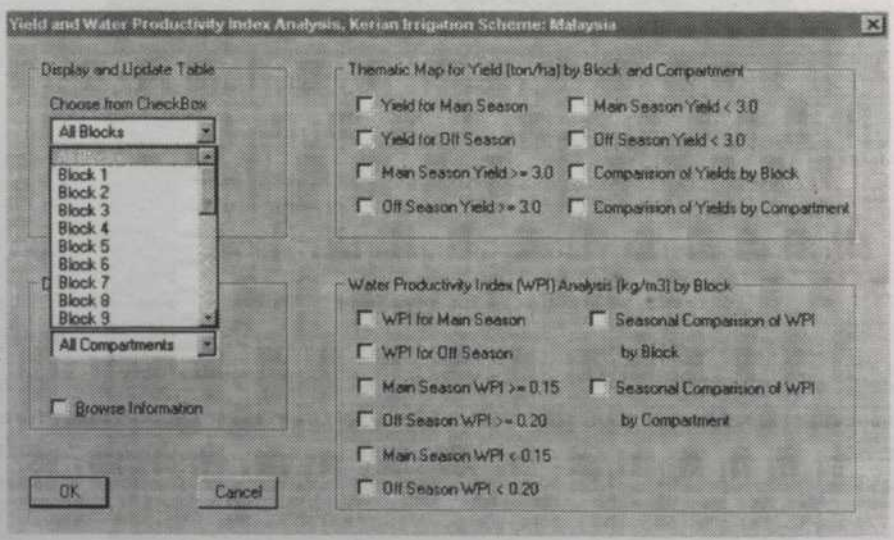

Fig. 8. Dialong window for post-season analysis of yield and WPI

RESULTS AND DISCUSSIONS

Recommended Irrigation Deliveries

Output of the interactive dialog window shown in *Fig. 5* computes irrigation deliveries for service areas under each CHO of any selected compartment. The results are shown in *Fig. 9* which is the recommended irrigation supply for each hydraulic unit (CHO) of compartment F during 10 to 16 October 1997 in the main season. The thematic bar chart together with browser window shows discharges for all CHOs of compartment F in *Fig. 10* when the user clicks on the CheckBox dialog "Display water distribution system". The name of the CHO is also displayed on the screen when the cursor is targeted on the map object.

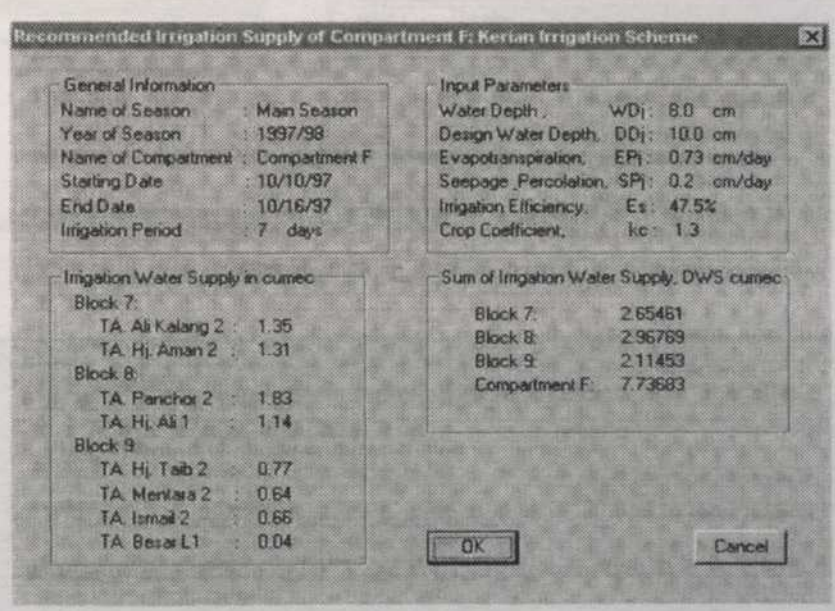

Fig. 9. Weekly recommended irrigation supply for the main season

Monitoring Periodic Irrigation Delivery

The daily, weekly, and periodic appraisal can characterize the irrigation delivery performance and improve the irrigation management as the season progresses. The water balance components are analyzed at the end of each period. This module allows the irrigation manager to monitor the situation within a block as well as the spatial and temporal irrigation performance between blocks within the compartment. The color-coded maps and graphs are displayed instantly when users select the CheckBox "Display Thematic Maps" from the dialog window shown in *Fig. 6*. It views computed results together with detailed information for a given period as illustrated in *Fig. 11*. *Fig. 12* represents spatial variation of RWS and WUE displayed as thematic bar chart.

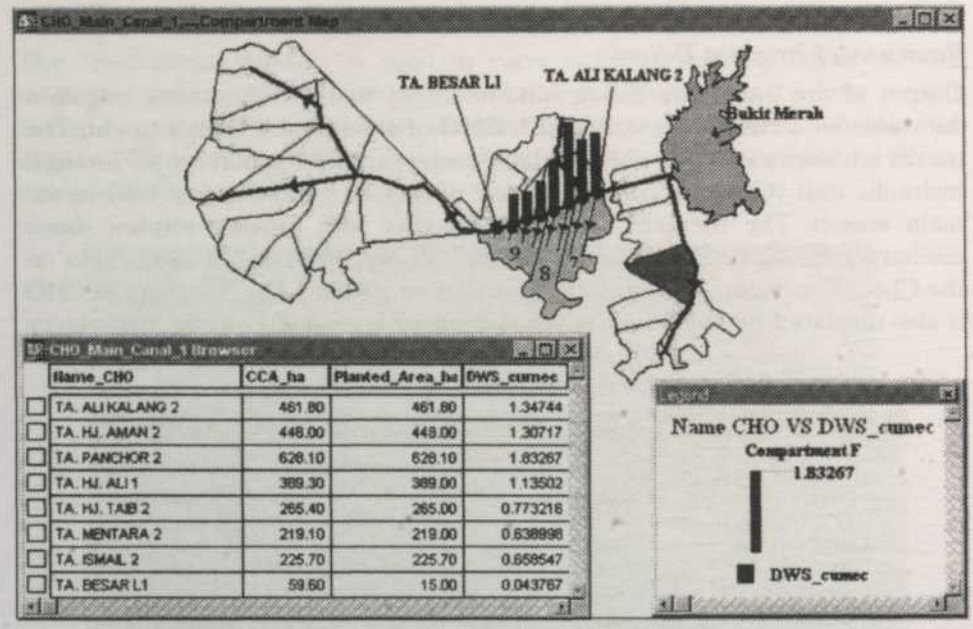

Fig. 10. Recommended irrigation supply for Compartment F shown on a map

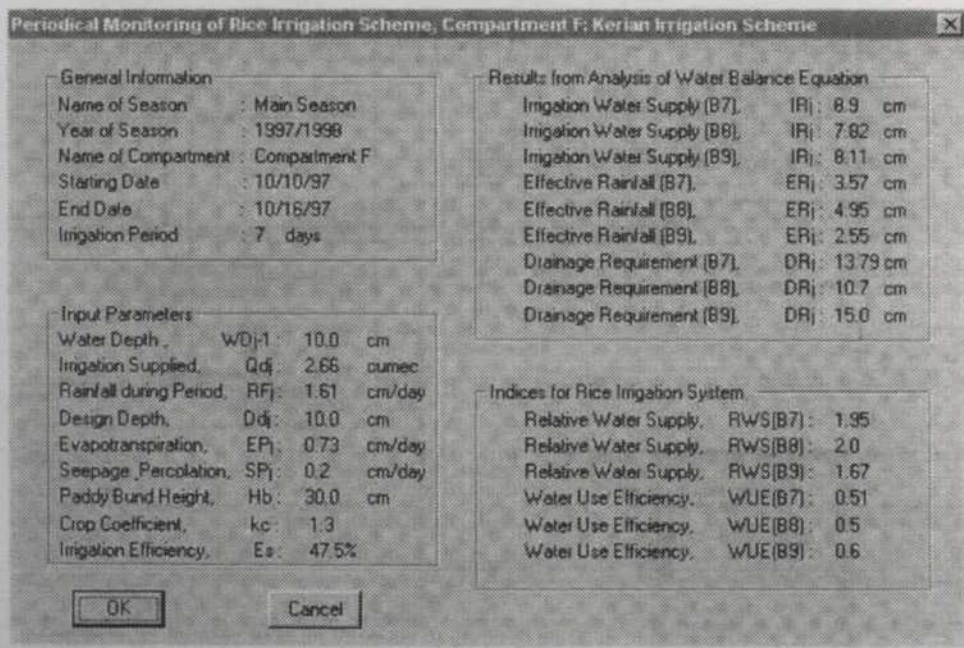

Fig. 11. Monitoring Module: Computed results for compartment F in main season, 1997/98

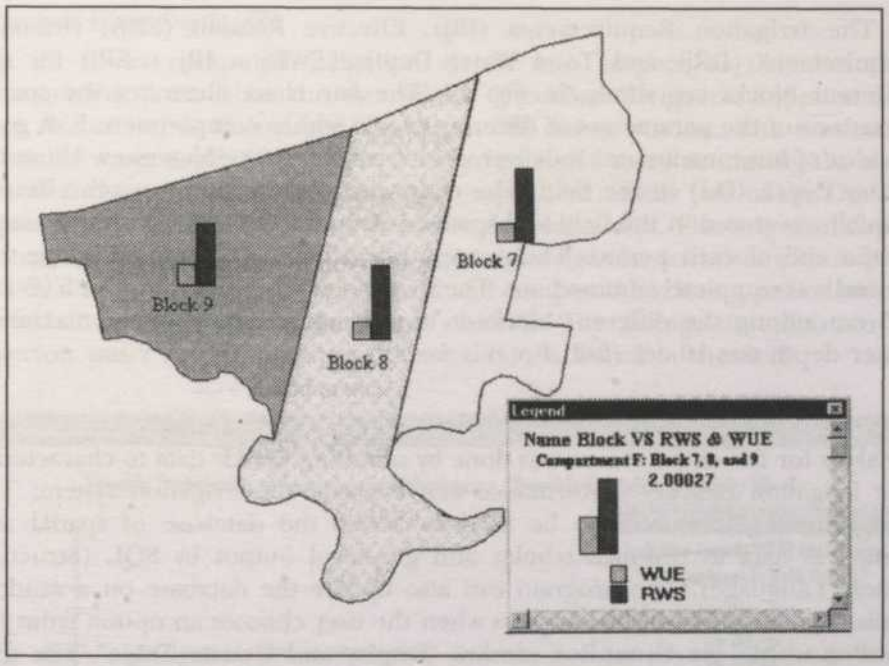

Fig. 12. Thematic Bar Chart showing the spatial variation of RWS and WUE

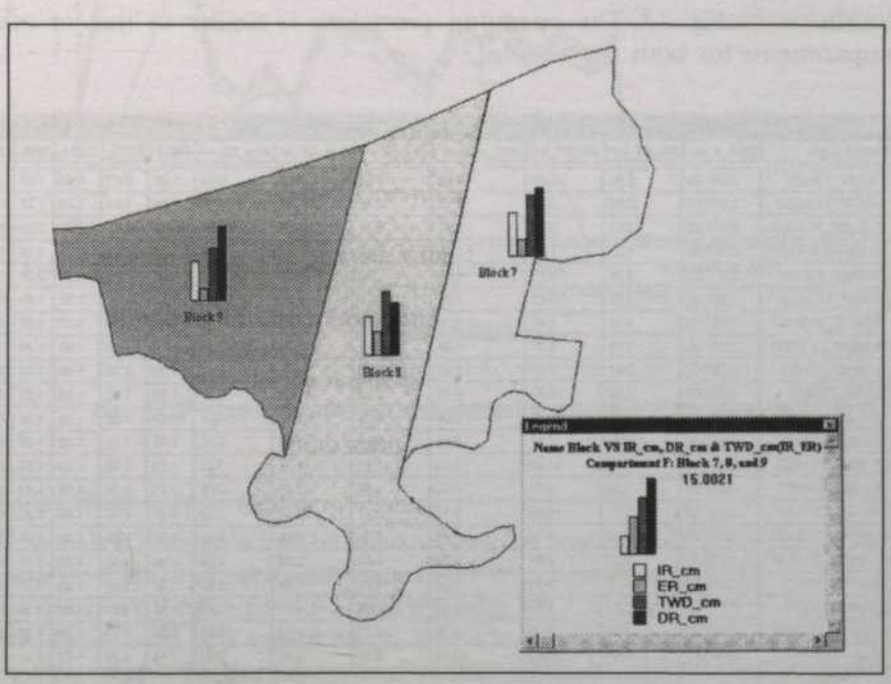

Fig. 13. Spatial variation of the IR_j, ER_j, DR_j, and TWD_j among the blocks of compartment F for a week

The Irrigation Requirements (IRj), Effective Rainfall (ERj), Drainage Requirement (DRj) and Total Water Depth (TWDj = IRj + ERj) for the different blocks are shown in *Fig. 13.* The bar chart illustrates the spatial variations of the parameters of different blocks within compartment F. It gives an idea of how much water is delivered with respect to the Maximum Allowable Water Depth (Dd) in the field. The chart also illustrates how much effective rainfall was stored in the field and spatial distribution of drainage requirement at the end of each period. The average rainfall of 1.61 cm/day during that period was completely drained out. The irrigation deliveries were 6.98, 5.95 and 6.5 cm among the different blocks in the compartment F where maximum water depth was 10 cm (full) for this week.

Post-season Analysis of the Irrigation System

Analysis for the entire season was done by summing weekly data to characterize the irrigation delivery performance and evaluate the irrigation system. The programming modules can be used to access the database of spatial and temporal data to produce tabular and graphical output by SQL (Structure Query Language). The program can also update the database on a random basis. The browser window displays when the user chooses an option from the ListBox within the GroupBox window "Display and Update Table". The user can update weekly information during ongoing seasons through options available in the dialog windows. The analyzed data for the main season of compartment F is shown in *Fig. 14.* The operation procedure is similar to that of other compartments for both the seasons.

CompartF_MS Browser

Period_Days	CCA_F_ha	SW_ET_cm	SW_RF_cm	DWS_cumec	Avg_IR_cm	Avg_DR_cm	Avg_ER_cm	RWS7	RWS8	RWS9	RWS	WUE
1 Aug97_7 Aug97	2,697.00	2.60	0.00	3.93	4.22	0.13	0.00	1.06	0.93	1.03	1.01	1.00
8 Aug97_14 Aug97	2,697.00	3.85	0.00	6.13	6.72	1.48	0.00	1.76	1.54	1.70	1.67	0.60
15 Aug97_21 Aug97	2,697.00	3.57	3.08	8.49	9.11	4.22	2.02	2.32	2.12	2.27	2.24	0.45
22 Aug97_28 Aug97	2,697.00	4.27	7.98	7.93	8.52	8.82	3.72	2.22	2.07	2.18	2.16	0.46
29 Aug97_4 Sep97	2,697.00	4.46	4.13	8.31	8.92	4.20	2.81	2.67	1.92	2.03	2.21	0.46
5 Sep97_11 Sep97	2,697.00	3.85	9.45	4.92	5.28	9.49	3.37	1.69	1.59	1.67	1.65	0.61
12 Sep97_18 Sep97	2,697.00	3.15	1.47	4.29	4.58	1.50	1.11	1.29	1.19	1.27	1.25	0.80
19 Sep97_25 Sep97	2,697.00	3.78	4.27	4.84	5.19	4.31	2.33	1.50	1.40	1.48	1.46	0.69
26 Sep97_2 Oct97	2,697.00	2.94	2.17	4.07	4.37	2.21	1.44	1.38	1.28	1.36	1.34	0.75
3 Oct97_9 Oct97	2,697.00	5.18	10.57	6.18	6.64	10.62	4.05	1.66	1.56	1.64	1.62	0.62
10 Oct97_16 Oct97	2,697.00	4.97	11.27	5.99	6.43	11.32	4.07	1.68	1.59	1.66	1.64	0.61
17 Oct97_23 Oct97	2,697.00	4.83	3.57	5.86	6.29	3.62	2.26	1.41	1.31	1.39	1.37	0.73
24 Oct97_30 Oct97	2,697.00	4.06	11.62	5.16	5.53	11.66	3.72	1.73	1.63	1.70	1.68	0.59
31 Oct97_6 Nov97	2,697.00	3.43	3.57	4.52	4.85	3.61	2.04	1.47	1.38	1.45	1.43	0.70
7 Nov97_13 Nov97	2,697.00	5.11	10.08	6.12	6.57	13.13	2.13	1.38	1.27	1.35	1.33	0.75
14 Nov97_20 Nov97	2,697.00	4.62	6.18	5.49	6.04	8.20	2.02	1.39	1.28	1.36	1.34	0.75
21 Nov97_27 Nov97	2,697.00	5.25	2.87	6.22	6.68	2.92	1.99	1.35	1.25	1.33	1.31	0.76
28 Nov97_4 Dec97	2,697.00	4.27	5.60	5.34	5.73	7.64	1.82	1.37	1.27	1.35	1.33	0.75
5 Dec97_11 Dec97	2,697.00	5.32	3.08	5.95	6.39	4.13	1.74	1.32	1.22	1.30	1.29	0.78
12 Dec97_18 Dec97	2,697.00	4.27	4.55	5.34	5.72	6.59	1.63	1.34	1.23	1.31	1.29	0.77
19 Dec97_25 Dec97	2,697.00	5.04	0.70	5.70	6.12	0.75	0.65	1.15	1.04	1.13	1.11	0.90

Fig. 14. Database for main season of the compartment F in the browser window

Irrigation Water Depth (IR_j)

Fig. 15 shows computed irrigation depth with respect to the desirable management limits when the user selects CheckBox "Irrigation Supplied and Max. Water Depth Maintained, cm" from the dialog window. The maximum allowable water depth (Dd) in the field varies from 0 to 10 cm during the crop season and starts from the origin of the graph. The middle part of the Dd line represents the peak crop water demand during the season. The irrigation depth among the blocks of a compartment shows the irrigation deliveries with respect to Dd. The gap between the lines of Dd and computed IR during peak demand period illustrates the contribution of rainfall. The savings in utilization of reservoir water can be significant if more rain is stored in the field.

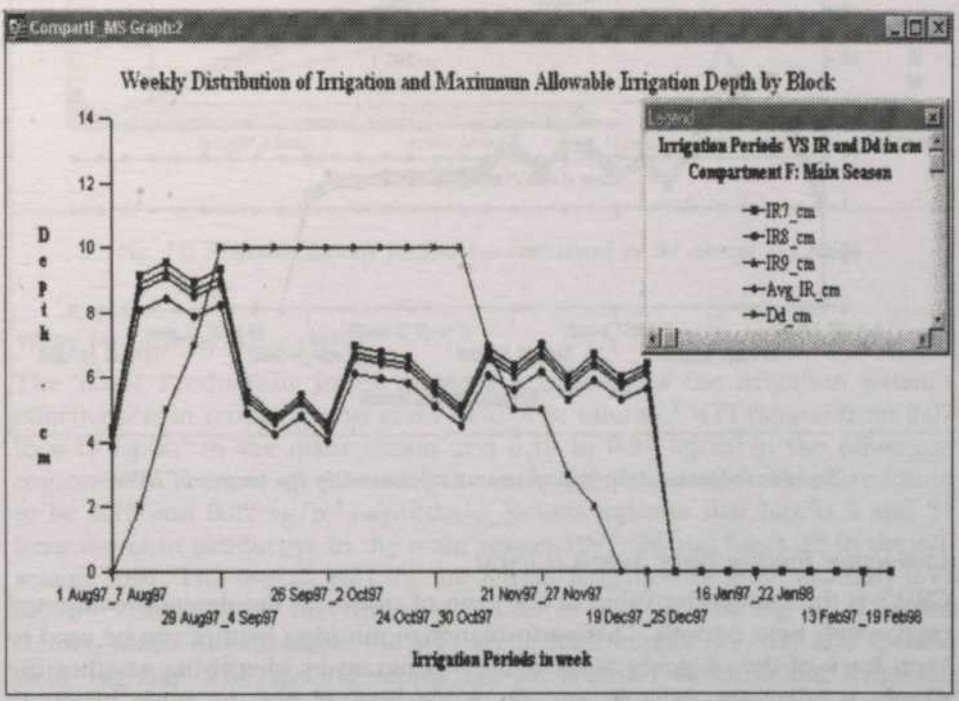

Fig. 15. Irrigation requirement and maximum allowable irrigation depth

Relative Water Supply, RWS

The weekly RWS values for the main season are represented in *Fig. 16.* In order to analyse the actual performance, actual RWS values have been compared with the critical RWS value for 1.0 and RWS value for 1.5. If RWS = 1.0 at any given week, at the level of a typical block, then the implication is that the combined irrigation supply by the system and rainfall in that week exactly matches the actual demand. RWS value for a particular week should be between above 1.0

to 1.5 for an adequate supply relative to demand. RWS values higher than this range indicate over supply and a value lower than the critical level indicates under supply.

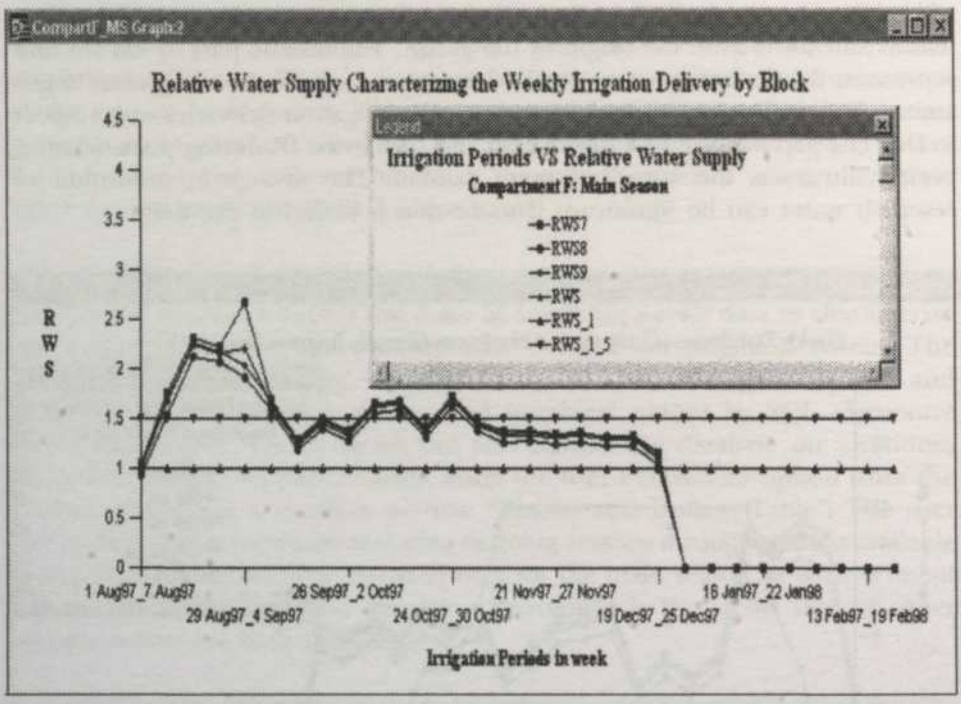

Fig. 16. Irrigation delivery performance represented by the concept of RWS

Cumulative Relative Water Supply (CRWS)

CRWS is the cumulative value of the ratio of supply to the demand computed over weekly time periods. This performance monitoring feature can be used to keep track of the on-going water delivery program by identifying whether the supply is adequate, reliable and equitable and, if not, to apply necessary adjustments and management interventions to rectify the situation. This is shown in *Fig. 17.* In adopting the CRWS curves, it is possible to select an operational range of upper and lower bound RWS values. The upper bound value may be determined assuming there is no rainfall whilst the lower bound value indicates that even if rainfall occurs, it has to be maintained either at RWS = 1.0 or at a slightly higher. If there is an increasing slope of the CRWS curve with CRWS being closer to the upper bound value it means that irrigation supply can be slightly curtailed in the next period. On the other hand, if the slope is downwards and is reaching the lower bound value, supply has to be increased to maintain it within the desired boundaries.

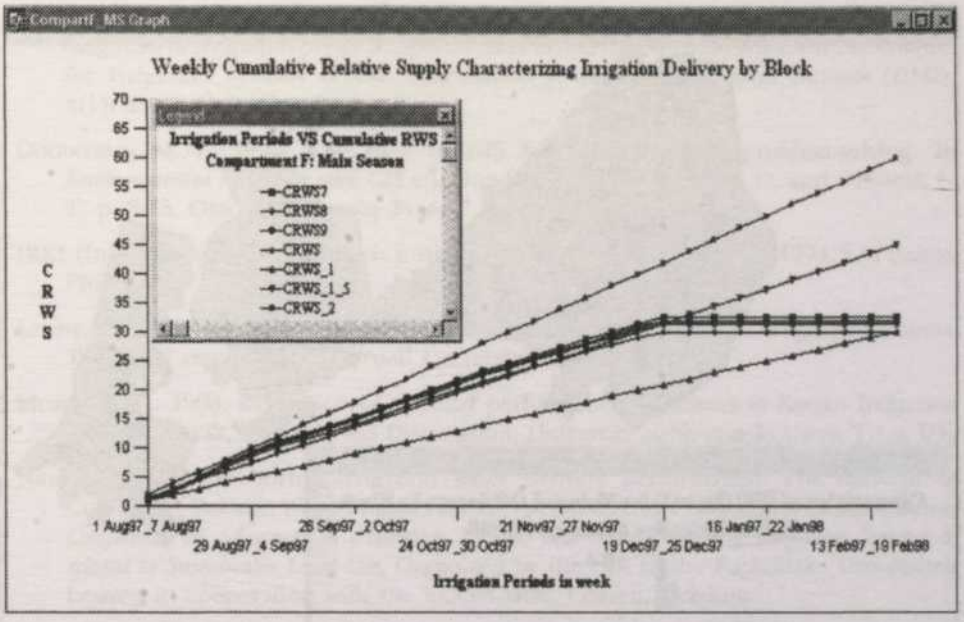

Fig. 17. Irrigation delivery performance represented by the concept of CRWS

Water Productivity Index (WPI)

The Water Productivity Index provides a measure of the irrigation system's effectiveness in terms of gross grain yield. The values of WPI ranged from 0.07 to 0.19 kg/m^3 in the main season and 0.10 to 0.31 kg/m^3 in the off-season respectively. The average values for the main season and off-season were found to be 0.13 and 0.22 kg/m^3 respectively. Results indicate that blocks 3 and 21 were the most productive in the main season 1997/98 and block 15 in the off-season 1997. The overall WPI for the Kerian Irrigation Scheme was only 0.17 kg/m^3. This is below the desirable targets of 0.30 to 0.60 kg/m^3. The two factors, which directly affect the WPI are specific supply (m^3/ha) and specific yield (kg/ha). The specific supply can be reduced by curtailing irrigation deliveries during the rainy days. With the effective use of irrigation and rainfall, better yield targets for water productivity from 0.30 to 0.60 kg/m^3 can be within reach.

CONCLUSION

The development of sustainable rice farming depends on the urgent necessity of achieving sustainable management of water resources. Improved management of water allocation systems, monitoring techniques and post-season analysis in the existing irrigation scheme using advanced technology such as Geographical Information System (GIS) can greatly help to achieve efficient water management

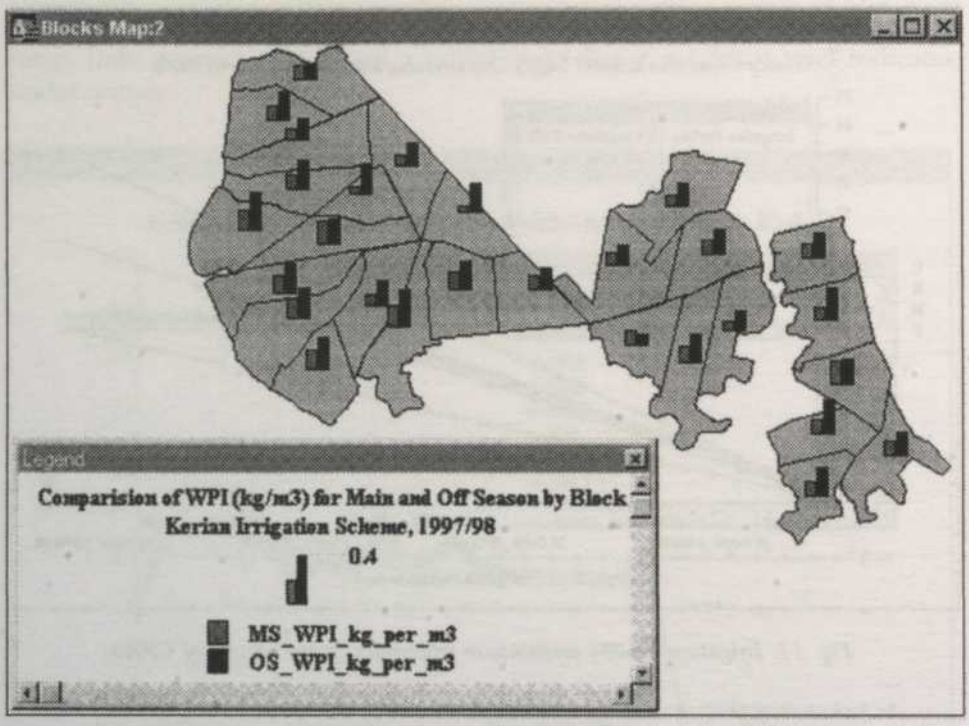

Fig. 18. Seasonal WPI by the thematic bar chart on the block layer

and targeted rice production. GIS interface is suitable as its features allow it to process and analyze a vast amount of spatially distributed information. This study would be useful for improving the irrigation system management when combined with actual feedback from the field.

ACKNOWLEDGEMENTS

The authors are indebted to the Ministry of Science, Technology and Environment, Government of Malaysia for funding this work through an IRPA Grant (Project No. 01-02-04-131), and to the Department of Irrigation and Drainage, Ministry of Agriculture, Malaysia for their assistance in data collection.

REFERENCES

ANON. 1998. JICA and DID Report. The study on modernization of irrigation water management system in the granary areas of Peninsular Malaysia. Nippon Koei Co., Ltd.

BRADLEY, R. L. 1993. Geographical information systems for agricultural decision support. *Agric. Eng.* **48:** 102-105.

FRANCOIS, M. and K. PONGPUT. 1997. NAGA- A GIS based software for the monitoring and diagnosis of irrigation projects. Special Issue on RS and GIS, Information Techniques for Irrigation Systems (ITIS). *International Irrigation Management Institute* (IIMI), **4(1)**: 23-25. Colombo, Sri Lanka.

GOODCHILD, M. F. 1993. The state of GIS for environmental problem-solving. In *Environmental Modeling with GIS* ed. Goodchild, M. F., Parks, B. O. and Steyaert, L. T. p. 8-15. Oxford University Press.

IRRI (International Rice Research Institute). 1977. Annual Report for 1974. Los Banos, Philippines.

LEVINE, G. 1982. Relative water supply: An explanatory variable for irrigation systems, Technical report no. 6, Cornell University, New York.

MORRIS, K. A. 1993. Evaluation of selected performance indicators at Kerian Irrigation Scheme, Perak, Malaysia. MS Dissertation, University of Newcastle Upon Tyne, UK.

NIHAL F. 1992. Monitoring irrigation water delivery performance: The concept of Cumulative Relative Water Supply (CRWS). p. 525-534. In *Proceedings of an International Conference on Advances in Planning, Design, and Management of Irrigation Systems as related to Sustainable Land Use*, Organized by the CIE of the Katholieke Universiteit Leuven in cooperation with the ECOWARM, Leuven, Belgium.

SALMAN, A., Y. CHEMIN and A. SAMIA. 1997. Using GIS and RS to monitor and evaluate irrigation and drainage projects: Example from IIMI Pakistan National Program. Special Issue on RS and GIS, Information Techniques for Irrigation Systems (ITIS), *International Irrigation management Institute* (IIMI). **4(1)**: 19-20. Colombo, Sri Lanka.

TEOH, B. P. 1995. Assessment of selected performance indicators for paddy irrigation schemes. p. 125. Department of Drainage and Irrigation, Perak Darul Ridzuan.

TEOH, B. P. and T. D. NGOH. 1997. Drainage problems in Kerian irrigation scheme. In *Proceedings of 7th ICID International Drainage Workshop*, vol. 3. Penang, Malaysia. p. M14-1 to M15-15.

WYSEURE, G. C. L and J. W. GOWING. 1992. Field studies in Malaysia: A joint program by Universiti Pertanian Malaysia and University Newcastle Upon Tyne. Pages. In *An International Proceedings on Advances in Planning, Design, and Management of Irrigation Systems as Related to Sustainable Land Use*, Leuven, Belgium, 14-17 September 1992. Organized by the CIE of the Katholieke Universiteit Leuven in cooperation with the ECOWARM.

WYSEURE, G. C. L., KWOK CHEE YAN, J. W. GOWING and A. A. ZAKARIA. 1994. Performance evaluation of paddy irrigation: A case study at Kerian Irrigation Scheme, Malaysia. p. 17-20. Institution of Agricultural Engineers, Winter.

Pertanika J. Sci. & Technol. 10(2): 229 - 250 (2002)
ISSN: 0128-7680

Instability Analysis of the Jamuna River, Bangladesh

Md. Hazrat Ali[1] & Harumichi Kyotoh[2]
[1]Department of Civil Engineering,
Bangladesh Institute of Technology (BIT), Chittagong,
Chittagong-4349, Bangladesh
E-mail: md_hazrat_ali@yahoo.com
[2]Institute of Engineering Mechanics,
University of Tsukuba, Ibaraki 305, Japan

Received: 26 November 1999

ABSTRAK

Perubahan-perubahan besar yang berlaku pada topografi dasar dan planform Sungai Jamuna, Bangladesh, khususnya semasa musim banjir, dan kesan perubahan-perubahan tersebut diselidiki dalam kertas ini dalam bentuk satu analisis stabiliti oleh teknik pengganggguan. Satu model pengangkutan keladak dan aliran dua dimensi di dalam sebuah sungai yang mengandungi aluvium dengan dasar yang terhakis dan tebingnya tidak terhakis dibangun dan digunakan di Sungai Jamuna, Bangladesh. Kesan gerakan berpilin disebabkan oleh kelengkungan saluran tegasan ricih dasar, dan kesan rintangan geseran akibat bentuk dasar diambil kira dalam model tersebut. Model 2-D boleh digunakan untuk memeriksa ketidakstabilan disebabkan oleh dasar mengandungi aluvium yang dilitupi bukit pasir. Satu teori kestabilan dibangunkan yang menentukan mod tak stabil, kepantasan dan rambatan bukit pasir, dan nombor gelombang sejajar dengan ketidakstabilan maksimum. Teori tersebut juga boleh membezakan antara fenomena gabungan dan berkelok-kelok. Beberapa implikasi model yang dicadangkan juga dibincangkan. Model yang dicadangkan digunakan untuk menganalisis kedua-dua paten sungai iaitu berkelok-kelok. Hasil daripada analisis Sungai Jamuna menunjukkan bahawa ketidakstabilan maksimum kerana aspek nisbahnya yang sangat rendah dan lebih daripada tiga gabungan.

ABSTRACT

Major changes take place in the planform and bed topography of the Jamuna River, Bangladesh, particularly during the flood season, and the effect of these changes are investigated in this paper in the form of a stability analysis by perturbation technique.

A two-dimensional model of flow and sediment transport in an alluvial river with erodible bed and non-erodible banks is developed and applied to the Jamuna River, Bangladesh. The effect of transverse slope resulting from the effect of secondary currents, the effect of spiral motion due to curvature of the channel on the bed shear stress, and the effect of frictional resistance occurring from pure skin friction and friction due to bedforms, are considered in the model. The 2-D model can be used to check the instability due to the dune-covered alluvial bed. A stability theory has been developed which determines the most unstable mode, the celerity and propagation of the sand dunes, and the wavenumber corresponds to maximum instability. The theory is also capable of differentiating between braiding and meandering phenomena.

Several implications of the proposed model are also discussed. The proposed model is used to analyze both the meandering and braided patterns of the river. The results from the analyses of the Jamuna River show that instability always exists in the Jamuna River under maximum instability conditions because of its very low aspect ratio (≈1/1000) and more than three braids.

Keywords: Instability, perturbation technique, dune-covered bed, 2-D model, aspect ratio

INTRODUCTION

The Jamuna River is the lowest reach of the Brahmaputra River, a large braided sand-bed river. The numbers of braids during low flow vary between 2 and 3 and the total width of the channel patterns ranges from 5 to 17 km. Leopold and Wolman (1957) made clear that the slope and discharge characterize the braiding. Consequently, the presence of a sequence of bifurcation and confluence is considered to be an essential feature for braided rivers. Sedimentation also plays an important role in developing braiding.

River channels possess three characteristic fluvial morphologies: straight, meandering and braiding. Braided rivers are defined as rivers containing more than one (low-flow) channel and bar/island in between the channels. A braided pattern probably brings to the minds of many authors, the concept of an aggrading stream. It has been observed that the banks of braided rivers are generally straighter than that of meandering rivers. Leopold and Wolman (1957) plotted bankfull discharge against channel slope and derived an equation for separation between braiding and meandering, i.e. $i = 0.0116 Q_b^{-0.44}$, where Q_b is the bankfull discharge in m^3/s and i is the channel slope. A river would be braided if its slope is above the threshold slope. Parker (1976) demonstrated that sediment transport and channel frictions are the essential features for the occurrence of fluvial instability. According to him, a river would follow meandering, transition from meandering to braiding, and braiding, depending on the degree of instability and the relationship between $\frac{S}{F}$ and $\frac{d_0}{B}$, where S is the local energy slope, F is the Froude number, d_0 is the mean water depth, and B is the channel width. He confirmed that meandering streams usually have gentle slopes and rather narrow channels, while braided streams generally have steep slopes and wide channels. He introduced bed perturbations into the balance equations and concluded that instability requires $\phi_i > 0$, where ϕ_i is the imaginary part of the complex celerity, ϕ. He deduced the bed patterns corresponding to various values of number of braids m and presented that for $m = 1$, the bed pattern consisting of a single braid of submerged alternating bars characteristic of the early stages of meandering. Increased values of m imply an increased tendency towards incipient braiding, with m equaling the number of braids. Thus, a range of wavenumbers for which ϕ_i is positive, always exists and instability characteristics of meandering or braiding always occur. Engelund and Skovgaard (1973) introduced the effect of a transverse bed slope on the sediment transport and found that this effect is of great significance, because

the theory predicts that the river will braid into an infinite number of branches if it is not included.

In this paper, a linear stability analysis of the Jamuna River by perturbation technique, investigation of fluvial instability, and differentiation between braiding and meandering regimes, will be presented in the following sections.

GOVERNING EQUATIONS

The flow in an alluvial channel with erodible bed and impermeable banks is considered. It is further considered that the flow is basic (undisturbed) on which a bed perturbation is superimposed. The momentum and mass balance equations in the x and y directions over this periodic bed (*Fig. 1*) are described as follows:

$$\frac{\partial u}{\partial t} + u\frac{\partial u}{\partial x} + v\frac{\partial u}{\partial y} = -g\frac{\partial H}{\partial x} - \frac{\tau_x}{\rho d} \tag{1}$$

$$\frac{\partial v}{\partial t} + u\frac{\partial v}{\partial x} + v\frac{\partial v}{\partial y} = -g\frac{\partial H}{\partial y} - \frac{\tau_y}{\rho d} \tag{2}$$

$$\frac{\partial}{\partial x}(ud) + \frac{\partial}{\partial y}(vd) + \frac{\partial d}{\partial t} = 0 \tag{3}$$

$$\frac{\partial (H-d)}{\partial t} + \frac{1}{1-\lambda_p}\left(\frac{\partial q_x}{\partial x} + \frac{\partial q_y}{\partial y}\right) = 0 \tag{4}$$

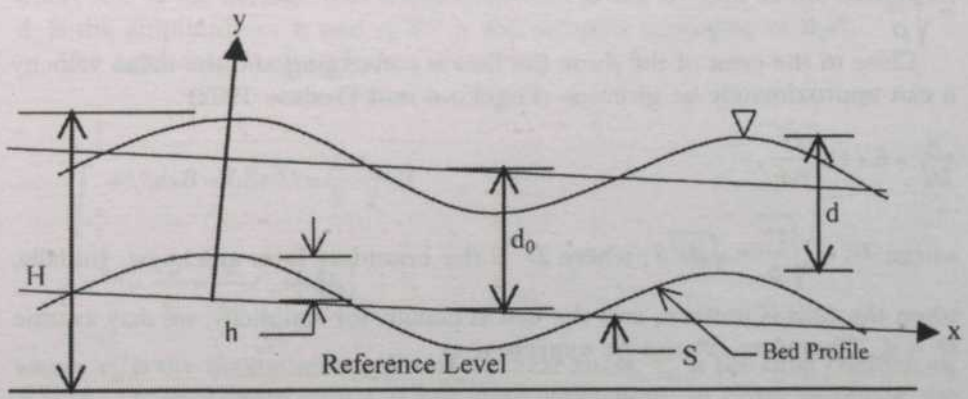

Fig. 1: Definition sketch

where u and v are the velocity components in the x and y directions, d is the local water depth, H is the water surface elevation above reference level, g is the acceleration due to gravity, ρ is the density of water, τ_x and τ_y are the local bed shear stress components in the x and y directions, q_x and q_y are the sediment

transports per unit width of the channel in the x and y directions, t is time, and λ_p is the bed-material porosity. Eqns. (1), and (2) are valid if the vertical accelerations of the fluid are ignored (hydrostatic pressure), if vertical variations of the velocity are neglected and if the tractive force on the bed has the direction of the velocity vector.

Constitutive Relations

The variation of the friction factor with flow velocity in a river channel is rather complicated because different bedforms exist for different flow conditions. Perturbations about a steady flow with dune covered bed are to be considered. In this study, this effect is considered based on the drag force coefficient and the shear stress due to bedforms is considered to change with time and space.

The total bed shear stress τ is equal to the sum of pure skin friction $\tau^{\wedge}$ and friction due to bedforms $\tau^{\wedge\wedge}$, i.e.

$$\tau = \tau^{\wedge} + \tau^{\wedge\wedge} \tag{5}$$

The Shields parameter can be given by

$$\theta = \frac{U_*^2}{(s-1)gd_s} = \frac{\tau}{\rho(s-1)gd_s} \tag{6}$$

where θ is the Shields parameter, s is the relative density, d_s is the size of the sediment grain, assumed to be constant, and U_* is the friction velocity = $\sqrt{gd_0S}$ $= \sqrt{\frac{\tau}{\rho}}$.

Close to the crest of the dune the flow is converging and the mean velocity u can approximately be given as (Engelund and Fredsoe 1982)

$$\frac{u}{U_*'} = 6 + 5\ln\frac{D'}{5d_s},$$

where $U_*' = \sqrt{\frac{\tau^{\wedge}}{\rho}} = \sqrt{gD'S}$, where D' is the boundary layer thickness. Initially, when the flow is uniform and the bed is planar, for simplicity, we may assume $D' = d$. Therefore, $\tau^{\wedge}$ can be expressed as

$$\tau^{\wedge} = \rho(U_*')^2 = \rho\left(\frac{u}{6 + 2.5\ln\frac{d}{2.5d_s}}\right)^2 = f(u,d) \tag{7}$$

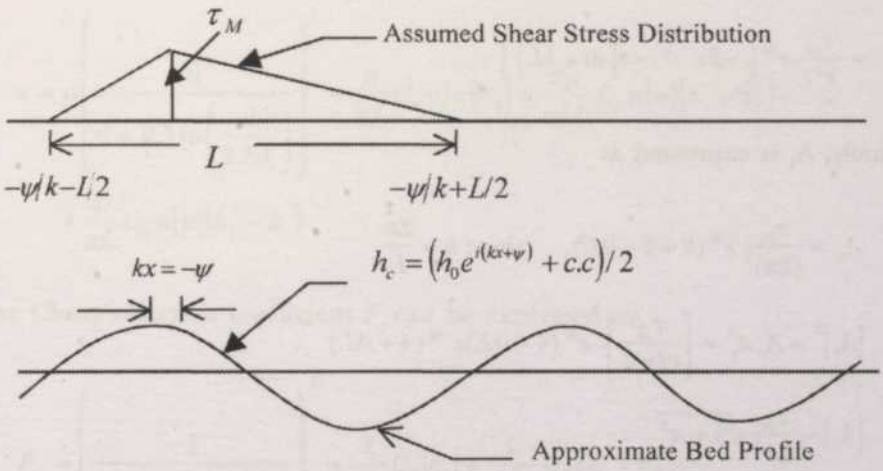

Fig. 2: Approximate bed profile and assumed shear stress distribution

For simplicity, the shear stress distribution can be approximated by *Fig. 2* and its peak is assumed to occur at lag $kx = -\psi$ from the peak of the bedform. The maximum stress generally occurs at flow separation point and is assumed to be τ_M. In *Fig. 2*, c.c is the abbreviation of complex conjugate. Applying Fourier series expansion, $\tau^{\wedge\wedge}$ can be expressed as

$$\tau^{\wedge\wedge} = \tau^{\bar{\wedge}\wedge} + A_\tau e^{ikx} + A_\tau^* e^{-ikx}$$

where $\tau^{\bar{\wedge}\wedge}$ is the average unit shear stress due to the friction of the bedforms, A_τ is the amplitude of τ, and $A_\tau^* e^{-ikx}$ is the complex conjugate of $A_\tau e^{ikx}$.

The total drag is given by

$$\int_{-\frac{\psi}{k}-\frac{L}{2}}^{-\frac{\psi}{k}+\frac{L}{2}} \tau^{\wedge\wedge} dx B = LB\tau^{\bar{\wedge}\wedge} = \frac{L}{2}\frac{\tau_M}{2}B$$

$$\therefore \tau^{\bar{\wedge}\wedge} = \frac{\tau_M}{4} = \frac{\rho}{2L} C_D u|u||h_0|$$

where τ_M is the maximum amplitude of shear stress, C_D is the drag coefficient, B is the channel width, and L is the dune wavelength. In order to obtain the amplitude A_τ, the integration is considered as follows:

$$\int_{-\frac{\psi}{k}-\frac{L}{2}}^{-\frac{\psi}{k}+\frac{L}{2}} \tau^{\wedge\wedge} e^{-ikx} dx = LA_\tau = \int_{-\frac{\psi}{k}-\frac{L}{2}}^{-\frac{\psi}{k}+\frac{L}{2}} \left\{\tau_M - \frac{\tau_M}{L/2}\left(x+\frac{\psi}{k}\right)e^{-ikx}\right\} dx$$

$$= \frac{\tau_M}{k^2 L} e^{i\psi} \left(-2e^{-\frac{ikL}{2}} - i\{2i + kL\} \right)$$

Finally, A_τ is expressed as

$$A_\tau = \frac{\tau_M}{(2\pi)^2} e^{i\psi}(2 + 2 - ikL), \quad \text{since } k = \frac{2\pi}{L}$$

$$|A_\tau|^2 = A_\tau A_\tau^* = \left\{ \frac{\tau_M}{(2\pi)^2} \right\}^2 e^{i\psi}(4 - ikL) e^{-i\psi}(4 + ikL)$$

$$|A_\tau| = \frac{\tau_M}{2\pi^2} \sqrt{4 + \pi^2}$$

$$\therefore \tau^{\wedge\wedge} = \bar{\tau}^{\wedge\wedge} + A_\tau e^{ikx} + A_\tau^* e^{-ikx}$$

$$= \bar{\tau}^{\wedge\wedge} + \frac{2\tau_M}{\pi^2} \cos(kx + \psi) \tag{8}$$

To express $\tau^{\wedge\wedge}$ by bed profile, the following expression is considered:

$$e^{ikx} A_\tau = \frac{\tau_m}{(2\pi)^2}(4 - ikL) e^{i(kx+\psi)} = \frac{2\rho}{L} C_D u|u||h_0| \left(\frac{4 - ikL}{(2\pi)^2} \right) e^{i(kx+\psi)}$$

$$= \frac{2\rho}{L} C_D u|u| \left(\frac{4 - ikL}{(2\pi)^2} \right) h_c, \text{ since } h_c = |h_0| e^{i(kx+\psi)}$$

and $$e^{-ikx} A_\tau^* = \frac{\tau_M}{(2\pi)^2}(4 - ikL) \bar{e}^{i(kx+\psi)} = \frac{2\rho}{L} C_D u|u| |h_0| \left(\frac{4 + ikL}{(2\pi)^2} \right) e^{-i(kx+\psi)}$$

$$= \frac{2\rho}{L} C_D u|u| \left(\frac{4 + ikL}{(2\pi)^2} \right) h_c^*,$$

where, $h_c^* = |h_0| e^{-i(kx+\psi)}$ is the complex conjugate of h_c.

Finally, $\tau^{\wedge\wedge}$ can be expressed as,

$$\tau^{\wedge\wedge} = \frac{\rho}{2L} C_D u|u||h_0| + \frac{2\rho}{\pi^2 L} C_D u|u|(h_c + h_c^*) + \frac{i\rho}{\pi L} C_D u|u|(h_c^* - h_c) \tag{9}$$

$$\tau = \rho\left(\frac{u}{6 + 2.5\ln\left(\frac{d}{2.5d_s}\right)}\right)^2 + \frac{\rho}{2L}C_D u|u|\|h_0| + \frac{2\rho}{\pi^2 L}C_D u|u|\left(h_c + h_c^*\right) + \frac{i\rho}{\pi L}C_D u|u|\left(h_c^* - h_c\right)$$

The Chezy's friction coefficient F_c can be expressed as

$$F_C = \left(\frac{1}{6 + 2.5\ln\left(\frac{d}{2.5d_s}\right)}\right)^2 + \frac{1}{2L}C_D|h_0| + \frac{2}{\pi^2 L}C_D\left(h_c + h_c^*\right) + \frac{i}{\pi L}C_D\left(h_c^* - h_c\right) \quad (10)$$

Since $\tau = \rho F_C u|u|$

The real component of the bed height fluctuation can be given as

$$h_c = |h_0|\cos(kx + \psi)$$

The most general possible constitutive relation for Chezy's resistance can be of the form:

$$F_C = \phi_c\left(u, v, d, h_c, h_c^*, L\right) \quad (11)$$

The total sediment transport is traditionally divided into (i) bed-material load, consisting of bed load and suspended load and (ii) wash load. Ignoring wash load, the total sediment transport can be expressed in dimensionless form as

$$\phi = \frac{q}{\sqrt{(s-1)gd_s^3}} \quad (12)$$

Engelund and Hansen (1967) established a relation between the dimensionless transport parameter ϕ and the dimensionless flow parameter θ as follows:

$$F_C\phi = 0.05\theta^{5/2} \quad (13)$$

where $\phi = \dfrac{q}{\sqrt{\Delta g d_s^3}}$ (14)

where Δ is the relative density difference, and

$$\theta = \frac{\tau}{(\rho_s - \rho) g d_s} = \frac{\tau}{\rho \Delta g d_s}$$

$$= \frac{1}{\rho \Delta g d_s} \left[\rho \left(\frac{u}{6 + 2.5 \ln\left(\frac{d}{2.5 d_s}\right)} \right)^2 + \frac{\rho}{2L} C_D u|u| h_0 \right.$$
$$\left. + \frac{2\rho}{\pi^2 L} C_D u|u| \left(h_c + h_c^*\right) + \frac{i\rho}{\pi L} C_D u|u| \left(h_c^* - h_c\right) \right]$$

Rearranging terms and simplifying, ϕ can be expressed as

$$\phi = \frac{0.05}{F_c} \left(\frac{1}{\rho \Delta g d_s} \left[\rho \left(\frac{u}{6 + 2.5 \ln\left(\frac{d}{2.5 d_s}\right)} \right)^2 + \frac{\rho}{2L} C_D u|u| h_0 \right. \right.$$
$$\left. \left. + \frac{4\rho}{\pi^2 L} C_D u|u| \left(h_c + h_c^*\right) + \frac{2i\rho}{\pi L} C_D u|u| \left(h_c^* - h_c\right) \right] \right)^{\frac{5}{2}} \quad (15)$$

Combining Eqns. (14), and (15), one can obtain

$$q = \frac{K}{F_c} \left(\left[\rho \left(\frac{u}{6 + 2.5 \ln\left(\frac{d}{2.5 d_s}\right)} \right)^2 + \frac{\rho}{2L} C_D u|u| h_0 \right. \right.$$
$$\left. \left. + \frac{4\rho}{\pi^2 L} C_D u|u| \left(h_c + h_c^*\right) + \frac{2i\rho}{\pi L} C_D u|u| \left(h_c^* - h_c\right) \right] \right)^{\frac{5}{2}} \quad (16)$$

where $K = \dfrac{0.05}{\rho^{\frac{5}{2}} \Delta^2 g^2 d_s}$.

Influence of Transverse Slope on Sediment Transport

Let us consider the local direction of sediment transport with an average direction of particles trajectory that deviates an angle δ from the direction of average shear stresses under the action of gravity. Thus, one can write

$$q^* = \left(q_x, q_y\right) = (\cos\ \delta,\ \sin\ \delta)q$$

where q^* is the sediment transport parameter.

$$q_x = \frac{K}{F_C}\left(\left[\rho\left(\frac{u}{6+2.5\ln\left(\frac{d}{2.5d_s}\right)}\right)^2 + \frac{\rho}{2L}C_D u|u|h_0| + \frac{4\rho}{\pi^2 L}C_D u|u|\left(h_c + h_c^*\right) + \frac{2i\rho}{\pi L}C_D u|u|\left(h_c^* - h_c\right)\right]\right)^{\frac{5}{2}} \cos\ \delta, \text{ and}$$

$$q_y = \frac{K}{F_C}\left(\left[\rho\left(\frac{u}{6+2.5\ln\left(\frac{d}{2.5d_s}\right)}\right)^2 + \frac{\rho}{2L}C_D u|u|h_0| + \frac{4\rho}{\pi^2 L}C_D u|u|\left(h_c + h_c^*\right) + \frac{2i\rho}{\pi L}C_D u|u|\left(h_c^* - h_c\right)\right]\right)^{\frac{5}{2}} sin\ \delta$$

For relatively small values of δ, the following formula can be adapted following the equation of Engelund (1981):

$$\sin\ \delta = v\left(u^2 + v^2\right)^{-\frac{1}{2}} - \frac{r}{B\theta^{1/2}}\frac{\partial}{\partial y}(H - d)$$

where r is a constant which Engelund (1981) suggested to assume the value = (0.5-0.6). In accordance with Olesen's (1983) results, lower value of r (around 0.3) may lead to more satisfactory prediction of alternate-bar formation. Hence, the most general possible constitutive relation for sediment transport can be of the form:

$$q^* = \phi_q\left(u, d, L, h_c, \delta\right) \qquad (17)$$

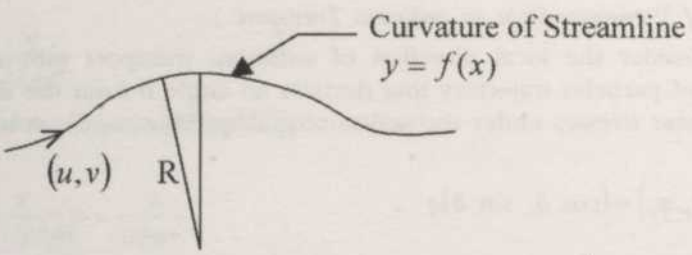

Fig. 3: Sketch of assumed curvature of streamline

The Effect of Secondary Flow Due to Curvature of River Bank

The magnitude of the secondary flow effect on the bed shear stress can be approximated as $\frac{A_1 d_o}{R}$, where A_1 is a constant, and R is the radius of curvature. R can be approximated as

$$\frac{1}{R} \cong f^{11} = \frac{d}{dx}\left(\frac{v}{u}\right) = \frac{\frac{dv}{dx}u - v\frac{du}{dx}}{u^2}$$

Now, $$\frac{dv}{dx} = \frac{\partial v}{\partial x} + \frac{\partial v}{\partial y}\frac{\partial y}{\partial x} = \frac{\partial v}{\partial x} + \frac{v}{u}\frac{\partial v}{\partial y}$$

Similarly, $$\frac{du}{dx} = \frac{\partial u}{\partial x} + \frac{v}{u}\frac{\partial u}{\partial y}$$

$$\therefore \frac{1}{R} = \frac{1}{u^2}\left(u\frac{\partial v}{\partial x} - v\frac{\partial u}{\partial x}\right)$$

Since $u = U + u'$, and $v = v'$

$$\frac{1}{R} \cong \frac{1}{U^2} = \left(U\frac{\partial v'}{\partial x}\right) \cong \frac{1}{U}\frac{\partial v'}{\partial x} \qquad (18)$$

The Perturbed Equations of Motion

The balance equations are considered for slight perturbations about steady uniform flow, i.e.

$$u = U + \varepsilon u'(t, x, y), \qquad v = \varepsilon v'(t, x, y),$$

$$d = d_o + \varepsilon d'(t, x, y), \qquad h_c = 2\varepsilon h'(t, x, y),$$

$$|u| = \sqrt{u^2 + v^2}, \qquad H = d_0 - Sx + \varepsilon h'(t, x, y) + \varepsilon d'(t, x, y),$$

$$F_C = \left(\frac{1}{6 + 2.5 \ln\left(\frac{d}{2.5 d_s}\right)} \right)^2 + \frac{1}{2L} C_D |h_0| + \frac{2}{\pi^2 L} C_D \left(h_c + h_c^*\right) + \frac{i}{\pi L} C_D \left(h_c^* - h_c\right),$$

$$\tau_x = \rho F_C \left(\sqrt{u^2 + v^2}\right) u, \qquad \tau_y = \rho F_C \left(\sqrt{u^2 + v^2}\right) v,$$

$$\theta = \frac{\tau_x}{\rho \Delta g d_s}, \qquad q = \frac{K \tau_x^{\frac{5}{2}}}{F_c},$$

$$q_x = q \cos \delta, \qquad q_y = q \sin \delta,$$

$$\delta = \varepsilon \delta'(t, x, y),$$

$$\delta'(t, x, y) = Lim_{\varepsilon \to 0} \frac{\partial}{\partial \varepsilon} \left[v\left(u^2 + v^2\right)^{-\frac{1}{2}} - \frac{r}{B\theta^{\frac{1}{2}}} \frac{\partial}{\partial y}(H - d) - \frac{A_1 d_0}{U} \frac{\partial}{\partial x} v'(t, x, y) \right]$$

where $\frac{\left(u'^2 + v'^2\right)^{\frac{1}{2}}}{U} << 1$. In the equation of $\delta'(t, x, y)$, the last term $\frac{A_1 d_0}{U} \frac{\partial}{\partial x} v'(t, x, y)$ is the effect of spiral motion on the bed shear stress due to the effect of the curvature of the river banks and the first two terms are due to the effect of the transverse slope of the sediment transport as explained before. If these perturbations are inserted into the steady uniform flow and put $\varepsilon \to 0$, zero-order perturbed equations will be obtained. Similarly, if these perturbations are inserted into the steady uniform flow, thereafter differentiate with respect to ε and set $\varepsilon \to 0$ gives first-order perturbed equations.

Stability of Spatially Periodic Disturbance

In this section, the stability of the river meandering and braiding will be discussed. To conduct a stability analysis, the following generalized sinusoidal perturbations are introduced into the balance equations:

$$\left.\begin{aligned} u' &= \hat{u}(y) \exp i\left(kx - \phi t\right)/2 \qquad v' = \hat{v}(y) \exp i\left(kx - \phi t\right)/2 \\ h' &= \hat{h}(y) \exp i\left(kx - \phi t\right)/2 \qquad d' = \hat{d}(y) \exp i\left(kx - \phi t\right)/2 \end{aligned}\right\} \tag{19}$$

Here, k is the dimensionless fluvial instability wavenumber, related to dimensional wavelength L by the relation $k = 2\pi/L$, and ϕ is the complex celerity, its real part

ϕ_r being related to the disturbance wave speed c by $c = \phi_r / L$, and its imaginary part ϕ_i being the temporal exponential growth rate. Instability requires that $\phi_r > 0$.

These perturbations will be introduced into the balance equations and are reduced with the aid of the boundary condition of impermeable banks; i.e. $v = 0$ at $y = \pm B/2$. The sidewalls will suppress the growth of the lateral disturbance.

As a result, for odd number of braids (m = 1, 3, 5, ...), it is found that $\hat{u}$, $\hat{v}$, $\hat{d}$, $\hat{h}$ can take the following forms:

$$\hat{u}(y) = \hat{u} \sin(k_B y), \qquad \hat{v}(y) = \hat{v} \cos(k_B y),$$
$$\hat{d}(y) = \hat{d} \sin(k_B y), \qquad \hat{h}(y) = \hat{h} \sin(k_B y)$$

In these equations, $k_B = m\pi/B$, and m is the number of braids. For $m = 1$, the bed pattern consists of a single braid of submerged alternating bars, i.e., the case of meandering river. Increasing values of m imply an increased tendency towards incipient braiding and increased instability.

After inserting sinusoidal perturbations and their forms into the basic equations, the resulting nonlinear algebraic equation (Eigen equation) for the complex celerity ϕ is obtained as follows:

The complex celerity ϕ must satisfy the dispersion equation (Eigen equation), i.e., Eqn. 20.

$$0.0625\phi^4 + \frac{10678.8k^2Km^2U^5}{B^3} + \frac{109375ik^3Km^2U^5}{B^3} + \frac{210791Km^4U^5}{B^5}$$
$$+ \frac{1.07949 \times 10^6 ikKm^4U^5}{B^5} + 570.457ik^3KU^6 + (163489 + 107800i)k^4KU^6$$
$$+(-1.10412 \times 10^6 + 1.73435 \times 10^6 i)k^5KU^6 - \frac{2321.96ikKm^2U^6}{B^2}$$
$$+ \frac{(-1.12784 \times 10^6 - 709297i)k^2Km^2U^6}{B^2}$$
$$+ \frac{(-1.08972 \times 10^7 + 1.71173 \times 10^7 i)k^3Km^2U^6}{B^2} + \frac{30.9806ikKm^2U^7}{B^3}$$
$$- \frac{417.64k^2Km^2U^7}{B^3} - \frac{1027.59ik^3Km^2U^7}{B^3} + (32.9612 - 51.7753i)k^3KU^8$$
$$+(-1060.59 - 675.195i)k^4KU^8 + (10373.3 - 16294i)k^5KU^8$$
$$+\phi\left(0.0183065iU - 0.1875kU + \frac{1027.59iKm^2U^4}{B^3} + (-10373.3 + 16294.3i)k^2KU^5\right)$$

$$+\phi^2\left(\begin{array}{l}-6.65241k^2-\dfrac{65.6566m^2}{B^2}-0.00119156U^2-0.0437082ikU^2+0.1875k^2U^2\\-5570.8k^2KU^4-\dfrac{10996.3Km^2U^4}{B^2}-\dfrac{300.985Km^2U^5}{B^3}-\dfrac{3082.77ikKm^2U^5}{B^3}\\+(530.297+337.598i)k^2KU^6+(31119.9-48883i)k^3KU^6\end{array}\right)$$

$$+\phi\left(\begin{array}{l}-0.649505ik^2U+6.6524k^3U-\dfrac{12.8207im^2U}{B^2}+\dfrac{65.6566km^2U}{B^2}\\+0.0018843kU^3+0.0254017ik^2U^3-0.0625k^3U^3-\dfrac{109375ik^2Km^2U^4}{B^3}\\-\dfrac{1.07949\times10^6iKm^4U^4}{B^5}-543.903ik^2KU^5+11413.6k^3KU^5\\+(1.10412\times10^6-1.73435\times10^{6i})k^4KU^5-\dfrac{2147.24iKm^2U^5}{B^2}\\+\dfrac{24676.9kKm^2U^5}{B^2}+\dfrac{(1.08972\times10^7-1.71173\times10^7i)k^2Km^2U^5}{B^2}\\-\dfrac{19.591iKm^2U^6}{B^3}+\dfrac{718.625kKm^2U^6}{B^3}+\dfrac{3082.77ik^2Km^2U^6}{B^3}\\(-131.845+207.101i)k^2KU^7+(530.297+337.598i)k^3KU^7\\+(-31119.9+48883i)k^4KU^7\end{array}\right)$$

$$=0 \qquad (20)$$

Eqn. (20) contains four Eigen values for ϕ. The number of parameters is large, and a general solution for ϕ is tedious. Here asymptotic expansions in the small parameter K are considered, i.e. $\phi=\phi_0+K\phi_1+K_2\phi_2+\ldots$. To investigate instability, it is necessary to obtain the Eigen values of this polynomial equation for the complex celerity. We need to distinguish the physical phenomena, i.e. free surface displacement, velocity disturbance, and bed profile change, involved in river morphology. In order to do this, one needs to consider the following cases:

(i) Dune celerity c computed by $\dfrac{\mathrm{Re}[\phi]}{k}$, (ii) Wavenumber k, and (iii) Amplification rate $\mathrm{Im}[\phi]$.

In order to study river morphology, the last Eigen value will be taken into consideration and the flow is assumed to be quasi-steady. The equation for the lowest-order term in the expansion for the fourth root (proportional to

sediment transport), vanishing as $K \to 0$, has implications to the morphological processes and can be written in the form:

$$\phi_4 \begin{pmatrix} -0.00129901ik^2U + 13.3048k^3U - 2.04887 \times 10^{-10} im^2U \\ +1.04926 \times 10^{-6} km^2U + \left(-3.93608 \times 10^{-7} + 0.000051422i\right)k^2U^3 \\ +\left(-0.131333 - 0.0040314i\right)k^3U^3 \end{pmatrix}$$

$$+K \begin{pmatrix} 3.50675 \times 10^{-13} k^2 m^2 U^5 + 3.5917 \times 10^{-9} ik^3 m^2 U^5 + 5.53104 \times 10^{-20} m^4 U^5 \\ +2.83252 \times 10^{-16} ikm^4 U^5 + 0.00124612ik^3 U^6 - 12.7631k^4 U^6 \\ -3.33932 \times 10^{-11} ikm^2 U^6 - 2.61896 \times 10^{-7} k^2 m^2 U^6 \\ +\left(1.79261 \times 10^{-16} - 1.06257 \times 1.06257 \times 10^{-16} i\right)k^2 m^2 U^7 \\ +\left(1.08831 \times 10^{-12} - 1.83604 \times 10^{-12} i\right)k^3 m^2 U^7 - 1.94852 \times 10^{-24} m^4 U^7 \\ -9.97864 \times 10^{-21} ikm^4 U^7 + \left(-1.74585 \times 10^{-7} + 2.74237 \times 10^{-7} i\right)k^3 U^8 \\ +\left(-0.00561762 - 0.00357629i\right)k^4 U^8 + \left(18.3147 - 28.7686i\right)k^5 U^8 \\ +9.55814 \times 10^{-21} ikm^2 U^9 + \left(-1.28845 \times 10^{-16} + 3.7433 \times 10^{-21} i\right)k^2 m^2 U^9 \\ +\left(-3.83399 \times 10^{-17} - 3.16972 \times 10^{-13} i\right)k^3 m^2 U^9 \end{pmatrix}$$

$$=0 \qquad (21)$$

Properties of the Total Load-Dependent Solution

The imaginary part $\mathrm{Im}[\phi_4]$ of the solution to Eqn. (21) is:

$$
\left(\begin{array}{l}
\left(\left(\begin{array}{l}
\left(\begin{array}{l}
6.65241k^3U+\dfrac{65.6566km^2U}{B^2}+ \\
0.0018843kU^3-0.0625k^3U^3
\end{array}\right) \\
-\left(\begin{array}{l}
\dfrac{109375k^3m^2U^5}{B^3}+\dfrac{1.07949\times10^6km^4U^5}{B^3} \\
+570.457k^3U^6+107800k^4U^6+1.73435\times10^6k^5U^6 \\
-\dfrac{2321.96km^2U^6}{B^2}-\dfrac{709297k^2m^2U^6}{B^2}+\dfrac{1.71173\times10^7k^3m^2U^6}{B^2} \\
+\dfrac{30.9806km^2U^7}{B^3}-\dfrac{1027.59k^3m^2U^7}{B^3}-51.7753k^3U^8 \\
-675.795k^4U^8-16294.3k^5U^8
\end{array}\right)
\end{array}\right) \\
2.7431\times10^{-8}K+\left(-0.649505k^2U-\dfrac{12.8207m^2U}{B^2}+0.0254017k^2U^3\right) \\
\left(\begin{array}{l}
\dfrac{10678.8k^2m^2U^5}{B^3}+\dfrac{210791m^4U^5}{B^5}+163489k^4U^6 \\
-1.10412\times10^6k^5U^6-\dfrac{1.12784\times10^6k^2m^2U^6}{B^2} \\
-\dfrac{1.08972\times10^7k^3m^2U^2}{B^2}-\dfrac{417.64k^2m^2U^7}{B^3} \\
+32.9612k^3U^8-1060.59k^4U^8+10373.3k^5U^8
\end{array}\right)
\end{array}\right)
$$

$$
\left(\begin{array}{l}
\left(-0.649505k^2U-\dfrac{12.8207m^2U}{B^2}+0.0254017k^2U^3\right)^2+ \\
\left(\begin{array}{l}
\left(\begin{array}{l}
6.65241k^3U+\dfrac{65.6566km^2U}{B^2}+0.0018843kU^3 \\
-0.0625k^3U^3
\end{array}\right)
\end{array}\right)
\end{array}\right) \tag{22}
$$

In order to find the instability wavelength that can be expected to be one at which $\mathrm{Im}[\phi_4]$ is positive and maximum, i.e.,

$$\frac{d\,\mathrm{Im}[\phi_4]}{dk}=0 \tag{23}$$

We need to check the number of positive roots, which might be related to physical phenomena, such as, ripples, dunes or antidunes, mega-dunes and sand-bars or islands. If we consider the largest scale, the smallest value of k will be investigated. Under the indicated restrictions, a range of wavenumbers for which $\mathrm{Im}[\phi_4]$ are positive always exist and instability characteristic of meandering or braiding always occurs.

After incorporating the real and maximum positive root of k which is an implicit function of the number of braids m in Eqn. (22), we can find the maximum instability that is also a function of m. Let us assume one value of m, say $m = 1$, and calculate $\mathrm{Im}[\phi_4]$. Consider again higher values of m, say $m = 3$, and calculate $\mathrm{Im}[\phi_4]$. Comparing two values of $\mathrm{Im}[\phi_4]$, one can differentiate whether the river is braided or meandering corresponds to maximum instability.

RESULTS AND DISCUSSION

The agreement between the theoretical stability analysis and the observation does not necessarily mean that the model is in accordance with the actual mechanism of instability. Some numerical examples on the stability of alluvial rivers will be discussed in order to figure out the extent to which the 2-D mathematical model describes the features known from other authors' works or from the nature. The effect of secondary currents on sediment transport, the effects of spiral motion and drag force on the bed shear stress are considered in the present model. The flow is treated as unsteady, the dunes will change their forms with time, because the dune dimensions vary with the hydraulic conditions. If one neglects C_d, the effect of spiral motion, and the transverse slope δ, the imaginary part of the fourth root of the Eigen equation, e.g., $\mathrm{Im}[\phi_4]$ will be similar with respect to power of the wavenumber k of the equation obtained by Parker (1976).

It is needed to choose some representative data on Jamuna River. In order to reduce the model parameters, some numerical values are taken into considerations, which will also be of great importance in reducing the memory needed by the computer during programming. Such numerical values are the fluid density, $\rho = 1000$ kg/m^3; the representative grain size, $d_s = 0.22 \times 10^{-3} m$; the depth-averaged water depth, $d_0 = 10.85$ m (PWD); the width of the river at J 6-1, $B = 11187.00$ m; the porosity of the sediment grains, $\lambda p = 0.4$; the relative density difference, $\Delta = 1.65$; the Von Karman constant, $k_1 = 0.4$; $r = 0.5$ (the constant appeared in the evaluation of transverse slope); and the acceleration due to gravity, $g = 9.81$ m/s^2.

The imaginary part of ϕ of the fourth root of the Eigen equation , i.e., $\mathrm{Im}[\phi_4]$, the amplification factor, has been evaluated as the functions of the number of braids m, the channel width B, the uniform flow velocity U, and the wavenumber k.

As instability is observed to occur at coherent finite wavelengths, the observed instability wavelength can be expected to be one at which $\mathrm{Im}[\phi_4]$ is positive and a maximum. If the roots of Eqn. (23) are to represent the characteristic meander or braid wavelengths, they must be real and correspond

to positive, maximum instability for maximum real and positive root among all the roots of k. The unstable wavenumber against flow velocity for maximum instability condition is shown in *Fig. 4* for $m = 3$ and $m = 1$, respectively. It is seen

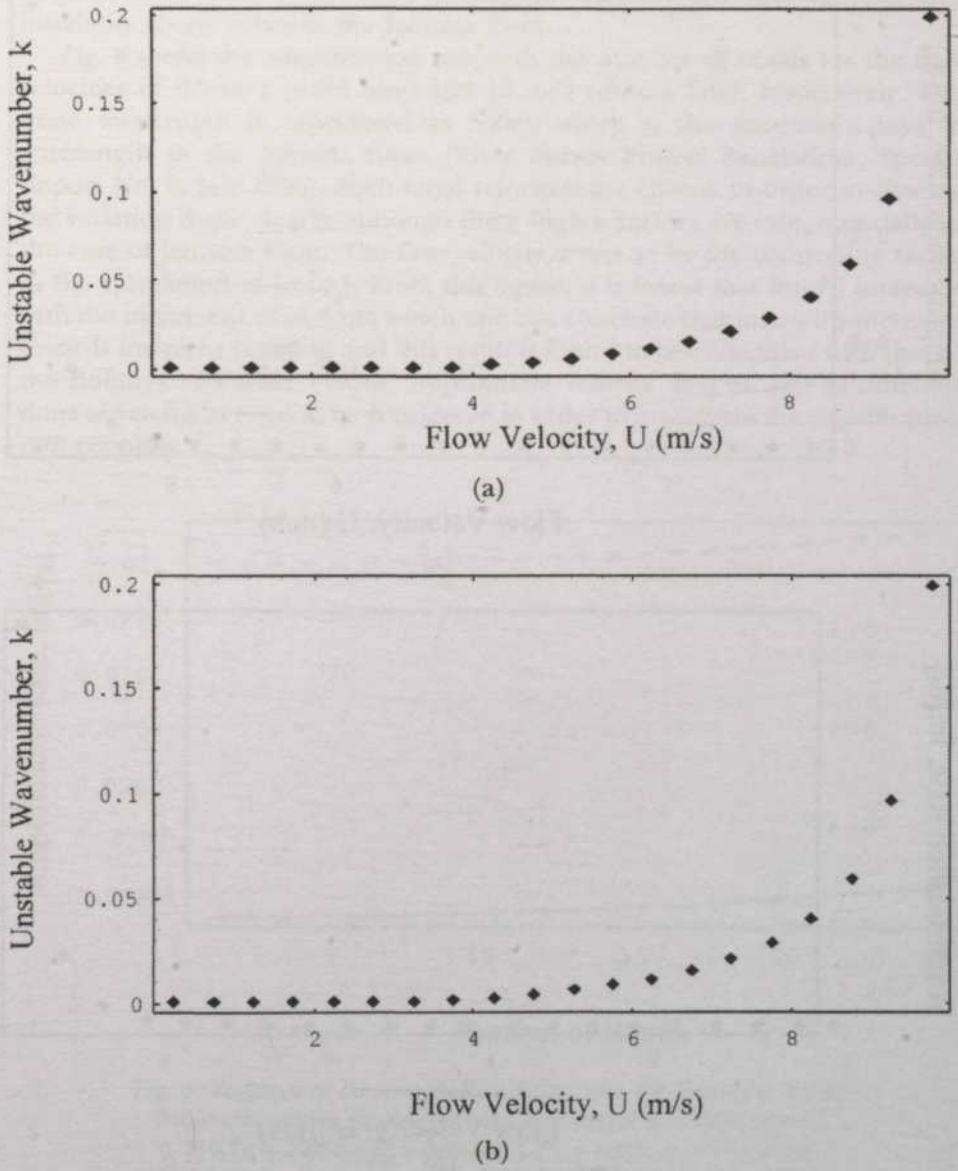

Fig. 4. Variations of unstable wavenumbers with flow velocity under maximum instability condition for (a) m = 3 and (b) m = 1
Parameter values considered are: $k_B = m\pi/B$; $\rho = 1000$ kg/m^3; $\lambda_p = 0.4$; $\Delta = 1.65$; $r = 0.5$; $g = 9.81$ m/s^2; $L = 2\pi/k$ m; $C_d = 1$; $k_1 = 0.4$; $d_0 = 10.85$ m; $d_s = 0.22*10^{-3}$ m; and $B = 11187$ m

that the wavenumber exponentially increases with the increment of the flow velocity for both the cases. Although it is difficult to guess, the maximum instability is found to occur in the case of meandering stream (*Fig. 5*). The

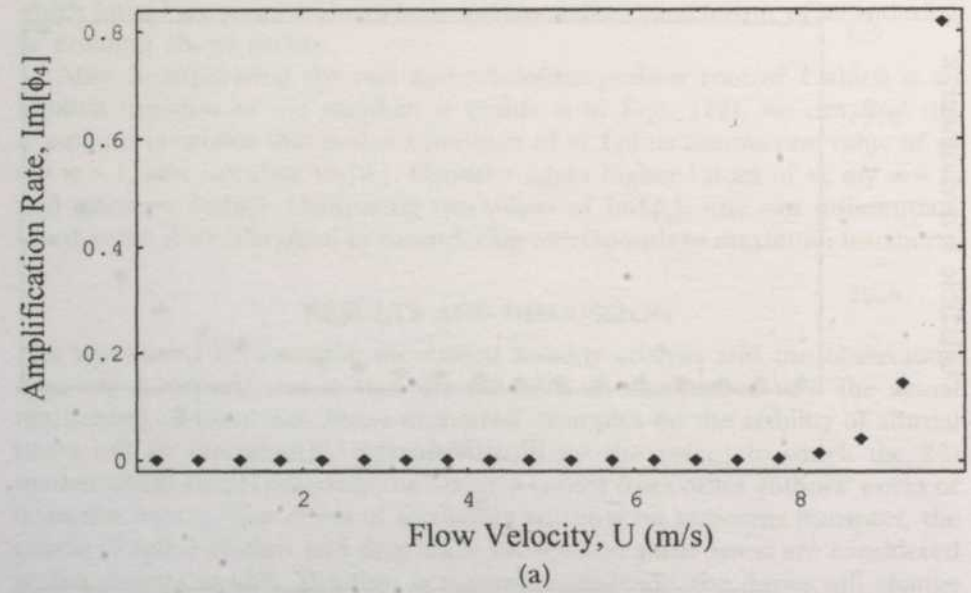

(a)

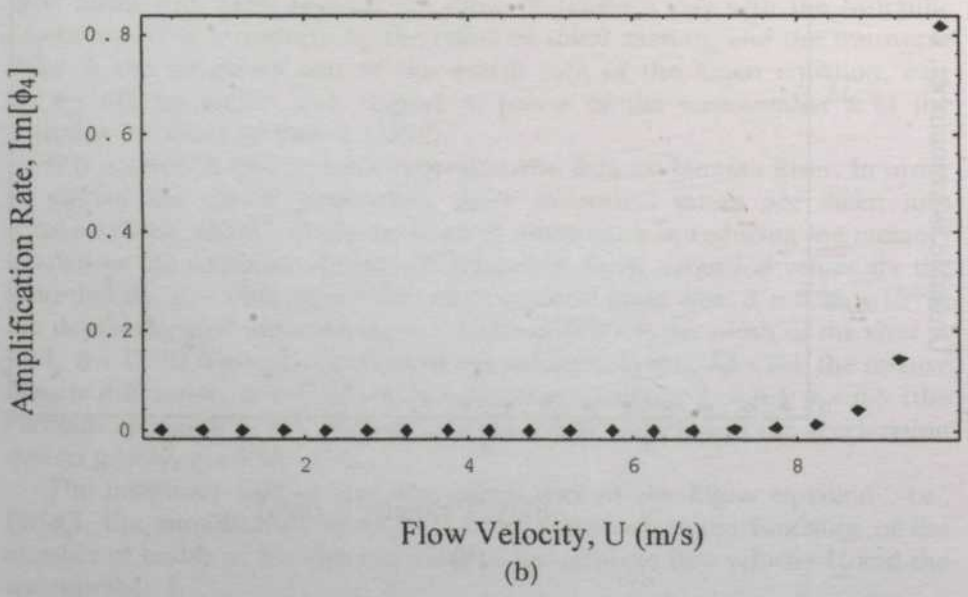

(b)

Fig. 5. Amplification factor against flow velocity under maximum instability condition for (a) m = 3 and (b) m = 1

Parameter values considered are: $k_B = m\pi/B$; ρ = 1000 kg/m^3; λ_ρ = 0.4; Δ = 1.65; r = 0.5; g = 9.81 m/s^2; $L = 2\pi/k$ m; C_d = 1; k_1 = 0.4; d_0 = 10.85 m; $d_s = 0.22*10^{-3}$ m; and B = 11187 m

amplification rate and the unstable wavenumber are directly proportional to the flow velocity. It is also found that $\mathrm{Im}[\phi_4]$ always takes positive values, meaning there is no critical velocity for which instability appears. This could be due to the very large width of the Jamuna River and its very small aspect ratio (*Depth/Width*), 1/1000. Thus, to predict the stability is rather difficult and instability always exists in the Jamuna River.

Fig. 6 shows the amplification rate with the number of braids for the flow velocities of 9.9 m/s (solid line) and 10 m/s (dotted line), respectively. The dune wavelength is considered as 350m, which is the maximum possible wavelength in the Jamuna River (River Survey Project Bangladesh, Special Report No. 9, July 1996). Such large velocities are chosen in order to observe the variation more clearly, although these high velocities are rare, especially in the case of Jamuna River. The flow velocity seems to be the controlling factor in the calculation of $\mathrm{Im}[\phi_4]$. From this figure, it is found that $\mathrm{Im}[\phi_4]$ increases with the increment of m, from which one can conclude that instability increases towards incipient braiding and this result is found to be coincident with that of the findings of Parker (1976). Appropriate velocity data as well as different dune wavelengths need to be considered in order to investigate the amplification rate properly.

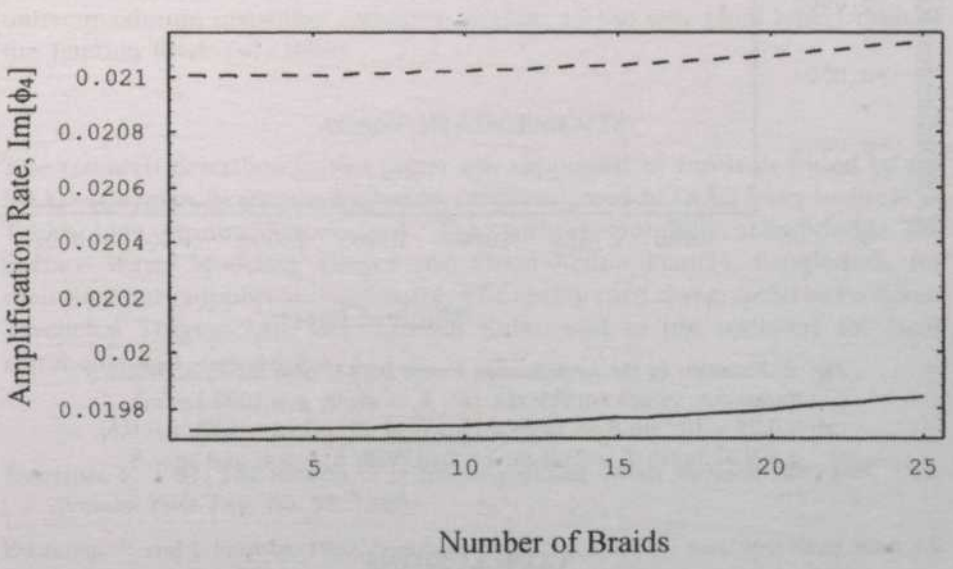

Fig. 6. Variation in the Amplification Factor with the Number of Braids
Parameter values considered are: $k_B = m\pi/B$; $\rho = 1000$ kg/m^3; $d_s = 0.22 \times 10^{-3}$ m; $\lambda_p = 0.4$; $\Delta = 1.65$; r = 0.5; g = 9.81 m/s^2; $L = 2\pi/k$ m; $C_d = 1$; $k_1 = 0.4$; k = 0.017952; and B = 11187 m

Referring to Eqn. (22), the effect of river width B on the amplification rate is shown in *Fig. 7*. The amplification rate increases towards increasing B, but its variation is almost negligible. It can be said that the larger the channel width, the larger will be the aspect ratio, which could be the case of braided stream. If the dotted line is plotted separately, it can be guessed that $\mathrm{Im}[\phi_4]$ is more pronounced up to a certain value of B; thereafter its increment is quite negligible, indicating instability is on the state of nearly constant. The authors have tried to find the peak of the instability, but no peak is found. However, critical value could be between these two values to initiate instability.

The aspect ratio of the Jamuna River is very low (1/1000), which means that the instability always exists under maximum instability conditions and the prototype experiment is rather difficult to perform. Also, this fact indicates that it might have many braids, i.e., the number of braids will be more than 3.

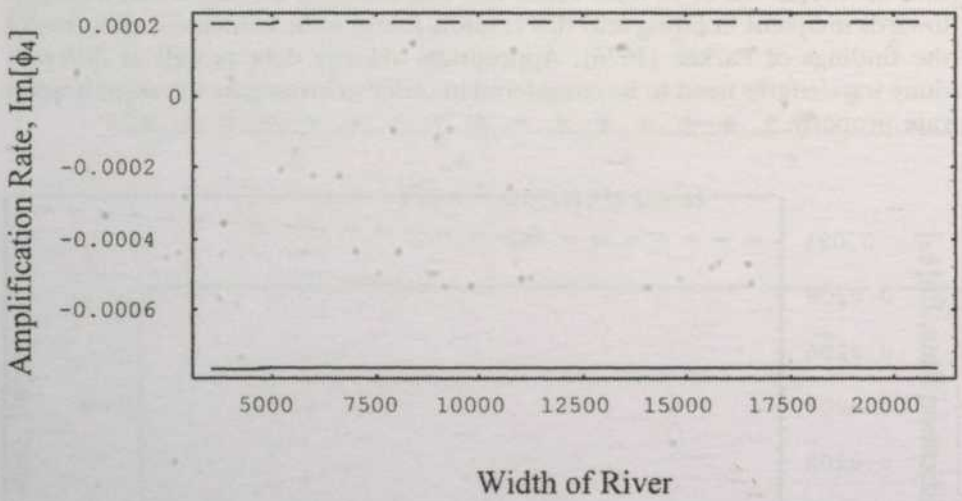

Fig. 7. Variation in the Amplification Factor Im[ϕ4] with the River Width B
Parameter values considered are: $k_B = m\pi/B$; $\rho = 1000$ kg/m^3; $d_s = 0.22 \times 10^{-3}$ m; $d_0 = 10.85$ m; $\lambda_p = 0.4$; $C_d = 1$; $\Delta = 1.65$; r = 0.5; g = 9.81 m/s^2; $L = 2\pi/k$ m; k = 0.017952; $k_1 = 0.4$; and m = 3

CONCLUSIONS

The developed 2-D model appears to explain some physical features satisfactorily: instability increases towards incipient braiding; instability is proportional to the width-depth ratio (aspect ratio); and the instability wavelength corresponds to maximum instability. A stability theory has been developed by applying perturbation technique which determines the real and positive roots of k corresponding to maximum instability and hence the maximum instability wavelength. Several implications of the proposed model based on the data of

the Jamuna River, are discussed. The approximated ϕ value is also compared with the actual ϕ value. The theory may yield better results, if (i) the phase shift of the bedforms; (ii) the accurate description of the behavior of the sand dune on the river bed; and (iii) the proper estimate of the frictional resistance due to pure skin friction and bedforms; are properly included in the model. The purpose of including the effect of the transverse bed slope is that the river will braid into an infinite number of branches if it is not included. The aim of including the spiral motion on the bed shear is that the lateral bed shear stress will adapt faster to changing curvature of the channel than the intensity of the spiral motion. The choice of a specific sediment transport formula may also have influence on the model. The linear aspects of the present theory differs from that of Parker (1976) because of the consideration of transverse slope effect on the sediment transport, the effect of spiral motion on bed shear stress and the estimate of frictional resistance from pure skin friction and friction due to bedforms. Furthermore, the major inadequacy of the linear stability theory is that it cannot explain the longitudinal asymmetry embodied in the sand dunes or bars properly which may appear to be associated with nonlinear effects. From the analyses, it can be concluded that the instability increases towards incipient braiding, increased channel width, and dune wavelength. It is further concluded that stability will never be achieved in the Jamuna River under maximum instability condition because of the very small aspect ratio of the Jamuna River ($\approx$1/1000).

ACKNOWLEDGEMENTS

The research described in this paper was supported by funds provided by the DAAD (German Academic Exchange Program), and AITAA (Asian Institute of Technology Alumni Association). The authors gratefully acknowledge the Surface Water Modeling Center and Flood Action Plan-24, Bangladesh, for their necessary support and assistance. The authors are also grateful to Professor Tawatchai Tingsanchali, Dr. Naritaka Kubo, and to the reviewers for their comments and suggestions.

REFERENCES

ENGELUND, F. 1981. The motion of sediment particles on an inclined bed. *Tech. Univ. Denmark ISVA Prog. No.* **53:** 15-20.

ENGELUND, F. and J. FREDSOE. 1982. Sediment ripples and dunes. *Ann. Rev. Fluid Mech.* **13:** 13-37.

ENGELUND, F. and E. HANSEN. 1967. *A Monograph on Sediment Transport in Alluvial Streams.* Copenhagen: Danish Technical Press.

ENGELUND, F. and O. SKOVGAARD. 1973. On the origin of meandering and braiding in alluvial streams. *J. Fluid Mech.* **57:** 289-302.

LEOPOLD, L.B. and M.G. WOLMAN. 1957. River channel patterns: Braided, meandering and straight. U.S.G.B. Professional Paper, 282-B.

Olesen, K. W. 1983. Alternate bars in and meandering of alluvial rivers. *Commun. Hydraul., Rep.* 7-83. Delft Univ. of Technology.

Parker, G. 1976. On the cause and characteristic scales of meandering and braiding rivers. *J. Fluid Mech.* **83:** 457-480.

Swmc-Danida. 1996. River survey project Bangladesh. Surface Water Modeling Center, Dhaka, Bangladesh, Special Report No. 9.

Pertanika J. Sci. & Technol. 10(2): 251 - 259 (2002)
ISSN: 0128-7680

Service and Voltage Sag Study of Humid and Dry Weather Utilities

N. Khan, N. Mariun, S. M. Bashi & S. Yusof
Department of Electrical and Electronic Engineering
Faculty of Engineering, Universiti Putra Malaysia
43400 UPM Serdang, Selangor, Malaysia
E-mail: khan@eng.upm.edu.my

Received: 13 September 2000

ABSTRAK

Kertas ini membandingkan masalah lendut voltan yang teruk dua utiliti yang biasa terdapat beroperasi di persekitaran yang lembap dan panas kering. Berdasarkan kepada data kualiti kuasa dan analisisnya, ia cuba untuk membandingkan kualiti perkhidmatan kepada pelanggan rupa bumi cuaca lembab dan kering. Untuk menyempurnakan kajian ini Tenaga Nasional Berhad (TNB) Malaysia dan Pihak Berkuasa Pembangunan Kuasa dan Air Pakistan(WAPDA) telah dipilih. Sejarah kegagalan sistem pengagihan elektrik kedua-dua utiliti, membawa kepada kepincangan tugas atau tiada diskriminasi operasi komputer mengawal proses industri, geganti pelindung dan penyentuh elektromagnetik jenis AC, dengan demikian menguatkuasakan penutupan pengguna akhir sedar kualiti, telah dianalisis untuk memperkukuhkan keagresifan lendut voltan di kedua-dua kawasan. Indeks keboleharapan kualiti kuasa telah dikira untuk mengukur persembahan sistem operasi. Kajian tersebut difokuskan untuk merumuskan algoritma bagi menganggar kemungkinan gangguan di luar pengurusan industri beroperasi dalam persekitaran lembap dan panas kering. Pengaruh kualiti kuasa yang rendah ke atas industri seperti perlindungan utiliti dan peralatan kawalan telah dianggarkan daripada data berkaitan beberapa tahun lalu. Kajian keboleharapan kualiti kuasa membuat kesimpulan bahawa lebih tinggi tahap penebatan untuk persekitaran lembap dan cuaca panas rata. Semasa perbandingan ini projek kajian kualiti kuasa ke atas sebab lendut voltan dan indeks keboleharapan bocoran keadaan stabil, didapati bahawa 77% lendut voltan adalah disebabkan oleh kesilapan litar pintas pada rangkaian, 11% disebabkan kesilapan antara kemudahan tetapi tiada sebab boleh dikaitkan dengan baki 14% lendut voltan yang terhasil dalam belantikan pemacu, kipas alir bebas, pemampat PLC, pam amonia, penunu dan pengawal proses. Indeks keboleharapan utiliti lembab didapati secara relatifnya lebih lemah daripada yang setara dengannya. Kemungkinan lendut voltan yang teruk di persekitaran lembab didapati lebih banyak daripada utiliti rupa bumi cuaca panas kering.

ABSTRACT

This paper compares the voltage sag severity problems of two typical utilities operating in humid and dry hot environments. Based on power quality data and its analysis, it has been attempted to compare the quality of services to the customers of humid and dry weather terrains. To accomplish this study Tenaga Nasional Berhad (TNB) Malaysia and Water and Power Development Authority (WAPDA) Pakistan were chosen. Electrical distribution system fault histories of

two utilities, leading to malfunctioning or indiscriminate operation of industrial process controlling computers, protective relays and AC type electromagnetic contactors thereby imposing costly shutdowns to quality conscious end users, were analyzed to establish the severity of voltage sag aggressiveness in both areas. Power quality reliability indices were calculated to measure the operational system performance. The study has been focused to formulate algorithm for estimating probability of nuisance trip outs in industrial organizations operating in humid and hot dry environments. Influence of poor power quality on industrial as well as utility protection and control equipment has been estimated from the field data spread over a few years. This power quality reliability study concludes that there are higher insulation levels for humid environments than the plain hot weathers. During this comparative power quality study project on the causes of voltage sags and steady state outages reliability indices, it was found that some 77% voltage sags were caused by short circuit faults on utility network, 11% due to inter facility faults but no cause could be assigned to remaining 14% voltage sags resulting in tripping of drives, draft fans, compressors PLCs, ammonia pumps, incinerators and process controllers. The reliability indices of humid utilities were found relatively poorer than its counterpart. The probability of severe voltage sags in humid environments was found to be much more than the dry hot weather terrain utilities.

Keywords: Voltage sags, SAIDI, SAIFI, CAIFI and power quality

INTRODUCTION

Power quality (PQ) problems are unwanted guests to both the utility and the facility. Power system disturbances do result in revenue loss to utility and costly downtime in industry. In industrialized countries power quality is a burning issue. Customers blame utilities for supplying unreliable power and utilities accuse customers for injecting electrical pollution into transmission and distribution systems. US color books (IEEE series) have established some criteria by suggesting limits on utilities as well as facilities. A utility can improve the quality of its power by the use of active power line conditioners, storage devices, filters and periodic routine maintenance of the protective relays. Previous studies have reported some 36 out of 49 trippings are due to simple causes aggravated by problems related to the protective relaying system (Tamronglak, S. and S.H. Horowitz *et al.* 1996). These problems are often caused by bad wiring of control circuits, AC/DC grounding, moisture in airtight pockets such as monostats, water ingress on transformer top mounted devices, undetected inbuilt problems and improper settings on relays. Power quality problems such as voltage sags, surges, impulses, swells, notches, flickers and harmonics may cause infrequent mal-operation of drives process controllers, computers, magnetic contactors, PLCs, industrial lights and compressor motors. Compressors and PLCs are usually the heart of a continuous process, which upon tripping causes a shutdown of the plant. Critical equipment are mostly affected by voltage sags and switching surges. There is a great deal of jargon used to describe momentary disturbances. Several authors (Key 1978; Koval and

Leonard 1990; Koval 1990) and IEEE color books have attempted to standardize momentary disturbances but still others have their own point of view. The anatomy of generally referred power system disturbances is defined in several publications (WAPDA GUJRANWALA 1996; Conrad and Little 1991; Dugg and Ray 1996). Voltage sag was poorly understood in the past but now there is a complete consensus that the voltage sags are caused by short-circuit faults on the utility transmission or distribution network and are the major source of industrial sensitive equipment disruptions.

Power Quality Study

PQ study mainly consists of determining momentary variation of voltage, current and frequency relative to their steady state values. If the sensitive equipment works as desired, then there is no need for conducting power quality studies. Otherwise it becomes necessary to identify the causes to opt for economically justified ride-through devices. It is well known that the PQ sensitive devices are themselves often the cause of inducting surges in the distribution system. Electrical control and protection equipment such as PLCs, magnetic contactors, AC/DC drives, relays and communication devices are usually sensitive to many types of power system disturbances. The electrical system susceptibility is best illustrated by computer business equipment manufacturers associations (CBEMA) susceptibility envelope described elsewhere (Tamronglak and Horowitz 1996; Key 1996; Koval and Leonard 1990; Koval, 1990; WAPDA GUJRANWALA 1996). Common types of disturbance recorders may include TR-16 40 (Rochester), 626-PA (Dragnets), AMX-1600 digital oscillograph (Kinkei system corp.), YR-8 (Yoshio Electric Co. Ltd.) and power scope (BMI model 4800). As part of this study, power and service quality data were collected from WAPDA and TNB. The threshold pick-ups and sensitivities of the various types of equipment found in this PQ study are shown in Table 1 (Conrad and Little 1991). These settings were found on sensitive industrial customer relays, which were suffering from voltage sags problems.

TABLE 1
Threshold pickups and dropouts of voltage sag sensitive equipment

Equipment	Pick up		Drop out	
	Sag (%)	Duration (cycles)	Sag (%)	Duration (cycles)
AC Contactors	20	4	>20	4
DC Contactors	20	8	>20	4-8
Industrial drives	5-15	1-5	>5-15	1-5
PLCs	15-20	instant	>15-20	instant
Process Computers	10	5-10	>10	5-10
Mercury Lamps	50	2	>50	2
High Discharge lamps	10-15	1	>10-15	1

It is well known that if both leading edges of voltage and current are positive or negative going then the impulse is likely to have originated from utility side. However, if voltage polarity is positive going and current is negative going or vice versa then the source of disturbance may be somewhere on the load side (Price 1993). Similarly, if the voltage sag continuously goes down on an analyzer in industry then fault lies downstream. However, if the voltage sag recovers after a few cycles back to the normal, then the source of voltage sag is somewhere upstream (Reason 1992). If the analyzer record is a voltage sag followed by a continuously decaying DC voltage, then it is nothing except discharge of capacitors after tripping of the controlling circuit breaker. There may be an interesting record of continuously decreasing voltage and frequency which are often caused by motor's generator action during voltage sags or sudden disruption of a process involving high inertia loads (Conrad and Little 1991).

UTILITIES DATA ANALYSIS

To estimate utility performance and its impact on industrial downtime, the SS & T Division WAPDA Gujranwala, a model town Subdivision Gujranwala and the Ghakhar Subdivision Ghakhar, under AEB, WAPDA Gujranwala were chosen as random samples to determine overall performance of WAPDA. A similar PQ study was focused on TNB sub transmission and distribution network feeding to Selangor, which is the most developed state of Malaysia. Utilities tripping data analysis was conducted in comparison to industrial electrical failure history. The findings obtained by data analysis of WAPDA and TNB tripping histograms has shown that short circuit faults on the lines cause voltage sags that result in tripping of most of the industrial equipment and often the utility's own protection and control devices. A reasonable number of indiscriminate trippings is recorded by WAPDA and TNB. Both TNB and WAPDA need to give attention to high numbers of indiscriminate trippings on their networks. The main cause of indiscriminate tripping on TNB network may be the highest isokeraunic level and humidity leading to insulator flashover. The data for Malaysian thunderstorm days (TD)/year) as compared to some international cities is shown in Table 2.

TABLE 2
Thunderstorms Days/Yr Data

Name of City	TD/Yr
Tokyo (Japan)	20
Subang (Malaysia)	330
Lahore (Pakistan)	330
Miami (USA)	100
Penang (Malaysia)	290

The causes of voltage sags may vary but the average number of voltage sags caused by faults on utility networks in Pakistan and TNB Malaysia is much more than the practices adopted in standard international utilities. The frequency of faults in TNB is less than WAPDA but the number of unidentified trippings is much higher. Some of the international utilities have reported 80% of voltage sags caused by lightning and the others declare the number of voltage sags to be directly proportional to short circuit faults on utility or facility distribution networks. Thus the voltage sags are considered to originate from short circuit faults. Therefore, to minimize voltage sags on systems the utilities need to increase maintenance to reduce frequency of faults on their networks.

Voltage sag severity may be represented by several methods. 3-D plot of TNB voltage dip magnitudes, duration and frequency of occurrence are shown in *Fig.1.* TNB and its customers record voltage sag profiles but WAPDA and its customers normally do not record them except for a few cases. We estimated WAPDA sag durations from the controlling circuit breakers and magnitudes by making reactance diagrams of the 11 kV feeders. The sag magnitudes were found similar to the standard published and generally recorded values. Based on field experience and present research on TNB and WAPDA Gujranwala, it is concluded that the frequency of severe voltage sags in radial systems are far more than meshed networks. Average number of sags/yr in WAPDA is more than TNB but less than many South Eastern utilities operating in similar environmental conditions.

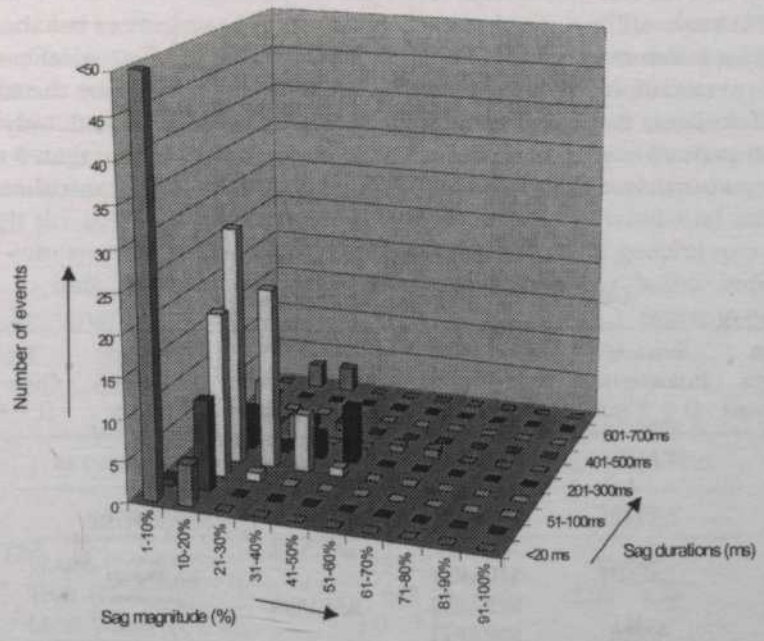

Fig. 1. A typical TNB 3D plot of voltage sags durations, magnitudes and frequency of occurrence

SERVICE QUALITY CRITERIA

Competitiveness of a utility performance depends upon the quality of service provided to its customers. If the customers are satisfied with the supply services then there is no more question about it, otherwise, the utility performance may be estimated from its statistical service in respect of outages, sustained interruptions, momentary interruptions, harmonics and transient indices. Long ago, the utilities progress could only be weighted in terms of its outages based indices such as system average interruption duration index (SAIDI), system average interruption frequency index (SAIFI), customer average interruption duration index (CAIDI), customer average interruption frequency index (CAIFI) and average system availability index (ASAI) [7, 10, 11]. The customers were supposed to be affected only during outages due to simple loads. Development in semiconductor VLSI technology has resulted in quite sensitive devices that can easily be interrupted by surges and transients. Thus the above concept of indices was substantially modified to incorporate the effects of sustained interruptions on distribution systems. Most of the utilities still use above five types of indices to evaluate their performance but more efficient utilities have started to measure their competitiveness in terms of momentary and transient indices in view of sensitive equipment reported to be affected even by transients. This study is limited to calculation of outages (>5 min) based indices, SAIDI, SAIFI, CAIFI, CAIDI and ASAI, but the details of other indices are shown in Table III for information and further pursuance of work both in WAPDA and TNB.

WAPDA as a utility not only must calculate the above indices but should also prepare for self-assessment regarding quality of services to the critical customers. A perfect estimation of utility service quality is only possible by the above six types of indices, however, an average guess may be obtained only by the statistical evaluation of interruptions/outages occurring for more than 5 minutes. To the authors' knowledge, both TNB and WAPDA do not calculate all the

TABLE 3
Utility service quality reliability indices [10-14]

System Outages ($t \geq 5$ min)	Sustained Interruptions ($t > 1$ min)	Momentary Interruptions ($t < 1$ min)	Voltage Fluctuations (Steady state)	Harmonic Distortions (THD)	Transient Over voltages ($t <$ few ms)
SAIDI	SASIFI	SARFI			
		SIARFI	SAEVUR		
SAIFI	SATIFI	SMARFI		SAETHDRI	
		STARFI	SAENSR		SATMORI
CAIFI	SASIDI	SIPARFI		$SAEN_hRI$	
		S2PARFI	SAEVDR		
CAIDI	ASIDI	S3PARFI			
		ARDI			
ASAI					

above indices. However, TNB calculates SAIFI, SAIDI and CAIDI indices but WAPDA is still planning to start calculation of above indices in the near future. In the present study, the authors have attempted to calculate two of the above indices to compare it with TNB data.

UTILITIES SERVICES INDICES

Above indices were calculated for WAPDA on the basis of data of five 11 kV feeders of model town Subdivision feeding to 7956 domestic, 3256 commercial and 1230 industrial consumers. This choice shows a reasonably good admixture of sensitive industrial and commercial users. Due to time constraint and lack of desired data, only SAIDI and SAIFI indices could be calculated. To estimate the average value of SAIDI it was assumed that HV outages from grid station affect all the 11 kV customers on all feeders emanating from the grid. The 11 kV feeder faults just cause outages to the concerned customers without disturbing parallel feeder customers. Similarly for calculating SAIFI it was assumed that faults on 11 kV feeders not only disrupt customers connected to these feeders but also some 2% of the nearby customers on parallel feeders. Computation of these indices is based on the assumption that all the HV and 11 kV outages are cleared within 5 and 2 hours respectively. In view of limited information these indices may be considered approximate and rough representations where no such data is available.

Overall WAPDA performance may not be based on this study as the data was incomplete and the authors chose the worst area cases. The service quality of utility can also be measured in terms of its momentary and steady state outages on transmission and distribution systems. WAPDA uses the radial system and its performance comparison with TNB and other international utilities is shown in Table 5. Similarly, the causes of sags of different utilities are shown in Table 5.

The outages per year data are accurate but momentary interruptions per year data are approximate in light of the operator's ignorance to record it. Although the actual data supplied by the subdivision was compared to records of the concerned Shaheenabad Grid Station, still the general practice of utilities to hide or conceal their actual fault figures, for better impression, cannot be ignored during analysis. Further, to probe a more generalized

TABLE 4
Average SAIDI and SAIFI indices of WAPDA and TNB as compared to standard international most efficient utilities

Utility	SAIDI (Hrs)	SAIFI
WAPDA (Dry)	1271@	11.68@
TNB (Humid)	642	3.98 - 4.28
Ideal Utility	1.0 - 1.5	1.0

@ These values correspond to urban areas of District Gujranwala.

TABLE 5
Percentage contribution of causes of voltage sags in WAPDA and TNB.

Causes (Types)	WAPDA (Pakistan)	TNB (Malaysia)
Insulator flashover	31%	8%
Indiscriminate	32%	**43%**
External touches	**14%**	9%
Equipment failure	23%	40%

estimate of supply service quality it was decided to focus on distribution subdivision at WAPDA Ghakhar under Wazirabad Division. This Subdivision supplies electricity through six 11 kV feeders to some 15395 consumers.

These six feeders emanate from the 220/132/11 kV Grid station Ghakhar along with 11 other parallel feeders falling in jurisdiction of the other Subdivisions. All the 17 feeders supply electricity at 11 kV voltage level to some 38488 customers. The indices were calculated using the above-mentioned assumptions. Data collection showed those 2558 faults (resulting in tripping of circuit breakers) occurred on 17 radial 11 kV feeders in 1996. The measured data indicates 2364 faults on 11 kV parallel feeders and 194 on the WAPDA 220/132/66 kV transmission lines. These faults resulted in 2558 voltage sags on the 11 kV feeders. It is, therefore, estimated that (including severe and mild sags) some 2558 sags occurred for each of the 38488 consumers fed from 17 feeders. This is due to parallel connection of 17 feeders from the same substation. The traditional utility service quality indices were calculated on individual feeders and subdivision basis.

CONCLUSIONS

To minimize voltage sag problems WAPDA and TNB may adopt strategies including but not limited to reduction of number of faults, improvement in maintenance and repair, going for higher voltage transmission, increment of local VAR support during faults, increment of generation and spinning reserve, installation of shield wire, replacement of deteriorated cables and choice of better insulators on over head EHV lines. Based on the results of this power and service quality comparative case study, it can be concluded that the number of faults on utility transmission and distribution network is directly proportional to the voltage sags to the customers. The overhead transmission and distribution network appears to behave as more exposed to power quality issues than the underground/concealed systems. Higher number of indiscriminate trippings is alarming. WAPDA and TNB service quality indices reflect that they have not any self-imposed or adopted recent international practice. As TNB computes at least three indices so its underground trend is more competitive than WAPDA. This may partly be attributed to utility priorities and monopoly. Power and

service quality statistics are almost similar in most of the developing countries, but as international utilities, the WAPDA and TNB may consider adopting recent international practices to minimize the momentary interruptions to their consumers.

ACKNOWLEDGEMENTS

Authors are thankful to TNB and WAPDA for supplying data to complete this comparative study.

REFERENCES

CONRAD L. and K. LITTLE. 1991. Predicting and preventing problems associated with remote fault clearing voltage sags. *IEEE Trans. Indust. App.* **27** February: 167-72.

DUGG R. C. and L.A. RAY. 1996. Fast tripping of utility breakers and industrial load interruptions. *IEEE Indust. App Mag.* August: 55-64.

EPRI TR-107938, Reliability benchmarking methodology, May 1997.

EPRI TR-110346,Power quality for distribution planning, April 1998.

GUJRANWALA W. Transmission lines tripping data of SS&T Division for year 1996.

KOVAL DON. O. 1990. How long should power systems disturbance site monitoring to be significant. *IEEE Trans. Indust. App.* **26(4)** August: 705-710.

KOVAL DON. O. and J.J. LEONARD. 1990. Modeling rural power quality. In *Proc. of 22nd, Power Symposium*, PES, p. 317-326.

LT.THOMS S.KEY. 1978. Diagnosing power quality related computer problems, CPS p.48-59.

PRICE, K. 1993. Practices for solving end user power quality problems. *IEEE Trans on Indust. App.* **9(6)** December: 1164-1169.

REASON, J. 1992. Outage monitoring boosts power quality. *Electrical World*: 540-552.

SABIN D.D. and D.L. BROOKS. 1998. Indices for assessing harmonic distortion measurements: Definitions and benchmarking, Paper No. PE-063, PWRD.

TAMRONGLAK S. and S.H. HOROWITZ. 1996. Anatomy of power system blackouts: Preventive relaying strategies. *IEEE Trans. PD.* **11(2)**: 709.

TNB transmission and distribution faults data for periods 1995-99.

Transmission and distribution lines tripping and consumer data of model town and Ghakhar subdivision and XEN(SS&T) Division Wapda Gujranwala, for periods 1994-97.

Pertanika J. Sci. & Technol. 10(2): 261 - 267 (2002)
ISSN: 0128-7680

Penentuan Plumbum Menggunakan Kaedah Analisis Suntikan Aliran Berdasarkan Pembentukan Kompleks antara Plumbum dengan Reagen Galosianin

Nor Azah Yusof & Musa Ahmad
Pusat Pengajian Sains Kimia dan Teknologi Makanan
Fakulti Sains dan Teknologi
Universiti Kebangsaan Malaysia
43600 UKM Bangi, Selangor
Malaysia

Received: 4 September 2000

ABSTRAK

Analisis suntikan aliran (FIA) dengan sistem pengesanan UL-Nampak telah digunakan dalam kajian ini untuk pengesanan Pb(II) dalam persekitaran akues. Sistem FIA yang digunakan di dalam penyelidikan ini adalah berdasarkan tindak balas antara Pb (II) dengan reagen galosianin untuk membentuk suatu kompleks yang keserapannya maksimum pada panjang gelombang 550 nm. Kadar alir larutan pembawa, pH larutan dan kepekatan reagen telah dioptimumkan bagi meningkatkan kecekapan analisis bagi sistem FIA ini. Sistem FIA didapati optimum pada kadar alir 1.2 mL/min dan pH 8. Julat kepekatan dinamik bagi Pb(II) pula ialah 1.0×10^{-3} mg/L hingga 1.0×10^{1} mg/L. Kebolehulangan pengesanan Pb(II) adalah baik dengan nilai RSD 1.03%. Pada nisbah mol 1:1, Cd(II), Ni(II) dan Co(II) didapati mengganggu dengan masing-masingnya memberikan ralat relatif sebanyak 10.05 %, 10.15 % dan 10.25 %.

ABSTRACT

Flow injection analysis (FIA) with UV-Visible detection has been used in this study for Pb(II) detection in an aqueous environment. The FIA system used in this study was based on the reaction between Pb (II) and gallocyanine which formed a complex with maximum absorbance at around 550 nm. The carrier solution flow rate, solution pH and the reagent concentration have been optimised to increase the efficiency of the FIA system. The FIA system was found to be optimum at 1.2 mL/min flow rate and pH 8. The dynamic range for the Pb(II) concentration was found to be between 1.0×10^{-3} mg/L and 1.0×10^{1} mg/L. The reproducibility of the method was very good with RSD value of 1.03 %. At mole ratio of 1:1, Cd(II), Ni(II) and Co(II) were found to interfere with respective relative error of 10.05 %, 10.15 % and 10.25 %.

Kata kunci: Plumbum, kaedah analisis suntikan aliran, reagen galisianin, persekitaran akues

PENGENALAN

Sistem FIA telah diasaskan oleh Ruzicka dan Hansen pada tahun 1975 (Shpigun 1990). Ia merupakan suatu teknik yang sesuai untuk pengukuran secara kinetik bagi ion logam kerana keadaan tindak balas yang boleh dikawal dengan

pengoptimuman parameter-parameter eksperimen seperti kadar alir, panjang tiub, diameter tiub dan lain-lain.

Pengesanan ion Pb(II) menggunakan sistem FIA telah dilakukan oleh beberapa penyelidik terdahulu, contohnya pengesanan Pb(II) secara spektrofotometri menggunakan kaedah FIA dengan reagen 2-(5-nitro-2-piridilazo)-5-(N-propil-N-sulfo-propilamino) fenol sebagai pengkompleks (Yamane & Yamaguchi 1997), pengesanan Pb(II) menggunakan kaedah suntikan aliran dengan ekstraksi-fotometrik (Novikov *et al.* 1989), pengesanan Pb(II) menggunakan kaedah suntikan aliran 'stopped flow' (Mingshu & Pacey 1995) dan pengesanan Pb(II) dalam darah menggunakan kaedah voltametri hidrodinamik dengan sistem suntikan aliran dan alat pengesan 'wall jet' (Jaenicke *et al.* 1998).

Memandangkan pelbagai teknik telah wujud di dalam pengesanan ion Pb(II), adalah kurang berfaedah untuk memperkenalkan suatu teknik yang baru kecuali teknik tersebut dapat memberikan kadar pensampelan yang lebih tinggi, had pengesanan yang lebih rendah dan kaedah operasi yang lebih mudah tanpa melibatkan ekstraksi, pemekatan ataupun tindak balas yang rumit. Oleh itu kertas kerja ini memfokuskan kajian terhadap pengesanan Pb(II) menggunakan reagen galosianin yang sensitif terhadap Pb(II) melalui pembentukan kompleks Pb(II)-galosianin. Reagen yang digunakan ini adalah sensitif terhadap Pb(II) dan kaedah tindak balas yang terlibat ringkas tanpa melibatkan pemekatan analit dan juga ektraksi.

Kaedah FIA dengan sistem pengesan Spektrofotometer UL-Nampak digunakan dalam kajian ini. Kajian dilakukan untuk mendapatkan graf kalibrasi, menentukan kebolehulangan kaedah, mengoptimumkan kadar alir, mengkaji kesan kepekatan reagen terhadap pembentukan kompleks, mendapatkan pH optimum dan mengkaji kesan gangguan logam berat yang lain semasa penentuan ion Pb(II).

EKSPERIMEN

Bahan Kimia dan Reagen

Semua bahan kimia yang digunakan dalam kajian ini adalah dari gred analisis. Air nyahion digunakan dalam kajian ini untuk penyediaan semua larutan. Larutan stok galosianin (Fluka) dengan kepekatan 0.15 % (w/v) disediakan dengan melarutkan 0.15 g reagen ke dalam 100 mL larutan penimbal pH 8. Satu siri kepekatan larutan galosianin (0.03 – 0.15 %) disediakan melalui pencairan terhadap larutan stok galosianin.

Larutan stok Pb(II) dengan kepekatan 5.0×10^3 mg/L disediakan dengan melarutkan 0.5 g plumbum nitrat (Carlo Erba) dalam air nyahion dan isi padunya dijadikan 100 mL. Satu siri larutan Pb(II) dengan kepekatan 1.0×10^{-10} mg/L – 1.0×10^4 mg/L disediakan dengan melakukan pencairan terhadap larutan stok Pb(II).

Larutan penimbal yang digunakan disediakan berdasarkan kaedah dari Handbook of Basic Tables for Chemical Analysis (Bruno & Svoronos 1989).

Peralatan

Peralatan analisis suntikan aliran yang digunakan terdiri dari injap suntikan (Rheodyne 7727), pam peristaltik (Gelson Pump) dan tiub pam 1.85 cm (Astoria Pacific International). Peralatan ini disambungkan kepada Spektrofotometer UL-Nampak model Shimadzu 160A yang menggunakan sumber lampu tungsten dan deutrium.

Tatakaedah

Kesan kadar alir larutan pembawa terhadap pembentukan kompleks Pb(II)-galosianin dikaji untuk julat kadar alir dari 0.4 mL/min hingga 1.8 mL/min. Parameter-parameter yang lain seperti kepekatan reagen dan kepekatan Pb(II) dibiarkan tetap. Kesan pH terhadap tindak balas pengkompleksan pula dikaji pada julat pH antara 1 hingga 8.0. Larutan Pb (II) dengan isi padu dan kepekatan yang sama tetapi pH yang berbeza disuntik ke dalam sistem melalui injap suntikan.

Untuk kajian kesan kepekatan reagen terhadap serapan kompleks, larutan galosianin pada julat kepekatan 0.03% - 0.15% (g/mL) digunakan. Larutan galosianin yang berlainan kepekatan ini dipamkan ke sistem FIA dengan menetapkan parameter-parameter lain. Spektrum yang terhasil direkodkan dan graf ketinggian puncak melawan kepekatan galosianin diplotkan.

Kajian terhadap julat kepekatan dinamik Pb(II) dilakukan menggunakan larutan Pb(II) pada kepekatan 1.0×10^{-10} mg/L - 1.0×10^{4} mg/L. Setiap satu sampel disuntik sebanyak 10 kali ke dalam peralatan FIA melalui injap suntikan menggunakan penyuntik 25 ml. Reagen galosianin (0.03%) dialirkan menggunakan pam peristaltik dengan kadar alir 1.2 mL/min. Puncak yang terhasil direkodkan menggunakan Spektrofotometer UL-Nampak pada panjang gelombang sekitar 550 nm. Kebolehulangan kaedah ini ditentukan menggunakan kaedah yang sama seperti untuk penentuan julat kepekatan dinamik Pb(II) tetapi hanya satu kepekatan Pb(II) sahaja yang digunakan iaitu 1.0×10^{-2} mg/L.

Kajian terhadap kesan gangguan oleh ion-ion asing dilakukan dalam kajian ini untuk melihat darjah gangguan oleh ion-ion berkenaan. Kajian dihadkan kepada kation-kation Mn(II), Cd(II), Ni(II), Mg(II), K^+, Co(II) dan Na^+ yang telah dikenal pasti sebagai mengganggu dalam penentuan Pb(II). Kajian dilakukan dengan menyuntik campuran Pb(II) dan ion berkenaan pada nisbah molar 1:1 ke dalam peralatan FIA melalui injap suntikan menggunakan penyuntik 25 µl.

KEPUTUSAN DAN PERBINCANGAN

Rajah 1 menunjukkan kesan kadar alir reagen terhadap serapan kompleks Pb(II)-galosianin. Keputusan ini menunjukkan bahawa rangsangan tindak balas

bertambah dengan pengurangan kadar alir. Pada kadar alir yang lebih rendah, analit akan berada di dalam reaktor tindak balas dalam jangka masa yang lebih lama berbanding kadar alir yang tinggi dan keadaan ini memberikan peluang untuk analit berinteraksi lebih lama dengan reagen yang dialirkan. Selain itu, pengurangan kadar alir akan mengurangkan juga serakan analit. Kedua-dua faktor ini membantu dalam meningkatkan kepekaan kaedah.

Kesan pH terhadap tindak balas di antara reagen dan analit ditunjukkan dalam *Rajah 2.* Seperti ditunjukkan, rangsangan optimum diperolehi pada pH 8.0 apabila puncak dengan ketinggian yang maksimum dihasilkan. Pada pH yang lebih tinggi, suatu mendakan berwarna putih didapati akan terbentuk. Oleh itu kesan pH yang melampaui pH 8.0 tidak dikaji dalam kajian ini.

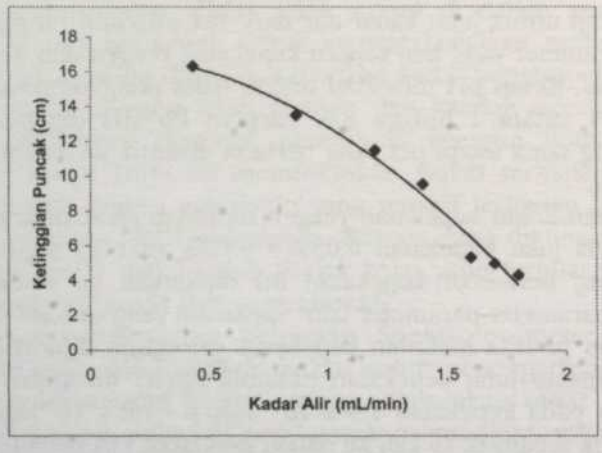

Rajah 1: Kesan kadar alir terhadap ketinggian puncak serapan kompleks Pb(II)-galosianin

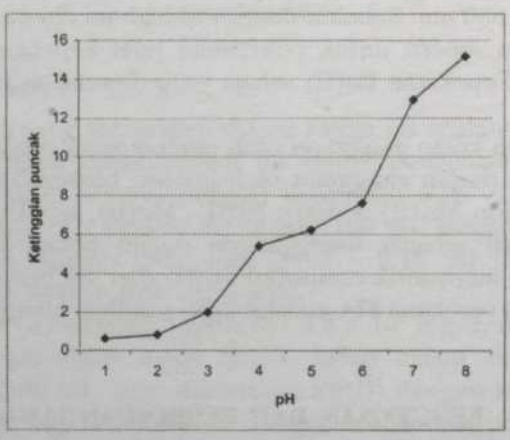

Rajah 2: Kesan pH terhadap ketinggian puncak serapan kompleks Pb(II)-galosianin

Rajah 3 menunjukkan keputusan yang diperolehi dalam kajian kesan kepekatan reagen galosianin terhadap ketinggian puncak spektrum untuk kompleks Pb(II)-galosianin yang terhasil. Serapan kompleks didapati meningkat dengan peningkatan kepekatan galosianin yang digunakan sehingga mencapai suatu tahap di mana serapan menjadi malar. Peningkatan serapan berlaku kerana tindak balas pengkompleksan antara galosianin dan Pb (II) meningkat dengan peningkatan kepekatan galosianin. Walau bagaimanapun, serapan kompleks menjadi malar akhirnya apabila semua Pb (II) yang hadir telah habis digunakan untuk bertindak balas dengan galosianin yang kini hadir secara berlebihan.

Hasil kajian terhadap penentuan julat kepekatan dinamik Pb(II) ditunjukkan dalam *Rajah 4*. Suatu garis lurus dihasilkan pada julat kepekatan Pb(II) yang digunakan iaitu 1.0×10^{-3} mg/L – 1.0×10^{1} mg/L. Untuk kajian terhadap kebolehulangan kaedah, hasil yang diperolehi menunjukkan bahawa kaedah ini mempunyai kebolehulangan yang baik dengan nilai RSD 1.03%.

Jadual 1 menunjukkan peratus gangguan kation asing semasa pengesanan Pb (II) dilakukan. Pada nisbah molar 1:1, kation-kation Ni (II), K, Cd (II) dan Co (II) didapati memberikan peratus gangguan yang agak tinggi iaitu sekitar 7.50 – 10.15 %. Kation-kation lain yang dikaji iaitu Mn(II), Mg(II) dan Na^{+} didapati memberikan peratusan gangguan di bawah 5.00 %. Di dalam keadaan di mana sampel Pb(II) yang ingin dianalisis diketahui mengandungi ion-ion pengganggu ini, adalah dicadangkan agar ion-ion pengganggu tersebut ditopengkan terlebih dahulu sebelum analisis dijalankan. Contohnya ion Ni(II) boleh ditopengkan dengan menggunakan Dimetilglioksin (DMG).

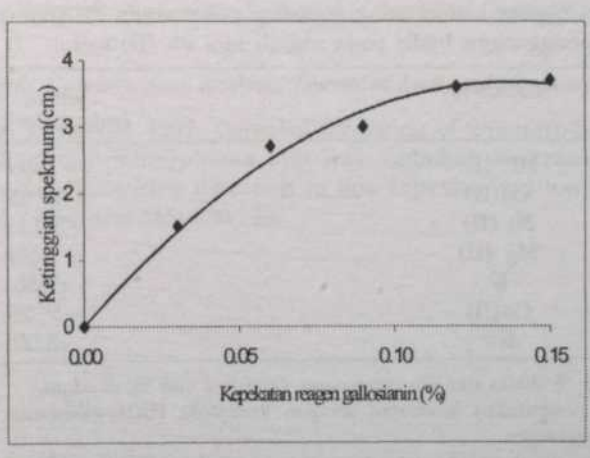

Rajah 3: Kesan kepekatan reagen galosianin terhadap ketinggian puncak serapan kompleks Pb(II)-galosianin

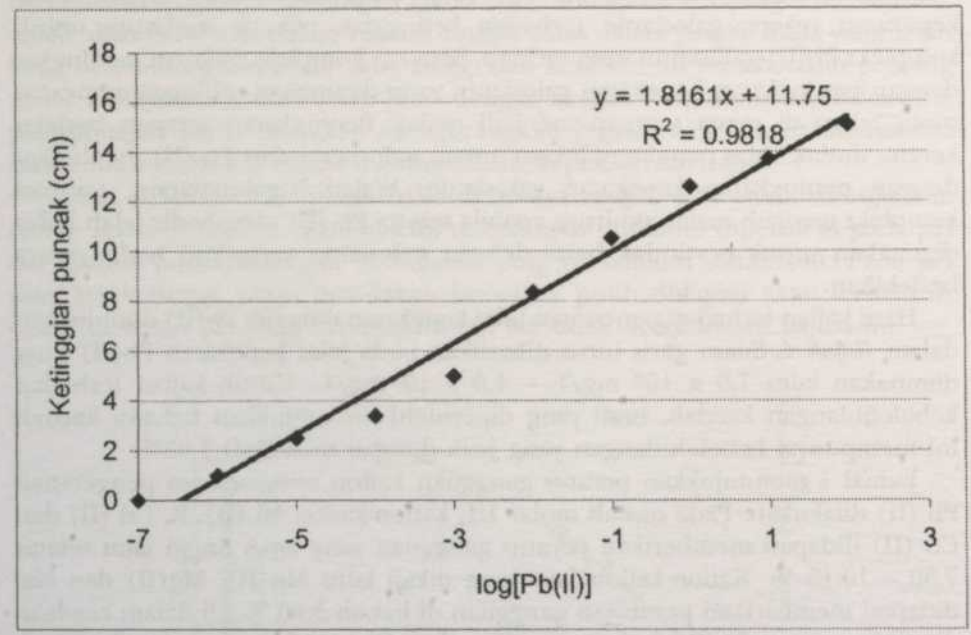

Rajah 4: Julat kepekatan dinamik ion Pb(II) menggunakan kaedah FIA dengan reagen galosianin

JADUAL 1
Kesan gangguan kation asing terhadap pengesanan Pb (II) apabila ion pengganggu hadir pada nisbah mol Pb (II):kation 1: 1.

Kation%	* gangguan (ralat relatif, %)
Mn (II)	+ 2.50
Cd(II)	+10.05
Ni (II)	+ 10.15
Mg (II)	+ 3.90
K^+	+7.50
Co(II)	+10.25
Na^+	+3.00

* ralat relatif, % dikira dengan persamaan (x-y)/y x 100 %, di mana:

x – purata (3 penentuan) keamatan serapan kompleks Pb(II)-galosianin dengan kehadiran kation pengganggu

y – purata (3 penentuan) keamatan serapan kompleks Pb(II)-galosianin tanpa kehadiran kation pengganggu

KESIMPULAN

Kajian yang telah dilakukan menunjukkan bahawa reagen galosianin merupakan reagen yang sensitif untuk penentuan Pb(II) dalam persekitaran air dengan menggunakan kaedah analisis suntikan aliran. Rangsangan linear diperolehi pada julat kepekatan Pb(II) 1.0×10^{-3} mg/L - 1.0×10^{1} mg/L dan had pengesanan yang dikira ialah 0.45 mg/L. Kebolehulangan kaedah sangat memuaskan dengan nilai RSD 1.03%. Kaedah ini walau bagaimanapun mengalami kesan gangguan yang agak tinggi daripada kation-kation seperti Ni (II), K, Cd (II) dan Co (II).

PENGHARGAAN

Penyelidik merakamkan penghargaan kepada IRPA kerana membiayai penyelidikan ini melalui gran projek IRPA 09-03-03-0028.

RUJUKAN

Bruno T.J. dan P.D.N. Svoronos. 1989. *CRC Handbook of Basic Tables for Chemical Analysia.* USA: CRC Press.Inc.

Jaenicke S., R.M. Sabarathinam, B. Fleet dan H. Gunasingham. 1998. Determination of lead in blood by hydrodynamic voltammetry in a flow injection system with wall-jet detector. *Talanta* **45**: 703-711.

Mingshu L. dan G.E. Pacey. 1995. Lead determination at the ppb level using stopped-flow FIA. *Talanta* **42**: 1857-1865.

Novikov E.A., L. K. Shpigun dan Yu. A. Zolotov. 1989. Flow injection analysis: Extraction-photometric determination of lead. *Journal of Analytical Chemistry of USSR* **44**: 1067-1071.

Shpigun, L. K. 1990. Flow injection analysis. *Journal of Analytical Chemistry of USSR* **78**: 145.

Yamane T. dan Y. Yamaguchi. 1997. Complex formation of 2-(5-nitro-2-pyridilazo)-5-(N-propyl-N-sulfo-propylamino)phenol with lead, cadmium and manganese for their sensitive spectrophotometric detection in flow injection and ion chromatography system *Anal. Chim. Acta* **345**: 139-146.

Pertanika J. Sci. & Technol. 10(2): 269 - 286 (2002)
ISSN: 0128-7680

Wireless Spread Spectrum Communication Channel Modelling and Simulation Technical Area: Wireless Communication

***Sabira Khatun, Ashraf Gasim Elsid Abdalla & Borhanuddin Mohd Ali**
Department of Computer & Communication System Engineering,
Faculty of Engineering, Universiti Putra Malaysia
43400 UPM, Serdang, Selangor, Malaysia
e-mail: sabira@eng.upm.edu.my

Received: 31 July 1999

ABSTRAK

Kertas ini berkait dengan pola Rangkaian Komunikasi Spektrum Sebaran Wayarles dan perancangan menggunakan teknik spektrum sebaran Jujukan Terus (DSSS) model-model teori dan matematik dibangunkan untuk simulasi dan penilaian persembahan. Sebab pensimulasian sistem adalah untuk memeriksa kesahan dan mengelak sebarang perubahan yang tidak perlu semasa pelaksanaan perkakasan sebenar sistem tersebut. Sebab lain pensimulasian sistem sebelum melaksanakan adalah untuk mencari cara yang sebaik mungkin atau kaedah utnuk membuatnya seperti teknik modulasi, lebar jalur, sekuriti dan sebagainya. Jenis rangkaian komunikasi ini memberikan kebolehan untuk mengelak sumber-sumber luaran lain daripada penyesakan dan gangguan dengan transmisi informasi disebabkan penggunaan teknik Jujukan Terus. Kertas ini menghuraikan pola, pembangunan dan simulasi saluran komunikasi wayarles digital dalam bangunan. Saluran komunikasi tersebut mengandungi unit penerimaan transmit beroperasi dalam frekuensi 900-915 MHz. Untuk rangkaian komunikasi wayarles yang selamat dan boleh diharap teknik Spektrum Sebaran Jujukan Terus (DSSS) digunakan. Bahagian yang paling mencabar adalah penerima di mana jujukan hingar pseudorawak perlu diselaraskan untuk memulihkan mesej sebenar yang dihantar. Lain-lain kawasan penting penyiasatan termasuklah kumpulan kod hingar pseudorawak (kod PN), Kekuncian Anjakan Amplitud (ASK), pemodulatan/penyahmodulatan Kekuncian Anjakan Fasa Perduaan Kebezaan (DBPSK), modulatan Kekuncian Anjakan Fasa Kebezaan (DPSK), pengesanan jelas lawan tidak jelas, dan sebagainya.

ABSTRACT

This paper deals with *Wireless Spread Spectrum Communication Link* design and planning using Direct Sequence Spread Spectrum (DSSS) technique. The theoretical and mathematical models are developed for simulation and performance evaluation. The purpose of simulating the system is to check validity and avoid unnecessary changes during the actual hardware implementation of the system. Another purpose of simulating the system before implementing it is to find the best possible way or method to fabricate it like the modulation technique, bandwidth, security etc. This type of

*Communicating Author

communication link gives the ability to prevent other external sources from jamming and interfering with the transmission of information due to the use of Direct Sequence technique. This paper describes the design, development and simulation of an indoor digital wireless communication channel. The communication channel consists of a transmit-receive unit operating in the 900-915 MHz frequency range. For a reliable and secure wireless communication link, the Direct Sequence Spread Spectrum (DSSS) technique is used. The most challenging part is the receiver where the pseudo-random noise sequences must be synchronized to successfully recover the original transmitted message. Other key areas of investigation include selection of the pseudo-random noise code (PN code), Amplitude Shift Keying (ASK), Differential Binary Phase Shift Keying (DBPSK) modulation/demodulation, *Differential Phase Shift Keying (DPSK)* modulation, coherent versus non-coherent detection, etc.

Keywords: Wireless, spread spectrum, direct sequence, differential phase shift keying

INTRODUCTION

Spread Spectrum Communication is a method to transmit information wirelessly and securely using the Direct Sequence Spread Spectrum (DSSS) technique (Wilheimsson and Zigangirov 1998; Chu and Mitra 1998; Qiao 1998; Host-Madsen and Cho 1999; Glistic *et al.* 1999; The American Radio Relay League 1996; Power Spectral Density Curve; Messier 1998). This paper describes the construction of a transmit / receive unit to operate in the range of 900 - 915 MHz band using the spread spectrum method (Prasad 1996; Peterson and Ziemer 1985; Freeman 1995). One such technique is direct sequence spread spectrum, which has become popular for many wireless communication systems (Wilheimsson and Zigangirov 1998; Chu and Mitra 1998; Qiao 1998; Host-Madsen and Cho 1999; Glistic *et al.* 1999; Glistic *et al.* 1999; The American Radio Relay Leaque 1996).

The communication channel involves the construction of a spread spectrum transmitter and receiver. In this paper two areas of investigation have been selected. The first stage is the simulation and modelling, such as channel modelling and Tx / Rx circuit design. The second stage involves the hardware implementation, which requires the determination of antenna impedance, radiation pattern, cost, durability and polarization, Tx / Rx switch for half duplex operation, amplifier impedance, bandwidth, gain, power, distortion, modulator/demodulator BPSK, QPSK, DPSK, local oscillator frequency, stability, power output and digital interference synchronization speed (Messier 1998). In this paper the main focus is on the system modelling and simulation.

The transmitter and receiver comply with self-defined standards and protocols to enable proper communication and data transfer described in detail in (Wilheimsson and Zigangirov 1998; Chu and Mitra 1998; Qiao 1998; Host-Madsen and Cho 1999; Glistic *et al.* 1999). The various blocks or program functions, which make up the overall system, are implemented by software simulation (Ong 1998; Proakis and Salehi 1998).

The challenge in implementing a working DSSS is in the receiver. In order to receive information successfully the receiver has to synchronize with the pseudo random noise (PN) sequence of the transmitter (Transmission Line Attenuation Chart). This involves extracting the sequence from the incoming signal, aligning the local sequence to the transmitted sequence, and then locking onto the incoming signal so that data can be correctly de-spread (Error Correction with Hamming Codes 1994; Blahut 1983). The Amplitude Shift Keying (ASK) and Differential Phase Shift Keying (DPSK) modulation and demodulation scheme have been selected (Peterson and Ziemer 1985). Because of its very low output power, it is not expected that the transmitted signal will interfere with any other communication equipment.

This paper is organised as follows. The next section describes the theoretical and mathematical models. The simulation model, the results and discussion and finally the conclusion follow this.

THE THEORETICAL AND MATHEMATICAL MODEL

The simulation has been carried out using MATLAB as the main simulation tool. This section details the concept of the simulation method and gives a description of the simulation model. In addition the simulation environment is presented.

The Concepts of the Method Applied

The primary advantage of a spread spectrum communication system is its ability to reject interference whether it is unintentional interference by another user simultaneously attempting to transmit through the same channel, or the intentional interference by a hostile transmitter attempting to jam the transmission. It also provides excellent narrow-band noise rejection characteristics. The fundamental concept of spread spectrum is to spread the baseband digital signal with a periodic binary sequence, noise-like in nature, called a pseudo random noise (PN) sequence.

In a DSSS system, a PN sequence is used to convert a narrow-band digital signal to a larger bandwidth signal, referred to as a spread signal. To transmit the spread signal through a channel such as the atmosphere, Amplitude Shift Keying (ASK) or Phase Shift Keying (PSK) techniques are applied to the spread signal. A sinusoidal carrier is multiplied by the spread data to produce ASK modulated data or the carrier is multiplied by differentially encoded spread data to produce DPSK modulated data. The received signal may be recovered by using coherent detection or a phase lock loop and a matched filter.

Synchronization is of concern with the recovery of the baseband digital signal. For proper operation, a spread spectrum system requires that the locally generated pseudo random noise sequence used to de-spread the received signal be synchronized with the pseudo random noise sequence used to spread the transmitted signal.

The locally generated pseudo random noise sequence is compared to an interval of the received signal, a measure of correlation is used to determine

when the two signals are satisfactorily aligned. After alignment, the remaining received signal is then correlated with the pseudo random noise sequence and is properly de-spread using a matched filter after which the baseband digital data is properly recovered.

Pseudo Random Noise Sequences

Sequence Spread Spectrum applies the principle of spreading the spectrum through the use of pseudo random noise sequences. The bit sequence is not truly random since the sequence is periodic. However, it is referred to as pseudo random because the periodicity is so large that usually more than one thousand bits occur before the sequence repeats. A random bit sequence generator forms the pseudo random noise sequence. The generator is a set of feedback shift registers operated by a single clock. During a pulse of the clock, the state of each flip-flop is shifted to the next one and the result is fed back as the input to the first flip-flop. This sequence is then employed in the transmitter and receiver for spreading and de-spreading.

Processing Gain in spread spectrum system is defined as the ratio of transmitted bandwidth to information bandwidth. This parameter can also be defined as the difference between the signal-to-noise-ratio (in dB) of the transmitted bandwidth to the information bandwidth. The spread spectrum technique results in a message signal with a transmission bandwidth (B_t) that is much larger than the information bandwidth (B_i) of the original signal (Prasad 1996). This can also be expressed in terms of dB by:

$$G_p(dB) = 10\log_{10}\left(\frac{B_t}{B_i}\right) \quad (1)$$

where, $(B_t/B_i) = L$, is the length of PN code.

For a spread spectrum system the ratio of the transmission bandwidth to information bandwidth is often the length of the PN code length. By doubling the length of the PN code, a 3dB increase in signal to interference ratio is obtained. By increasing the processing gain, the system will be better able to reject interfering signals, and more users will be able to reuse the same frequency band using different PN codes.

Model Description

Two modulation techniques have been implemented, the PN modulation (or coding) and ASK or DPSK, respectively.

Pseudo Random Noise Modulation

First, the incoming data sequence is modulated with a pseudo random noise sequence code. This noise-like code transforms the narrowband data sequence into a noise-like wide-band signal. The function of pseudo random noise

modulation is to spread each bit of binary data in the transmit packet which converts the original narrow-band digital signal into a wide-band spread spectrum signal. This requires the multiplication of every bit in the transmit packet by a predefined seven bit pseudo random noise sequence to form a noise-like spread digital signal. The bandwidth occupied by the pseudo random noise modulated data will be seven times larger than the original's transmit packet bandwidth. In general this process can be described as follows:

$$M(t) \times PN(t) = P(t) \tag{2}$$

where M(t) = the message signal, PN(t) = the PN code and P(t) = the PN modulated wave. However, the bit rate of this signal is $L * R_b$, where L is the length of the PN code and R_b is the bit rate of M(t).

PN demodulation takes place at the receiver. PN demodulation simply decodes the transmitted message by multiplying the transmitted message with the PN code. The demodulated signal, $\hat{M}(t)$, is a good approximation of the original message data and can be expressed as

$$\hat{M}(t) = P(t) \times PN(t) \tag{3}$$

ASK Modulation

In the second technique the resultant wide-band signal (PN modulated signal) is used to modulate a local carrier to produce an ASK signal. The ASK modulation is essential for conversion of the baseband signal into a radio frequency signal.

In ASK technique, the different amplitudes differentiate each binary sign example, 1 volt (or 'on') may represent a binary bit '1' and 0 volt (or 'off') may represent a binary bit '0'. In Differential Binary Phase Shift Keying (DPSK) the phase changes only at the transition from bit '1' to '0' or vice versa.

In ASK modulation, a baseband data signal P(t) is modulated by a complex envelop g(t) with carrier wave S(t) and the modulated signal Y(t) is

$$Y(t) = P(t) \times g(t)$$

where g(t) = A S(t), A is a sinusoidal amplitude for sending a binary bit '1' and $S(t) = \cos(2\pi f_c t)$, f_c is the operating frequency (915MHz).

$$\therefore Y(t) = AP(t) \cos(2\pi fct) \tag{4}$$

The radio frequency signal is then transmitted across the channel and received at the other end. Here two stages of demodulations are required. First, the received noise-like wide-band signal is passed through a ASK demodulator to demodulate the signal. A method of synchronization must be employed at

this stage to ensure proper de-spreading of the demodulated signal.

ASK demodulation is used to recover the baseband signals. Multiplying the received waveform (that deviates from the desired values frequency and amplitude by Δf and ΔA respectively due to channel noise) with carrier wave S(t), the demodulated wave is

$$Y(t) = \hat{Y}(t) \times S(t) \tag{5}$$

where the received waveform

$$\hat{Y}(t) = (A + \Delta A) \times (P(t) \times \cos 2\pi (fc + \Delta f)\, t.$$

Since ΔA and Δf are very small using an appropriate scaling factor 'K' the low pass filter (LPF) output can be represented as follows:

$$Y'(t) = \frac{1}{2} AP(t) \times \cos 2\pi \Delta f\, t \Rightarrow \frac{1}{2} A\, P(t) \times K \Rightarrow \hat{P}(t) \tag{6}$$

which is an approximation of the original signal P(t).

Hence, the steps taken to ASK modulate and detect a spread spectrum signal are as follows:

At the Transmitter:	PN modulation
	ASK modulation
At the Receiver:	ASK demodulation
	PN demodulation
	Message retrieval

DPSK Modulation

In DPSK technique the implementation of the DSSS system can be broken down into two main sections: i. e. hardware section and a software section. The software portion of the implementation performs all the DSP (Digital Signal Processing) while the hardware part of the implementation performs the DPSK modulation and demodulation.

There are mainly two steps in DPSK modulation: 1) differential encoding of the signal and 2) BPSK modulation.

1) Differential Encoding:

If the data from the information source is denoted by D_n and the initial reference bit is Cn-1, the differentially encoded data sequence C_n is (Peterson and Ziemer 1985):

$$C_n = D_n \oplus C_{n-1} \tag{7}$$

where, '⊕' represents the exclusive OR (XOR) operations. This operation

is used to produce the differentially encoded data sequence $\{C_n\}$ from original data sequence $\{D_n\}$. The next step is PN coding using $\{C_n\} = M(t)$ to obtain P(t) followed by BPSK modulation.

The differential decoding is performed by forming the sequence $\{\hat{D}\}$ as follows:

$$\hat{D}_n = C_n \oplus C_{n-1} \tag{8}$$

2) BPSK Modulation

P(t), the PN modulated wave is used to binary phase shift the carrier wave S(t), resulting in a DPSK modulated signal $Y_1(t)$. So the transmitted signal

$$Y_1(t) = P(t) \times S(t) \tag{9}$$

Let $\hat{S}(t) = \cos(2\pi(f_c+f_\Delta)t+\phi)$ represent the local oscillator carrier wave at the receiver where f_Δ is the carrier frequency offset between the transmitter and receiver and ϕ is the carrier phase. Hence the demodulated wave is

$$Y_2(t) = Y_1(t) \times \hat{S}(t) = P(t) \times S(t) \times \hat{S}(t) \tag{10}$$

Since f_Δ is very small, using an appropriate scaling factor 'R', the filter output is

$$Y_2(t) = \frac{1}{2} P(t) \times \cos(2\pi f_\Delta t - \Phi) \Rightarrow LPF \Rightarrow \frac{1}{2} P(t) \cos\Phi \times R \Rightarrow \hat{P}(t) \tag{11}$$

Hence, the steps taken to DPSK modulate and detect a spread spectrum signal are as follows:

At the Transmitter:	Differential encoding
	PN modulation
	BPSK modulation
At the Receiver:	BPSK demodulation
	PN demodulation
	Differential decoding
	Message retrieval

The results obtained from the two different modulation techniques have been compared. The main reason to compare the two different modulation techniques is to find out what is the best and the most suitable technique for this particular system.

Transmitter Design for ASK Modulation

The spread spectrum transmitter is designed in two stages consisting of the radio frequency component and the intermediate frequency component. The radio frequency component is used to up-convert the intermediate frequency

for wireless transmission at 915 MHz.

The primary purpose of the spread spectrum transmitter is to convert a narrow-band digital signal to a wide-band, noise-like, digital signal through pseudo random noise modulation. This wide-band digital signal is then used to modulate a sinusoidal carrier to produce an ASK modulated signal at the intermediate frequency. Before modulation occurs, the input string is first converted into binary and then a packet is created complete with preamble, start and stop characters, and the input string. Secondly, the packet is pseudo random noise modulated. ASK modulation is used since baseband information is not suitable for wireless transmission.

The spread spectrum transmitter design consists of multiple components that function together as shown in *Fig. 1.* Each component is designed using MATLAB. The user input on the transmit side is in the form of an ASCII string.

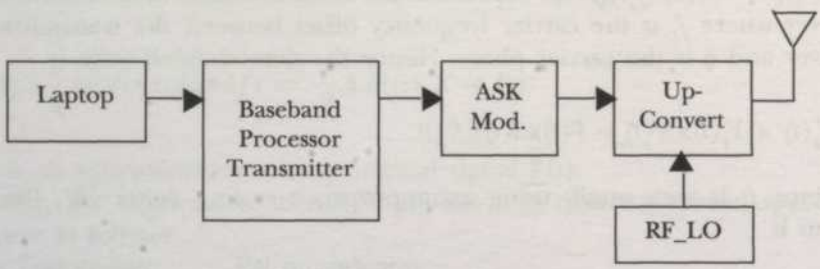

Fig. 1: Transmitter design model

This data is converted to binary and is included in the transmitted packet.

The mode of transmission employed in most spread spectrum systems is packet transmission. The general packet structure includes preamble, a start character, the message data, and a stop character (described in the Simulator section in *Fig. 5*). Preamble is used to ensure that the receiver has sufficient time to synchronise with the transmitted pseudo random noise sequence. The stop and start characters are added to ensure that the receiver does not need to know when transmission begins or ends.

Normally, the preamble consists of two hundred binary one bits. The start character consists of eight zero bits added at the front of the input binary message and after the preamble. The stop character consists of sixteen one bits and is appended to the end of the packet to form the packet for transmission.

Transmitter Design for DPSK Modulation

The simulation of this system is done by breaking up the whole system into various blocks. Each of these blocks has its own function and finally all these blocks are put together to form the simulation model. The various functions to represent these blocks are written in MATLAB M-files. The blocks of this system are shown in *Fig. 2.*

The first block is the **Text to ASCII** block. This block serves to convert the

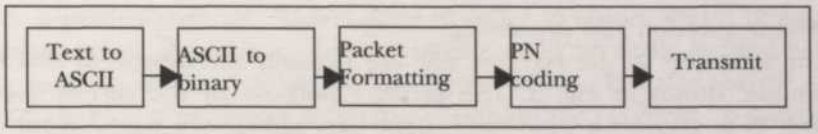

Fig. 2: Blocks in the transmission system

text data received into its ASCII code representation. To achieve this purpose, a function is written in MATLAB M-files with the name ***Te-xt2Asc***. This function uses a MATLAB built-in function ***abs***. This function changes string into a decimal representation. This representation is not equal to the ASCII code but for the simulation purpose, this representation would be sufficient. After changing the text to its ASCII format (for simulation purposes, a different decimal representation), the decimal numbers are converted into their binary equivalent. This is achieved by putting the information in the second block. This block, ***ASCII to binary***, converts any decimal number into its binary representation. This is to meet the requirement of a digital system. This block utilises the function ***de2bi***. The output of this function is a matrix with 7 columns and number of rows that are equal to the number of letters in the alphabet and/or numbers and/or punctuation. The output of this block is channelled to the third block.

This block would do all the necessary addition of bits to mark the header, tail and others. This block should actually add the headers, tail and also put the information into organised packets of fixed number of bytes / bits. Because all the previous functions have fixed the number of bits representing all possible data to 7 bits, formatting has been made simpler. So in this block only the header and tail are added. The header is placed at the start of the information being sent and the tail is appended at the back. For simulation purposes, the header has been set to 10 contiguous '1's and the tail to 6 contiguous '0's. It is used just to simplify the simulation process (since only one channel is used). There is no possibility that the information would contain these sequences of '1's and '0's because of the choice of representing the various letters in the alphabet, punctuation and numbers. The number of bits representing each data is 7 as stated earlier and thus '0's would not be sufficient to represent any of the sent data. Besides, all '0's would mean that the decimal equivalent is also '0' and there is no data represented by this value. As for the 10 '1', the equivalent value in decimal is '1023' and this also has no meaning. Additionally the decoding of this information does not look at the bits at all, for it counts the number of bits from the start of reception. This will be explained further in the reception section.

Receiver Design for ASK Modulation

The spread spectrum receiver is designed in two stages consisting of the radio frequency component and the intermediate frequency component. The radio frequency component is used to down-convert to the intermediate frequency

for data acquisition and processing.

The functions in the receiver side are basically the inverse of that of the transmitter shown in *Fig. 3.* The primary purpose of the spread spectrum receiver is to convert a wide-band, noise-like, signal to a narrowband digital signal. The received wide-band digital signal is demodulated to produce a spread baseband digital signal. These spreads signal is then demodulated to obtain the original transmit message.

The received signal is acquired using analogue to digital conversion at the intermediate frequency. Based on the input signal level, the sampled signal is amplified accordingly to obtain a two-volt peak-to-peak waveform. This is a form of automatic gain control employed in many receiver designs. The signal is in the form of an ASK modulated waveform. By detecting the amplitude change, the ASK signal is demodulated and converted to a baseband digital waveform.

Amplitude modulation is the result of the variance of the instantaneous amplitude of the received signal with time. The next step in the recovery of the received message is pseudo random noise sequence synchronization.

In order to ensure the receiver has enough time to synchronise, a preamble is appended to the transmitted message. The digital waveform is sampled over one bit interval, composed of seven chips, and correlated to the locally generated pseudo random noise sequence. From this, the level of correlation is measured. If the level is below a set threshold, the data is discarded and a new sample of the received data is taken. Simultaneously, the locally generated pseudo random noise sequence is shifted forward to provide better probability so that the received signal correlates to the pseudo random noise sequence. This process continues until synchronization is achieved. At this point, pseudo random noise demodulation occurs and the de-spread digital data is recovered. The receiver then parses the data to look for the start and stop characters and converts the extracted binary data into a string. This string should be the string entered at the transmitter end earlier.

Receiver Design for DPSK Modulation

The reception model is relatively just the opposite of the transmission model. It has several blocks too and these blocks tend to reverse the process of its peer in the transmission block. All blocks are independent of each other. The preceding or proceeding blocks do not have any knowledge of what has been

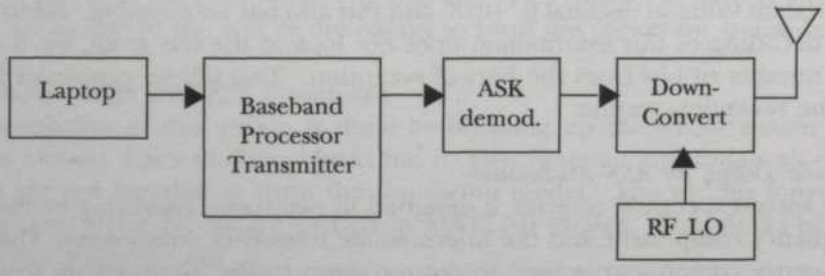

Fig. 3: Receiver design model

done at a particular block. This is done in order to ensure that if in any case a problem arises, the source of the problem could be easily located without having to go through every part of the whole system. It would suffice to just concentrate on the particular block that is causing the problem. A diagram of

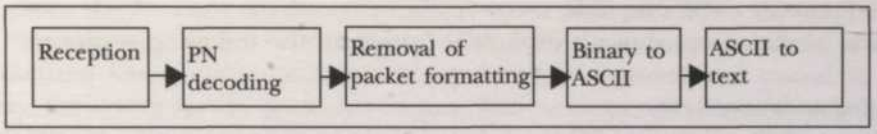

Fig. 4: Blocks in the reception system

the blocks in the reception model is shown in *Fig. 4* below.

As in the transmission model, this block - which is analogous to the Transmit block in the transmission model-is the most complicated of all the blocks in the reception model, though not as complex as the transmit block. The Reception block receives the transmitted signals from the channel and demodulates it to the baseband signal. This model represents a basic transmission and reception model.

In this block, several functions have been referred in order to achieve the desired results, Viz as Rx, Detect, and Diff dec. In fact, Rx constitutes the main function called in this block. Rx then calls the other functions, Detect and Diff dec, in order to demodulate the incoming signal. Diff dec performs differential decoding in accordance with the differential decoded incoming signal. This would then result in the signal being differentially decoded and this signal would then pass to the subsequent block, i.e. PN Decoding block.

THE SIMULATOR

Software development is broken down into two sub sections: transmitter and receiver. The receiving end is basically the opposite of the transmission end. The software is designed using the modular designing technique, i.e., a big task is subdivided into smaller tasks. Both transmitter and receiver have multiple modules, which work together to achieve the required functionality.

Transmitter Functions

The transmitter allows a user to input a text message to be transmitted. This text message is an array of ASCII character. Each character is converted into its ASCII representation. After this conversion, all the characters are stored in a binary array. This binary array of data is then converted into one or multiple packets depending upon the length of the entered message. Each packet is then PN coded and then stored in a two-dimensional array. The output two-dimensional array contains a packet in every row.

To achieve all the above-mentioned functionalities, the software is broken into the following sub modules:

* String to binary array module
* Arrangement of various matrix sizes $m \times n$ into $l \times (m*n)$ matrix form (matrix resizing) module
* Packet formatting module
* PN code data module
* Transmit packet module

Each of the sub-modules is explained further in the following sections.

String to Binary Array

This module takes an ASCII string input by the user and outputs a binary array. The output array contains binary representation of all the characters.

Matrix Resizing

This function resizes whatever size or shape of the matrix of the input binary array say $m \times n$ into $1 \times (m*n)$ matrix. This is done because all the input data at the latter stage will be required to be of this type.

Packet Formatting

The binary data array from the "String To Binary Array" module is broken into one or multiple packets. A packet consists of a header segment, data segment

Header segment	*Data segment*	*Stop Bit (s)*

and a stop bit segment.

The 'data length per packet' determines the number of data bits to be put in one packet. The 'stop bit(s)' sequence is set to six consecutive 0. The preamble is repeated in a packet ten times by default. The repetitions are used for packet synchronization in the receiver module. The output of this module is a double array, which contains a packet per row and number of packets made.

PN Coder transforms an input binary array into a PN coded array. The PN code forms the input to this module along with the binary data array.

Transmit

This function transmits the packetized data. It generates samples of a bandpass waveform using Amplitude Shift Keying (ASK) modulation technique. The carrier frequency modulates the baseband signal.

This module takes in a packet of information and creates a continuous waveform using the packet data bits as values for the waveform. This waveform is sent to the ASK modulator and then sent out to the channel.

The receiver module starts off by collecting a requested number of data packets. This large array of data is stored in the 'receive buffer array'. Once the array is full, the data is sent for processing. This processing includes non-coherent detection technique. Therefore, it needs to process the collected data

through two – decoding/demodulation process.

The first is ASK demodulation and the second is PN decoding. Note that before PN decoding can take place, synchronization between the received data and the PN code, needs to be done. The synchronization module is written and tested for a non-coherent simulation.

Once the PN code synchronization has taken place, the PN code is applied to the received data. The output of the PN code demodulation is the packetized binary data. Once the received data is obtained and stored in an array, the search for the preamble begins. The user can control the data length variable.

The data bits, once found, are converted into the ASCII value they represent. The ASCII number is translated into an ASCII character and displayed to the user.

To achieve all the above-mentioned functionality the software is broken into the following sub modules:

* Receive packet module
* Matrix resizing module
* PN decode data module
* Packet deforming module
* Inversion of matrix sequence module
* Binary to decimal module
* ASCII to string module

Receive

This function receives the transmitted data. The received data is then BPSK demodulated to get the PN coded packetized data.

PN Decoder

The received data bits are PN coded. Before doing any further processing, PN code synchronization is essential for decoding. This module makes use of shift registers to achieve synchronization. A PN coded data bit when multiplied with the PN code will result in all the chips being in the same state. This property is used for synchronization in this module. The received data is compared bit by bit. When a match is found (all the chips are of the same state) the search ends and the index of the match is stored for the next module.

The decoding starts by collecting the specified number of chips into a bit. The number of chips corresponds to the length of the PN code array. Each chip in a bit is multiplied with its corresponding chip from the PN code. All of the data bits are decoded in this fashion.

Packet Deforming

This module expects data that has been completely decoded. The purpose of this module is to extract the data field out of the received and decoded data. The module starts by finding the first preamble match. When a match is found, the location of the data portion of the packet is still unknown. The only piece of information known to the "depackc 1 " module is that the data section is

immediately after the preamble.

Inversion of Matrix Sequence

This function is important for arranging the data back to its original order. This is because the data is received in the inverted order. So, in order to correct this, we need to invert it back to its original order.

Example:

A = (1 0 0) , "invert" A = (0 0 1)

Binary to Decimal

This function converts the binary data into its decimal equivalent. The decimal value actually represents the ASCII code that has been predetermined. This output is then used in the next module.

ASCII to Text/String

This function converts the ASCII code back to the original data first keyed in by the sender. The function can be found in the usual MATLAB function library.

RESULTS AND DISCUSSIONS

A) ASK Modulation

The system developed above shows good functionality. It is able to receive, without error, the original information transmitted on the transmitter end. This is due to the fact that this system is simulated using AWGN channel within indoor environment. With ASK, this particular modulation is susceptible to any form of noise and distortion.

For ASK to differentiate between two different bits ('0' and '1'), a comparison with a threshold value is requested. So when any form of noise or distortion sets upon, it affects the accuracy of the matched filter deciding in which bit ('0' or '1') that particular signal falls into.

The simulation program is basically divided into two major groups, the Transmitting End and the Receiving End. Generally, the processes in the receiver are the inverse of the transmitter.

At the transmitter, the first step is to convert the string or text that has been keyed in by the user into decimal (in this case, the word is TESTING). The decimal value is actually in the form of ASCII code. For instance, 1 is represented by ASCII code of **49** and **a** is represented in ASCII as 97. This ASCII code is then converted into its binary equivalent because we need to transmit and receive based on a digital system. After that, the binary data sequence is arranged into a single row matrix form. This is to allow easier interpretation and for facilitating the next process, which is to packetize the binary sequence. The packet is completed with header, data and tail (stop bits). The header is meant for the packet to recognize where the last packet stopped and this is where it has to continue. The stop bits are to tell where that

particular packet ends. Next, the packetized binary data is spread by applying PN code for security. The spread data is the Amplitude Shift Keyed and transmitted.

At the receiver, the data is first ASK demodulated to get the spread data. Next, the data is arranged into the form of a single matrix to facilitate the next processes. Later, the data is Pseudo random noise decoded to get the packetized binary data. It is then depacketized to get the binary sequence data. At this point, the data has to be arranged again into the form of a single row matrix. Next, the data is rearranged into a 7-column matrix. This is because 7 bits represent each letter, and thus, this makes it easier to interpret and process. Next, the binary sequence data is converted into decimal, or in other words, the ASCII code. Later, the ASCII is converted into string or text. *Fig.*

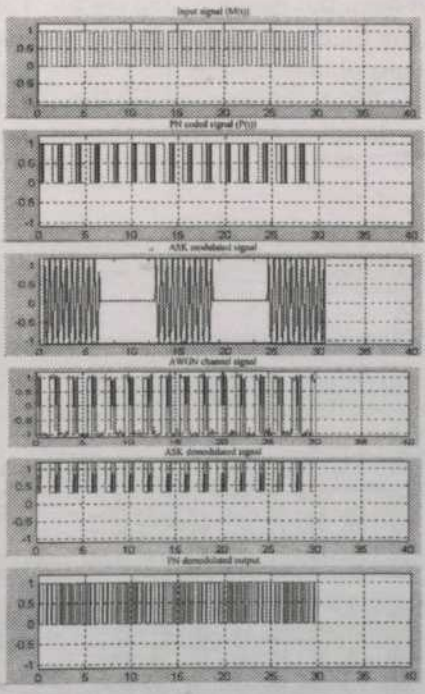

Fig. 6: The waveform results for ASK Modulation

6 shows the waveform results in time domain.

B) DPSK modulation

Simulation is done in the MATLAB environment. All functions are written in MATLAB M-files and the simulation progressed as a command line structure. A test with a few characters has been made and it was observed that transmitting and receiving blocks performed the expected operations on the data. The resulting output is found to be an approximation of the input because of the low noise and channel limitations.

It is clear from the simulation results that the expected objective has been achieved. In the simulation, differential coding is used before binary phase shift keying is done. This is to satisfy the condition of a DPSK system.

The simulation results showed that all the blocks in the transmission and reception models served their purpose well and each process is executed independently of the other processes. First, the data is converted from text to its ASCII code and then to the binary equivalent. This binary sequence is then rearranged into the form of single row matrix. This is to facilitate the transition into the next function. Next, packet formatting is done to the binary sequence. This is then coded with the pseudo-random noise sequence and finally modulated and transmitted.

At the receiving end, the transmitted signal is demodulated and the original binary data is retrieved from the demodulated signal. This demodulated signal is actually the same as the pseudorandom coded binary data in the transmission end. The payload is then obtained from this data by getting rid of the packet formatting. This payload is the binary representation and conversion back to decimal and finally text is done. *Fig. 7* shows the waveform results in the time domain for DPSK.

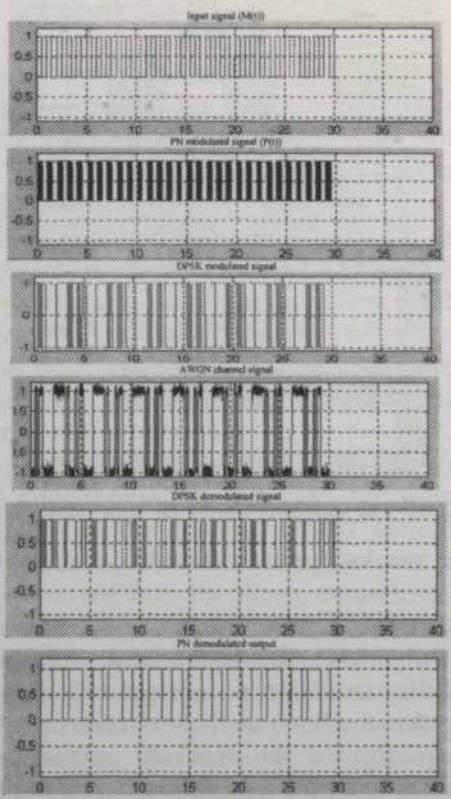

Fig. 7: The waveform results for DPSK Modulation

CONCLUSIONS

This paper describes the hardware model of the transmitter and receiver using Wireless Spread Spectrum Communication techniques using MATLAB communication toolbox. The aim of implementing such a system is to ensure a high security of the transmitted massage because spread spectrum signals are known to be noise-like and hard to detect. They are also hard to intercept and jam. These Low Probability of Intercept (LPI) and anti-jam (AJ) features are why the military personnel have been using Spread Spectrum for many years even until today. Presently IMT-2000 uses CDMA, a form of spread spectrum (SS). In future, an error control using block code (FEC) can be implemented to correct the channel error for both indoor and outdoor wireless spread spectrum communication system (WSSCS).

REFERENCES

BLAHUT R. E. 1983. *Theory and Practice of Error Control Codes.* Addison-Wesley Publishing Company, Inc.

CHEE-MUN ONG. 1998. *Dynamic Simulation of Electric Machinery: Using MATLAB/SIMULINK.* Prentice Hall.

CHU L. C. and U. MITRA. 1998. Performance analysis of an improved MMSE multiuser receiver for mismatched delay channels. *IEEE Transactions on Communications* **46 (10)**.

Error Correction with Hamming Codes, http://www-dos.uniine.msk.ru/tech1/1994/er_cont/hamming.html

FREEMAN R. L. 1995. *Practical Data Communications.* N.Y.: Wiley-interscience.

GLISTIC S.G., T.J. POUTANEN, W. W. WU, G. V. PETROVIC and Z. STEFANOVIC. 1999. New PN code acquisition scheme for CDMA network with low signal to noise ratio. *IEEE Transactions on Communications* **47(2)**.

HAYKIN S. 1994. *Communication Systems.* N.Y.: John Wiley.

HOST-MADSEN A. and K. S. CHO. 1999. MMSE/PIC multiuser detection for DSCDMA system with inter- and intra-cell interference. *IEEE Transactions on Communications* **47(2)**.

JOHN G. PROAKIS and MASOUD SALEHI. 1998. *Contemporary Communication Systems using MATLAB.* PWS Publishing Company.

MESSIER G. G. 1998. Private Communications, TRLabs, Calgary, March 12.

PETERSON R. L. and R. E. ZIEMER. 1985. *Digital Communications and Spread Spectrum Systems.* N.Y.: Collier Macmillan.

Power Spectral Density Curve, http:llwww.tapr.org/sslqexss .

PRASAD R. 1996. *CDMA for Wireless Personal Communications.* Norwood: Artech House Publisher.

QIAO C. 1998. A universal analysis model for photonic Banyan networks. *IEEE Transactions on Communications* **46(10)**.

The American Radio Relay League, The ARRL Handbook for Radio Amateurs, 1996.

Transmission Line Attenuation Chart, http://lwww.tapar.orgltaprlhtmlcoax.html.

WILHEIMSSON L. and K. S. ZIGANGIROV. 1998. Analysis of MFSK frequency-hopped spread spectrum multiple-access over a Rayleigh fading channel. *IEEE Transactions on Communications* **46(10)**.

Pertanika Journal of Science and Technology

Subject Index for Vol. 10, Nos. 1 and 2, 2002

Pertanika Journal of Science & Technology

Author Index for Volume 10, Nos. 1 & 2, 2002

ACKNOWLEDGEMENTS

The Editorial Board acknowledges the assistance of the following reviewers in the preparation of Volume 10, Numbers 1 & 2 of this journal

Prof. Dr. Abdullah Assuhaimi
Assoc. Prof. Dr. Abdul Aziz Jemain
Dr. Abdullah Embong
Dr. Abdul Halim Ghazali
Dr. Abu Hassan Shaari
Prof. Dr. Abdul Kariem Arof
Prof. Dr. Abdul Rashid Sarkar
Dr. Ahmad Ainuddin Nuruddin
Assoc. Prof. Ahris Yaakup
Dr. Anas Febrin Ismail
Prof. Dr. Anuar Ashrabor
Assoc. Prof. Dr. Azah Mohamad
Assoc. Prof. Dr. Azaini Maarof
Assoc. Prof. Dr. Azali Mohamed
Assoc. Prof. Dr. Fakrul Razi Ahamdun
Prof. Dr. Fatimah Mohd Yusuf
Assoc. Prof. Dr. Faujan Hj. Ahmad
Prof. Dr. Ganihodjaev N
Dr. Hadi Salamati
Assoc. Prof. Dr. Hishamudin Zainuddin
Assoc. Prof. Dr. Hj. Hassan Selamat
Assoc. Prof. Dr. Hj. Ismail Hj Mohamad
Prof. Dr. Hj. Mahamod Ismail
Prof. Dr. How Guan Aun
Dr. Kaharudin Dimyati
Assoc. Prof. Dr. Kwok Chee Yan
Dr. Lau Seng
Assoc. Prof. Dr. Leow Soo Kar
Prof. Dr. Lim Poh Eng
Prof. Dr. S.N. Maiti
Assoc. Prof. Dr. Md. Yazid Md. Saman
Assoc. Prof. Dr. Megat Johari Megat Mohd Noor
Assoc. Prof. Dr. Mohd. Amin Mohd. Soom
Prof. Dr. Mohamad Ridza Wahidin
Assoc. Prof. Dr. Muhammad Ismail Yaziz
Assoc. Prof. Dr. Noriah Bidin
Dr. O Ok Park
Assoc. Prof. Dr. Ong Seng Huat
Assoc. Prof. Dr. Roslan Shukor
Assoc. Prof. Dr. Shanuddin Zakaria
Dr. Suleyman Arumu Muyibi
Assoc. Prof. Dr. Tan Hui Boon
Assoc. Prof. Dr. Taufiq Yap Yun Hin
Dr. Thamer Ahmed Mohamed
Assoc. Prof. Dr. Wan Md Zin Md Yunus
Dr. Yahya Samian
Assoc. Prof. Dr. Zulkarnain Zainal

Preparation of Manuscript

General
The manuscript, including footnotes, tables, and captions for illustrations, should be typewritten double spaced on paper 210 x 297 mm in size, with margins of 40 mm on all sides. Three clear copies are required. Typing should be on one side of the paper only. Each page of the manuscript should be numbered, beginning with the title page.

Title page
The title of the paper, name of author and full address of the institution where the work was carried out should appear on this page. A short title not exceeding 60 characters should be provided for the running headline.

Abstract
Abstracts in Bahasa Melayu and English of not more than 200 words each are required for full articles and communications. No abbreviation should appear in the abstract. Manuscripts from outside of Malaysian may be submitted with an English abstract only.

Keywords
Up to a maximum of ten keywords are required and they should be placed directly below the abstract.

Footnotes
Footnotes to material in the text should not be used unless they are unavoidable. Where used in the text, footnotes should be designated by superscript Arabic numerals in serial order throughout the manuscript. Each footnote should be placed at the bottom of the manuscript page where reference to it is made.

Equations
These must be clearly typed, triple-spaced and should be identified by numbers in square brackets placed flush with the right margin. In numbering, no distinction is made between mathematical and chemical equations. routine structural formulae can be typeset and need not be submitted as figures for direct reproduction but they must be clearly depicted.

Tables
Tables should be numbered with Arabic numerals, have a brief title, and be referred to in the text. Columns headings and descriptive matter in tables should be brief. Vertical rules should not be used. Footnotes in tables should be designated by symbols or superscripts small italic letters. Descriptive materials not designated by a footnote may be placed under a table as a *note.*

Illustrations & Photographs
Illustration including diagrams and graphs are to be referred to in the text as 'figures' and photographs as 'plates' and numbered consecutively in Arabic numerals. All photographs (gloosy black and white prints) should be supplied with appropriate scales.

Illustrations should be of print quality; outputs from dotmatrix printers are not acceptable, Illustrations should be on separate sheets, about twice the size of the finished size in print. All letters, numbers and legends must be included on the illustration with the author's name, short title of the paper, and figure number written on the vereso. A list of captions should be provided on a separate sheet.

Unit of Measure
Metric units must be used for all measurements.

Citations and References
Items in the reference list should be referred to in the text by inserting, within parentheses, the year of publication after the author's name. If there are more than two authors, the first author should be cited followed by '*et al*'. The names of all authors, however, will appear in the reference list.

In the case of citing an author who has published more than one paper in the same year, the papers should be distinguished by addition of a small letter, e.g. Choa (1979a); Choa (1979b); Choa (1979c).

In the reference list, the names should be arranged alphabetically according to the name of the first author. Serials are to be abbreviated as in the *World List of Scientific Periodicals.*

The abbreviation for Pertanika Journal of Science and Technology is *Pertanika J. Sci. Technol.*

The following reference style is to be observed:

Monograph
Alefed, G. and J. Herzberger. 1983. *Introduction to Interval Computations.* New York: Academic Press.

Chapter in Edited Book
Muzzarell, R.A.A. 1980. Chitin. In *Polymers in Nature,* ed. E.A. MacGregor and C.T. Greenwood, p. 417-449. New York: John Wiley.

Serials
Kamaruzaman Ampon. 1991. The effect of attachment of hydrophobic imidoesters on the catalytic activity of trypsin. *Pertanika* **14(2)**: 18-185.

Proceedings
Mokhtaruddin, A.M. and L.M. Maene. 1981. Soil erosion under different crops and management practices. In *Agricultural Engineering in National Development,* ed. S.L. Choa, Mohd Zohdie Bardaie, N.C. Saxena and Van Vi Tran, p. 245-249. Serdang, Malaysia: Universiti Pertanian Malaysia Press.

Unpublished Materials (e.g. theses, reports & documents)

Sakri, I. 1990. Proper construction set-up of Malaysian Fish Aggregating Devices (Unjam). Ph.D. Thesis, Universiti Pertanian Malaysia, Serdang, Selangor.

Pertanika Journal of Science & Technology

Volume 10 No. 2, 2002

Contents

ISSN 0128-7680

07

9 770128 768083